NUMERICAL CALCULATION OF HOMOGENIZED PROPERTIES OF PIEZOELECTRIC COMPOSITES

A THESIS SUBMITTED TO
THE GRADUATE SCHOOL OF NATURAL AND APPLIED SCIENCES
OF
MIDDLE EAST TECHNICAL UNIVERSITY

BY

MUSTAFA KURT

IN PARTIAL FULFILLMENT OF THE REQUIREMENTS
FOR
THE DEGREE OF MASTER OF SCIENCE
IN
AEROSPACE ENGINEERING

NOVEMBER 2022

Approval of the thesis:

NUMERICAL CALCULATION OF HOMOGENIZED PROPERTIES OF PIEZOELECTRIC COMPOSITES

submitted by **MUSTAFA KURT** in partial fulfillment of the requirements for the degree of **Master of Science in Aerospace Engineering Department, Middle East Technical University** by,

Prof. Dr. Halil Kalıpçılar
Dean, Graduate School of **Natural and Applied Sciences** _____

Prof. Dr. Serkan Özgen
Head of Department, **Aerospace Engineering** _____

Assoc. Prof. Dr. Ercan Gürses
Supervisor, **Aerospace Engineering, METU** _____

Examining Committee Members:

Prof. Dr. Demirkan Çöker
Aerospace Engineering, METU _____

Assoc. Prof. Dr. Ercan Gürses
Aerospace Engineering, METU _____

Prof. Dr. Altan Kayran
Aerospace Engineering, METU _____

Assoc. Prof. Dr. Serdar Göktepe
Civil Engineering, METU _____

Assoc. Prof. Dr. Cihan Tekoğlu
Mechanical Engineering, TOBB ETU _____

Date: 25.11.2022

I hereby declare that all information in this document has been obtained and presented in accordance with academic rules and ethical conduct. I also declare that, as required by these rules and conduct, I have fully cited and referenced all material and results that are not original to this work.

Name, Surname: Mustafa Kurt

Signature :

ABSTRACT

NUMERICAL CALCULATION OF HOMOGENIZED PROPERTIES OF PIEZOELECTRIC COMPOSITES

Kurt, Mustafa
M.S., Department of Aerospace Engineering
Supervisor: Assoc. Prof. Dr. Ercan Gürses

November 2022, 110 pages

Piezoelectric materials are the materials we use in many parts of our lives without being aware. These materials can convert electrical energy into mechanical energy or vice versa. Although this ability renders piezoelectric ceramics very attractive materials for sensing and actuation applications, their use often remains limited, due to their weight and brittleness. As a result of these drawbacks, piezoelectric composites are developed, and they offer superior performance compared to monolithic piezoelectric materials.

The main aim of this study is to numerically calculate the effective material properties (elastic, piezoelectric, and dielectric) of piezoelectric composites to determine the behavior and performance of the piezoelectric composites. With micromechanical methods, the overall behavior of piezoelectric composites is obtained by using the properties of their constituents through a finite element analysis of a periodic representative volume element (RVE) or a unit cell model.

In this study, different piezoelectric fiber composites are studied. The most encountered piezocomposite in the literature is 1-3 type piezocomposites, whose full set of

material moduli is extracted using the homogenization method. The results are verified with experimental data and different numerical studies from the literature. The homogenization method is validated with a macro-scale boundary value problem and the results are compared with a numerical study from the literature. Moreover, porous piezoceramics are investigated. The effects of size, shape, and distribution of pores upon the effective material properties and performance coefficients are investigated. Finally, the porosity is incorporated into the 1-3 piezocomposites and its influence on the hydrostatic performance coefficients is investigated.

Keywords: Piezoelectricity, Composite, Homogenization, Finite element analysis, Porosity

ÖZ

PİEZOELEKTRİK KOMPOZİTLERİN HOMOJENLEŞTİRİLMİŞ ÖZELLİKLERİNİN SAYISAL OLARAK HESAPLANMASI

Kurt, Mustafa
Yüksek Lisans, Havacılık ve Uzay Mühendisliği Bölümü
Tez Yöneticisi: Doç. Dr. Ercan Gürses

Kasım 2022 , 110 sayfa

Piezoelektrik malzemeler hayatımızın birçok alanında farkında olmadan kullandığımız malzemelerdir. Bu malzemeler, elektrik enerjisini mekanik enerjiye veya tam tersine dönüştürme özelliğine sahiptir. Bu özellik, piezoelektrik seramikleri sensör ve aktüatör uygulamaları için oldukça cazip hale getirse de, ağır ve gevrek yapıda olmaları nedeniyle kullanımları genellikle sınırlı kalır. Bu dezavantajların bir sonucu olarak, piezoelektrik kompozitler geliştirilmekte ve monolitik piezoelektrik malzemelere göre daha üstün performans sunmaktadırlar.

Bu çalışmanın ana amacı, piezoelektrik kompozitlerin davranış ve performansını belirlemek için piezoelektrik kompozitlerin etkin malzeme özelliklerini (elastik, piezoelektrik ve dielektrik) sayısal olarak hesaplamaktır. Mikro mekanik yöntemlerle, piezoelektrik kompozitlerin genel davranışı, bileşenlerinin özellikleri kullanılarak, periyodik temsili hacim elemanının (RVE) veya bir birim hücre modelinin sonlu eleman analizi yoluyla elde edilir.

Bu çalışmada, farklı piezoelektrik fiber kompozitler incelenmiştir. Literatürde en çok

karşılaşılan piezokompozit, bu çalışmada homojenizasyon yöntemi kullanılarak tüm malzeme modülleri çıkarılan 1-3 piezokompozitlerdir. Sonuçlar, deneysel veriler ve literatürdeki birçok sayısal çalışma ile doğrulanmıştır. Homojenleştirme yöntemi, makro ölçekli bir sınır değer problemi ile doğrulanmış ve sonuçlar literatürdeki sayısal bir çalışma ile karşılaştırılmıştır. Ayrıca, gözenekli piezoseramikler de araştırılmıştır. Gözeneklerin boyut, şekil ve dağılımının etkin malzeme özellikleri ve performans katsayıları üzerindeki etkileri araştırılmıştır. Son olarak, gözenekli yapı 1-3 piezokompozitlere dahil edilmiş ve hidrostatik performans katsayıları üzerindeki etkisi araştırılmıştır.

Anahtar Kelimeler: Piezoelektrisite, Kompozit, Homojenleştirme, Sonlu elemanlar analizi, Gözenek

To my families,

ACKNOWLEDGMENTS

I would like to acknowledgment and give my deep and sincere gratitude to my advisor Assoc. Prof. Dr. Ercan Gürses for his guidance, critism, exemplarity and time allocated to me through all the stages of this thesis.

I would like to thank to the thesis committee members, Prof. Dr. Demirkan Çöker, Prof. Dr. Altan Kayran, Assoc. Prof. Dr. Serdar Göktepe and Assoc. Prof. Dr. Cihan Tekoğlu for their participation, criticism and contribution.

I would like to thank my parents for being my parents and my brother.

I would like to thank Funda Aksu Denli, who helped me to start this journey.

I would like to thank all my friends for their presence and supports.

TABLE OF CONTENTS

ABSTRACT v

ÖZ vii

ACKNOWLEDGMENTS x

TABLE OF CONTENTS xi

LIST OF TABLES xvi

LIST OF FIGURES xix

LIST OF ABBREVIATIONS xxiii

LIST OF SYMBOLS xxiv

CHAPTERS

1 INTRODUCTION 1

1.1 Motivation and Aim of the Thesis 3

1.2 Outline of the Thesis 3

2 LITERATURE REVIEW 5

3 PIEZOELECTRICITY 11

3.1 Fabrication 17

3.2 Poling 17

3.3 Properties of Piezoelectric Materials 19

3.4 Piezoceramics 19
3.5 Piezopolymers 20
3.6 Doping 22
3.7 Piezocomposites 23
3.8 Piezocomposite Design 24
3.9 Product Properties 25
3.10 Connectivity 25
3.11 Performance of Piezocomposites 28
3.11.1 Elastic Compliance 29
3.11.2 Permittivity (Dielectric Constant) 29
3.11.3 Density 30
3.11.4 Piezoelectric strain coefficient (d) 31
3.11.5 Hydrostatic strain constant (d_h) 32
3.11.6 Piezoelectric voltage coefficient (g) 32
3.11.7 Hydrostatic piezoelectric voltage constant (g_h) 33
3.11.8 Hydrostatic figure of merit ($d_h g_h$) 34
3.11.9 Hydrostatic Compliance (s_h) 34
3.11.10 Hydrostatic Coupling Coefficient (k_h) 34
3.11.11 Electromechanical Coupling Factor (k) 35
4 METHODOLOGY 37
4.1 Piezoelectric Constitutive Equations 37
4.2 Representative Volume Element 40
4.3 Homogenization 41

4.3.1 Linear Displacement Boundary Condition (DBC) 45
4.3.2 Constant Traction Boundary Condition (TBC) 45
4.3.3 Periodic Boundary Condition (PBC) 46
4.3.4 Comparison of Boundary Conditions 46
4.4 Application of PBCs 47
4.5 Loadings and Boundary Conditions 50
4.5.1 Axial Load 52
4.5.2 Simple Shear 53
4.6 Calculation of Effective Properties 55
5 TWO PHASE PIEZOCOMPOSITES 57
5.1 An analysis of 1-3 piezocomposite 58
5.1.1 FEM Model 58
5.1.1.1 Material 58
Elastic Properties: 59
Piezoelectric Properties: 59
Dielectric Properties: 59
5.1.1.2 Mesh 60
5.1.1.3 Loadings and BCs 60
5.1.2 Results and Discussion 60
5.1.2.1 Extraction of 11 Effective Coefficients 61
Coefficients C_{11}^{eff} and C_{12}^{eff}: 62
Coefficients C_{13}^{eff} and C_{33}^{eff}: 62
Coefficient ε_{11}^{eff}: 63

Coefficients e_{13}^{eff} , e_{33}^{eff} and ε_{33}^{eff}: 63

Coefficient C_{66}^{eff}: 64

Coefficients C_{44}^{eff} and e_{15}^{eff}: 65

5.1.2.2 PBC vs. DBC 66

5.2 Comparison with literature 67

5.2.1 Comparison with Tita et al. [19] and Berger et al. [12] 67

5.2.2 Comparison with Berger et al. [13] and Pettermann et al. [95] . 68

5.2.3 Comparison with experimental data 71

5.3 Application to a Macro-Scale Boundary Value Problem 74

6 POROUS PIEZOCOMPOSITES 79

6.1 Generation of Porosity 79

6.1.1 Sacrificial Template Method 80

6.1.2 Replica Technique 81

6.1.3 Direct Foaming 81

6.2 Calculation of Hydrostatic Performance Coefficients 81

6.3 Analysis of Porous Piezoceramics 82

6.3.1 Modelling 83

6.3.2 Comparison with literature data 85

6.3.3 Effect of Pore Shapes 87

6.3.4 Effect of Pore Size 89

6.3.5 Effect of Spherical Pore Configuration 90

6.3.6 Effect of Cylindrical Pore Configuration 92

6.4 Analysis of Porous Piezocomposites 94

7 CONCLUSION 97

REFERENCES 101

LIST OF TABLES

TABLES

Table 3.1 Properties of some piezoelectric crystals at room temperature 14

Table 3.2 Properties of PZT Ceramics Groups [57], [46] 20

Table 3.3 Properties of common piezoelectric ceramics 20

Table 3.4 Properties of PZT Ceramics 23

Table 3.5 Comparison of the Piezoelectric Properties of PZT-Polymer Composites with PVDF and PZT [1] 23

Table 4.1 Load cases and relevant material coefficient groups 50

Table 4.2 Boundary conditions on the RVE surfaces and corresponding effective coefficients 51

Table 5.1 Piezoelectric tensor format in ABAQUS [2] 59

Table 5.2 Material Properties of PZT-5A and Epoxy. Note that elastic, piezoelectric and dielectric coefficients are given in $\mathrm{GPa}, \mathrm{C/m^2}$ and $\mathrm{nF/m}$, respectively. 61

Table 5.3 Effective and constituent material properties of PZT-5A/Epoxy piezocomposite for 55.5% volume fraction. Note that elastic, piezoelectric and dielectric coefficients are given in $\mathrm{GPa}, \mathrm{C/m^2}$ and $\mathrm{nF/m}$, respectively. . . 62

Table 5.4 Comparison of mechanical and electrical parameter results of PBC and DBC 66

Table 5.5 Comparison for 55.5% volume fraction. Note that elastic, piezoelectric and dielectric coefficients are given in $\mathrm{GPa}, \mathrm{C/m^2}$ and $\mathrm{nF/m}$, respectively. 68

Table 5.6 Material Properties of PZT-7A and Epoxy. Note that elastic, piezoelectric and dielectric coefficients are given in $\mathrm{GPa}, \mathrm{C/m^2}$ and $\mathrm{nF/m}$, respectively. 69

Table 5.7 Comparison for 60% volume fraction. Note that the units are in GPa, $10^9\,\mathrm{Vm/C}$ and $10^9\,\mathrm{V/m}$, respectively. 70

Table 5.8 Material properties of PZT-7A and Epoxy. Note that elastic, piezoelectric and dielectric coefficients are given in $\mathrm{GPa}, 10^{-12}\,\mathrm{m/V}$ and $\mathrm{nF/m}$, respectively. 72

Table 5.9 Material properties of APC850 and shim. Note that elastic, piezoelectric and dielectric coefficients are given in $\mathrm{GPa}, 10^{-12}\,\mathrm{m/V}$ and $\mathrm{nF/m}$, respectively. 76

Table 6.1 Comparison of pore modeling techniques for 10% pore volume fraction. The units are in GPa, $\mathrm{C/m^2}$ and $\mathrm{nF/m}$, respectively. 85

Table 6.2 Comparison for 10% pore volume fraction. Note that the units are in GPa, $\mathrm{C/m^2}$ and $\mathrm{nF/m}$, respectively. 86

Table 6.3 Comparison for 30% pore volume fraction. Note that the units are in GPa, $\mathrm{C/m^2}$ and $\mathrm{nF/m}$, respectively. 86

Table 6.4 Comparison for 50% pore volume fraction. Note that the units are in GPa, $\mathrm{C/m^2}$ and $\mathrm{nF/m}$, respectively. 86

Table 6.5 Effective properties comparison of different pore shapes at the same volume fraction 10 $\%$. Note that the units are in GPa, $\mathrm{C/m^2}$ and $\mathrm{nF/m}$, respectively. 88

Table 6.6 Effective properties of porous piezoceramics with spherical pores at varying volume fractions. Note that the units are in GPa, $\mathrm{C/m^2}$ and $\mathrm{nF/m}$, respectively. 89

Table 6.7 Effective properties of piezoceramics with spherical pores at varying volume fractions. Note that the units are in GPa, $\mathrm{C/m^2}$ and $\mathrm{nF/m}$, respectively. 91

Table 6.8 Effective properties of piezoceramics with cylindrical pores at varying volume fractions. Note that the units are in GPa, $\mathrm{C/m^2}$ and $\mathrm{nF/m}$, respectively. 93

Table 6.9 Effective properties of porous piezocomposites with varying pore volume fraction and with fixed 40% epoxy content. Note that the units are in GPa, $\mathrm{C/m^2}$ and $\mathrm{nF/m}$, respectively. 95

LIST OF FIGURES

FIGURES

Figure 3.1 Crystal structure of Barium Titanate [37] 12

Figure 3.2 Schematics of a) Cubic and b) Tetragonal Lattices [39] 14

Figure 3.3 Atomic structure of Quartz [44] 15

Figure 3.4 Direct and inverse piezoelectric effect. [46] 16

Figure 3.5 Depiction of poling process under an applied electric field [54] . 19

Figure 3.6 Alpha-phase and Beta-phase structure of PVDF [63] 21

Figure 3.7 a) Product Effect and b) Combination Effect [1] 26

Figure 3.8 Connectivity Patterns of Two-Phase Composites [1] 27

Figure 3.9 a) 1-3 Piezocomposites and b) 2-2 Piezocomposites [67] 27

Figure 4.1 Composite built from duplicated RVEs [82] 40

Figure 4.2 An RVE model for 1-3 piezocomposites in ABAQUS 41

Figure 4.3 Illustration of homogenization example 42

Figure 4.4 Positive and negative boundary discretization [88] 46

Figure 4.5 Convergence comparison of the boundary conditions in a RVE [88] 47

Figure 4.6 Schematic of a matching pair of nodes on opposite faces of an RVE [82] 48

Figure 4.7 Part and Surface Designations in a Representative Volume Element [94] 49

Figure 4.8 Mechanical Loading applied in Z to calculate C_{13}^{eff} and C_{33}^{eff} . . 52

Figure 4.9 An example of an RVE with the constraint equations which are depicted with yellow circles. 54

Figure 5.1 An RVE model for 1-3 piezocomposites in ABAQUS 58

Figure 5.2 The subject RVE model with fiber volume fraction of 55.5% . . 61

Figure 5.3 Under mechanical loading in X, a) von Mises distribution in the deformed shape, b) stress distribution in X and c) stress distribution in Y in undeformed shapes 62

Figure 5.4 Under mechanical loading in Z, a) von Mises distribution in the deformed shape, b) stress distribution in X and c) stress distribution in Z in undeformed shapes 63

Figure 5.5 Under electrical loading in X, a) von Mises distribution in the deformed shape, b) electric displacement in X and c) electric field in X in undeformed shapes 63

Figure 5.6 Under electrical loading in Z, a) electric displacement in Z distribution in the deformed shape, b) stress distribution in X and c) stress distribution in Z in undeformed shapes 64

Figure 5.7 Under shear loading in X-Y, a) stress distribution in X-Y and b) strain distribution in X-Y in the deformed shapes 64

Figure 5.8 Under shear loading in Y-Z, a) stress distribution in Y-Z and b) electric displacement distribution in Y in the deformed shapes 65

Figure 5.9 Investigated fiber volume fraction ratios: a) 20%, b) 40%, c) 60% 70

Figure 5.10 a) C_{44}^{eff} and b) C_{66}^{eff} versus fiber volume fraction 70

Figure 5.11 a) k^{eff} $(= (C_{11}^{eff} + C_{22}^{eff})/2)$ and b) ε_{11}^{eff} versus fiber volume fraction 71

Figure 5.12 a) e_{13}^{eff} and b) e_{15}^{eff} versus fiber volume fraction 71

Figure 5.13 d_{33}^{eff} vs. PZT-7A volume fraction 72

Figure 5.14 d_{33}^{eff} vs. PZT-7A volume fraction ($d_{33} = 167{\times}10^{-12}\,\mathrm{m/V}$ for PZT-7A) 73

Figure 5.15 $\varepsilon_{33}^{T,eff}/\varepsilon_0$ vs. PZT-7A volume fraction ($d_{33} = 167{\times}10^{-12}\,\mathrm{m/V}$ for PZT-7A) 73

Figure 5.16 $s_{11}^{eff} + s_{12}^{eff}$ vs. PZT-7A volume fraction ($d_{33} = 167{\times}10^{-12}\,\mathrm{m/V}$ for PZT-7A) 74

Figure 5.17 Full scale of macroscale model and its quarter computational domain [97] 75

Figure 5.18 RVE model prepared for macro-scale problem 76

Figure 5.19 Material regions, mesh and mechanical BC surface of a) the heterogeneous and b) the homogeneous macro-scale models 77

Figure 5.20 Displacement contour of a) the heterogeneous and b) the homogeneous macro-scale models under 5 V electrical load. 77

Figure 5.21 Deflection of the middle point for various radii of the piezoelectric plate 78

Figure 6.1 Porosity Manufacturing Techniques [100] 80

Figure 6.2 Two modeling examples, in which a) pore is modeled and b) pore is not modeled 83

Figure 6.3 Under mechanical loading in X-direction, von Mises stress distribution in deformed shape of a) BC with pore geometry, b) PBC with pore geometry and c) PBC without pore geometry 84

Figure 6.4 d_h versus pore volume fraction 87

Figure 6.5 g_h versus pore volume fraction 87

Figure 6.6 Cut-views of the RVEs that contain 10 $\%$ pore in the shape of a) perfect sphere, b) ellipse aligned with Z axis c) cylinder aligned with Z axis 88

Figure 6.7 a) d_h and b) g_h versus pore shape 88

Figure 6.8 a) C_{11}^{eff} and b) C_{12}^{eff} versus pore volume fraction 89

Figure 6.9 a) C_{13}^{eff} and b) C_{33}^{eff} versus pore volume fraction 90

Figure 6.10 a) e_{13}^{eff} and b) e_{33}^{eff} versus pore volume fraction 90

Figure 6.11 ε_{33}^{eff} versus pore volume fraction 91

Figure 6.12 a) d_h and b) g_h versus pore volume fraction 91

Figure 6.13 Cut-views of the RVEs that contain 10 $\%$ pore in the shape of a) single sphere, b) two spheres, one in the middle and the other divided into 1/8 located at the corners, and c) two spheres aligned in the axis of isotropy 92

Figure 6.14 a) d_h and b) g_h versus spherical pore configuration 92

Figure 6.15 Cut-views of the RVEs that contain 10 $\%$ pore in the shape of a) a single cylinder, b) two cylinders, one at the center and the other divided into 1/4 located at the edges, and c) two cylinders aligned in the axis of isotropy 93

Figure 6.16 a) d_h and b) g_h versus cylindrical pore configuration 94

Figure 6.17 Cut-views of the RVE models of a) the porous piezoceramic and b) the porous piezocomposite 95

Figure 6.18 a) d_h and b) g_h versus pore volume fraction in piezocomposite made of PZT-5A and epoxy 96

LIST OF ABBREVIATIONS

ABBREVIATIONS	
BC	Boundary Condition
BT	Barium Titanate
DOF(s)	Degree(s) of Freedom
DOF(s)	Degree(s) of Freedom
FOM(s)	Figure(s) of Merit
PBC	Periodic Boundary Condition
PT	Lead Titanate
PZT	Lead Zirconate Titanate
RVE	Representative Volume Element

LIST OF SYMBOLS

SYMBOLS

$\boldsymbol{C^D}$	Elasticity tensor at a constant electric displacement
$\boldsymbol{C^E}$	Elasticity tensor at a constant electric field
$\boldsymbol{D}$	Electric displacement
$\boldsymbol{d}$	Piezoelectric strain coefficient tensor
d_h	Hydrostatic piezoelectric strain coefficient
$\boldsymbol{E}$	Electric field
$\boldsymbol{e}$	Piezoelectric stress coefficient tensor
G	Gibbs free energy
$\boldsymbol{g}$	Piezoelectric voltage coefficient tensor
g_h	Hydrostatic piezoelectric voltage coefficient
$\boldsymbol{h}$	Piezoelectric coupling tensor
$\boldsymbol{n}$	Surface normal vector
$\boldsymbol{S}$	Strain tensor
$\boldsymbol{s^E}$	Compliance tensor at a constant electric field
$\boldsymbol{T}$	Stress tensor
$\boldsymbol{t}$	Traction vector
U	Internal energy
$\boldsymbol{u}$	Displacement
$\boldsymbol{\beta}$	Dielectric tensor
$\boldsymbol{\epsilon}$	Strain tensor
ε_0	Absolute dielectric constant
$\boldsymbol{\varepsilon^S}$	Dielectric tensor at a constant strain
$\boldsymbol{\varepsilon^\sigma}$	Dielectric tensor at a constant stress
$\boldsymbol{\sigma}$	Stress tensor

ϕ	Electric potential

CHAPTER 1

INTRODUCTION

Piezocomposites, or piezoelectric composites, are composite materials consisting of a piezoelectrically active material and a piezoelectrically passive material host material, e.g., polymer or epoxy. The piezoelectrically active material is most commonly a piezoceramic or a piezoelectric ceramic, and this is the constituent that makes the composite piezocomposite. Due to their superior properties over conventional pure piezoceramics and tailorable properties, piezocomposites have been considered very promising and used in many different fields since then. Some special properties of piezocomposites are high electromechanical coupling, mechanical flexibility, and low acoustic impedance.

The high electromechanical coupling means better conversion between the mechanical and electrical energy. Low acoustic impedance helps the acoustic waves to be transmitted to new media such as water or human tissue. These properties render piezoelectric composites very beneficial for underwater sonar applications or ultrasonic transducer applications in medicine.

The properties that we obtain from a piezoelectric composite depend on the material selection, the volume fraction of the phases, and the topology of the phases. Therefore, by manipulating the aforementioned parameters, we can obtain different property values, meaning that the properties of the piezoelectric composites are tailorable, and this is generally not possible for a pure piezoelectric material.

The connectivity of the phases dictates the name of the piezoelectric composites and their nature. Depending on how the phases are interconnected, the geometry and the behavior of the piezocomposite change. For a two-phase piezoelectric composite,

there are 10 possible patterns: 0-0, 0-1, 0-2, 0-3, 1-1, 1-2, 1-3, 2-2, 2-3 and 3-3.

Especially a 1-3 piezocomposite configuration, which consists of PZT-rod and polymer-matrix as its constituents, has been considered the most useful because this composite configuration has features such as high coupling coefficients, mechanical flexibility, low acoustic impedance, decent acoustic matching to human tissue, and water [1]. These mentioned features make 1-3 piezoelectric composites quite beneficial for both underwater sonar applications and ultrasonic transducer applications of medical diagnosis.

Since these piezocomposite materials are among the important parts of the recent materials in engineering fields due to their unique advantages, the prediction of the material properties of the piezocomposites has become very necessary. The macroscopic properties of piezocomposites can be determined following the homogenization method. The concept of representative volume element (RVE) arises in the homogenization method. A representative volume element is said to be the smallest piece that can represent the entire structure homogeneously and is often modeled as a cube in three-dimensional numerical calculations. In the homogenization method, a macroscopic strain state is applied to an RVE, and the average of the non-uniform stress field over the RVE is computed. The homogenized material properties can then be computed using the macroscopic strain and the average stress values, assuming a linear constitutive relation. In this study, a representative volume element in the form of a cube is used for all the analyses using commercial finite element analysis software ABAQUS [2].

By obtaining these average (effective) properties, new homogeneous material with approximately the same mechanical and piezoelectrical behaviors as the original heterogeneous material can be created. This method is called homogenization, which will be explained in more detail in Chapter 4.

Finite element analyses are conducted with the commercial software program ABAQUS. Python programming language embedded in ABAQUS facilitated the application of boundary conditions and post-process calculations. Creating a Python script to do the pre or post-processing jobs or to automate the repetitive tasks decreases the time and effort required for analysis. Furthermore, for some specific jobs, it becomes a must

to do so. Applying periodic boundary conditions (PBCs) is an example of it. There are two main Python scripts developed for this thesis, one for applying PBCs and the other for post-processing.

1.1 Motivation and Aim of the Thesis

The fact that the monolithic piezoelectric materials do not meet the requirements of the specific applications necessitates the use of the piezoelectric composites, which are made of piezoelectric materials embedded in a piezoelectrically passive host material. Moreover, the computation of the effective material coefficients of these composites is a vital step reaching the optimum design with appropriate material selection and configuration. Numerical calculations also offer a great variety and convenience in estimating the effective material coefficient. Therefore, numerical calculation of effective properties of piezocomposites is essential and valuable.

1.2 Outline of the Thesis

Chapter 2 is a literature review chapter. Related studies in the literature are reviewed and briefly explained.

In Chapter 3, general information about piezoelectricity is thoroughly reported. It consists of sections that explain the fundamental principles of piezoelectric materials, such as their crystal structures, poling, and connectivity. Data of the piezoelectric materials are shared in tables. Two different types of piezoelectric materials, piezoceramics and piezopolymers, are briefly explained and piezocomposites and their advantages are stated. Material coefficients and performance coefficients of the piezoelectric materials are explained.

In Chapter 4, the following information regarding the calculation of the effective properties is expressed. Constitutive equations of the piezoelectric behavior, assumptions, and material tensors of transversely isotropic piezoelectric materials are stated. Homogenization method, the concept of RVE, types of boundary conditions, and particularly the periodic boundary condition (PBC) are explained. The application of

PBCs and the calculation of the effective properties are presented.

In Chapter 5, diphasic 1-3 piezocomposites are studied. Their full set of material moduli is extracted by analyzing RVEs in ABAQUS. An example model is analyzed, and the results are discussed. Effective material coefficients are tabulated, and contour plots of stresses, electric field, and electric displacements are shown. Furthermore, by using two different analysis models, the results of this study are compared with the four studies found in the literature.

In Chapter 6, porous piezoceramics are studied. Since only the performance coefficients regarding the hydrostatic applications are of interest, related material coefficients are evaluated, not all the material coefficients. It is observed that the presence of pores increased the hydrostatic performance of the piezoceramics. The effects of size, shape, and configuration are studied.

In Chapter 7, the conclusions will be remarked.

CHAPTER 2

LITERATURE REVIEW

In this chapter, important and related studies found in the literature about the homogenization of piezocomposites will be mentioned.

In 2019, Pramanik and Arockiarajan [3] wrote a comprehensive review article in which all the previous studies are mentioned, and important subjects such as porosity, interphase effects, and non-linearities are discussed.

Smith [4] discussed the effect of using polymer materials with negative Poisson's ratio on the coupling between the electrical and mechanical responses and concluded that it increased the electromechanical energy conversion of the piezocomposite. By doing so, the polymer matrix transformed the lateral stresses and helped in compressing the piezoelectric phase.

Upon that, Swart and Avellaneda [5] studied the limits of Poisson's ratio and concluded that using a negative Poisson's ratio improved performance. They also examined the effect of porosity in the matrix phase and obtained different homogenized properties and improved performance compared to composites with the non-porous matrix.

Bennett and Hayward [6] sought to get the maximum hydrostatic performance of a 1-3 piezocomposite. They achieved the best performance by using a piezocomposite with a low volume fraction PZT-5H and concluded that the polymer phase should be compliant and the Poisson's ratio should be as low as possible. The effect of Poisson's ratio was greater than Young's modulus of the polymer phase.

So far, researchers have investigated combinations of piezoelectrically active or pas-

sive phases and isotropic, transversely-isotropic, or anisotropic phases. As examples, the following can be given:

- Smith and Auld [7], Smith [8] and Chan and Unsworth [9] used transversely isotropic active fiber and isotropic passive matrix.
- Guinovart-Diaz et al. [10] studied transversely isotropic active fiber and transversely isotropic active matrix.
- Dunn and Taya [11], on the other hand, studied anisotropic active fiber and transversely isotropic active matrix.

Berger et al. [12], [13] focused on square arrangements of cylindrical fibers in 1-3 piezocomposites. In the study, an analytical and a numerical approach are presented to calculate the effective coefficients. These two studies can be considered benchmarks and have often been resorted to verifying other studies' results.

Just like Berger et al. [12], [13], the works of Kar-Gupta and Venkatesh [14]–[16] are also well-known. In their study, Kar-Gupta and Venkatesh [14] developed an analytical model for 1-3 piezoelectric composite and presented all the 45 independent material properties analytically. They also developed a FEM model and concluded that the analytical model successfully predicted the effective properties in the longitudinal direction of fiber (i.e., C_{33}, κ_{33}, and ε_{33}). However, the analytical model underpredicted the effective properties in the transverse directions like κ_{11} and κ_{22}. They stated that the differences were higher for matrix-dominant systems compared to fiber-dominant systems, and it was due to the approximation made in the FEM model, where the piezocomposite is modeled as a layered composite. Also, they noted that as the fiber volume fraction increases, the agreement between the FEM model and the analytical model worsens. They also studied in [16] the 1-3 piezoelectric composites according to their fiber arrangements.

Bowen and Kara [17] examined the influence of pore anisotropy on the hydrostatic properties for 3-3 piezocomposites, taking into account poling direction. They concluded that having pores aligned in the poling direction, permittivity in 3-direction (ε_{33}^{T}), hydrostatic strain coefficient (d_h), and hydrostatic figure of merit ($d_h g_h$) in-

creased, but hydrostatic voltage coefficient (g_h) is found to be insensitive to pore shape.

Moreno et al. [18] performed finite element analysis on 1-3 composites made of lead zirconate titanate (PZT) and the polymeric matrix. This study explained how the periodic boundary conditions should be applied in the computational homogenization of pizoelectric composites.

Tita et al. [19] evaluated the effective properties of smart composite materials with both perfect and imperfect fiber-matrix adhesion. They investigated different case studies to understand the influence of parameters, such as the geometry of the fiber cross-section, volume fraction, and imperfection in the interface, on the effective coefficients of composite materials. Their study concluded that more significant differences are observed for the effective coefficients of directions 1 and 2. Nevertheless, the effective coefficients in direction 3 (fiber direction) showed minute differences. This result is valid for different fiber volume fraction values and different levels of imperfect contact.

Mishra et al. [20] investigated a piezoelectric nanocomposite that is made of vertical arrays of piezoelectric zinc oxide (ZnO) nanowires and a SU8 photoresist as a polymeric matrix. In this study, the effective properties are evaluated by analyzing cubic RVE using finite element analysis. The results obtained were in agreement with the results that are obtained by a semi-analytical Eshelby Mori-Tanaka (EMT) method, in particular at low volume fractions. They investigated the influence of fiber arrangement, fiber volume fraction, and RVE size on the material properties. How the ZnO nanowires are arranged did cause differences in effective transverse elastic and piezoelectric coefficients but did not change the effective longitudinal (in fiber direction) properties much. Also, they studied two sizes of RVE and concluded that increasing the size of the RVE by two times did not affect the electromechanical properties of the piezocomposite, except for e_{15}.

According to Heiber et al. [21], PZT fibers can be produced for a wide range of diameters from 5 micrometers to 1000 micrometers. Della and Shu [22] studied the influence of three types of matrices on the performance of 1-3 piezoelectric composites: an active piezoelectric ceramic $\mathrm{BaTiO_3}$, an active piezoelectric polymer

[P(VDF-TrFE)], and a passive polymer Araldite D. PZT-7A fibers of circular cross section are used for all cases. They did the calculations using a micromechanics-based Mori-Tanaka model. They deduced that the active polymer matrix could seriously enhance the hydrostatic performance, yet the electromechanical coupling coefficient and acoustic impedance were not improved noticeably. Also, they discovered that using piezoelectric ceramic ($\mathrm{BaTiO_3}$) as a matrix does not improve performance.

To improve the thermal reliability and the performance of the 1-3 piezocomposites made of PZT and epoxy, Li et al. [23] introduced the reinforcement inclusions of glass spheres into the epoxy matrix. They fabricated the 1-3 piezocomposites and obtained the experimental results which revealed that while low content of glass spheres (≤ 4 $\%$) does not contribute to any improvement, the higher content of glass spheres ($\geq$ 12 $\%$) improved the dielectric permittivity, mechanical quality factor and lowered the thermal expansion coefficient of the piezocomposite.

Della and Shu [24] also investigated the possible effects of porosity in the matrix for 1-3 piezocomposites. They did a two-step analytical solution with Mori-Tanaka (MT) method [25], the first homogenized the porous matrix and then the whole structure, including the piezoelectric fiber and the porous matrix. Results showed that adding pores into the matrix significantly improved the figures of merits and the performance of the piezocomposite.

A similar but experimental study was conducted by Khanbareh et al. [26], in which they aimed to reduce the dielectric permittivity of the matrix phase and increase the flexibility for soft robotic skin applications by adding a gaseous phase into the matrix. They achieved the reduction of the dielectric permittivity, which resulted in an increase in the piezoelectric voltage coefficient (g_{33}) in return. New micro-porous piezocomposite can possess g_{33} coefficient up to twice as non-porous piezocomposite and five times as bulk PZT ceramics.

In a recent study about porosity, Isaeva and Topolov [27] studied the influence of a porous piezo-matrix on the piezoelectric properties and figures of merit compared to a non-porous piezo-matrix. Fiber material was chosen as KNNTL-Mn. Results showed that figures of merit like $d_{33}g_{33}$ and $d_{31}g_{31}$ improved with the addition of pores into the matrix. It is also stated that elliptic pores rather than spherical pores

can further improve the performance, inferring the influence of elastic anisotropy on the piezoelectric performance and the figures of merit (FOMs).

In the study of Martínez-Ayuso et al. [28], porous piezoelectric material (PZT-5A) is investigated through both analytical and numerical methods. With both methods, it was concluded that the figures of merit increased as the porosity increased. Porous piezoelectric materials are said to offer significant advantages for energy harvesting applications compared to monolithic piezoelectric materials. Also, it is deducted that the most favorable case is when the air inclusions are in the shape of perfect spheres and distributed spatially uniformly.

CHAPTER 3

PIEZOELECTRICITY

Piezoelectricity is the formation of electric charges in response to applied mechanical stress, which is called the direct piezoelectric effect. The other way around is also possible; by applying an electric field, the piezoelectric material undergoes a deformation, which is called the inverse piezoelectric effect. The word "piezo" is derived from the Greek word "piezein" and means "to press/squeeze". Therefore, the word piezoelectricity literally implies electricity from pressure [29].

These observed properties are defined as electromechanical coupling. The piezoelectricity results from the linear electromechanical interaction between the mechanical and electrical states in crystalline materials with no inversion symmetry [30]. This interaction relates a high amount of electric field to very small mechanical strains. For example, in Quartz, in response to 1000 V/cm electric field generates a mechanical strain of the order of 10^{-7} [31].

The piezoelectricity phenomenon was first discovered by French physicists Jacques and Pierre Curie in 1880 [32], [33]. Later, it began to be studied and understood as time went by. In 1917, Langevin and co-workers developed the first serious application of piezoelectricity around WWI, which was a transducer used to detect submarines and measure their depth. This application can be considered the basis of sonar. Although many applications are developed, the research field is active yet today. The main focus of the researchers has been the development of a composite material that possesses the desired properties that are not present in naturally found piezoelectric materials.

Quartz, tourmaline, sodium potassium tartrate, and Rochelle salt can be given as ex-

amples of naturally present crystals. Natural crystals are considered the most suitable piezoelectric materials for sensor applications because they are highly stable. Their highly stable properties provide a longer lifetime for the sensor used in the system. The low electromechanical coefficient of quartz causes it not to be preferred in applications where electromechanical energy conversion is essential. Because of their high piezoelectric voltage coefficient (g_h), lithium sulfate and tourmaline are two crystalline piezoelectric materials still used in commercial hydrophones. These crystals have also been used for shock and airflow measurements. Lithium niobate ($LiNbO_3$) and lithium tantalate ($LiTaO_3$) are preferred in high-temperature acoustic sensors due to their high sensitivity up to 4000 °C [34].

Ferroelectric materials can be defined as materials whose crystal structure has the ability to be instantly polarized under a high electric field ($\approx 10^6$ V/m). Ferroelectric materials are a type of piezoelectric materials, and the polarization of the crystal structure observed in piezoelectric materials under a high electric field is called the ferroelectric property. Quartz (SiO_2) and zinc oxide (ZnO) are piezoelectric materials, but they are not ferroelectric.

During World War II, Barium Titanate ($BaTiO_3$, BT), the most famous ceramic ferroelectric, was discovered independently by three countries, Japan, the USA, and Russia [35]. $BaTiO_3$ was actually the first commercialized ferroelectric and piezoelectric material [36].

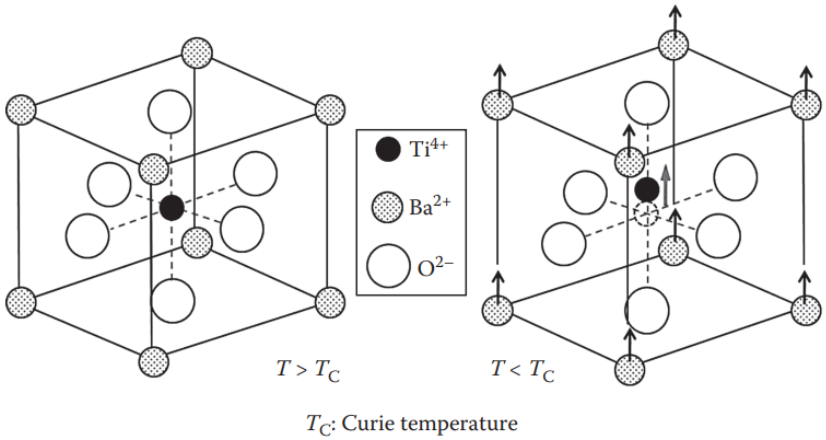

Figure 3.1: Crystal structure of Barium Titanate [37]

Common applications of the piezoelectric effect are based on ferroelectric ceramic

materials, and their advantages can be explained as [31]:

- Ferroelectric materials contain a high piezoelectric effect.
- Ceramics are easy to access and can be produced cost-effectively.
- Depending on the geometrical shaping and physical properties, ceramics offer a high degree of variation.

The piezoelectric effect has been used in many applications, such as in sonar applications, actuators, sensors, piezoelectric inkjet printing, as a clock generator in electronic devices, instrument pick-ups, and micro-robotics [31]. We also make use of the piezoelectric effect in our everyday lives, such as sparking to ignite gas cooking and heating devices, torches, and cigarette lighters. For example, quartz watches consist of a quartz crystal which is a piezoelectric material. Quartz crystal vibrates at one of its resonance frequencies, and time is measured more accurately compared to mechanical watches. Until today, Barium Titanate ($\mathrm{BaTiO_3}$) and Lead Zirconate Titanate (PZT) single or multi-component solid solutions have been mainly studied and used.

The solids in which the atoms are arranged in one pattern over the whole structure are called crystals or crystalline solids. Most piezoelectric materials are said to be crystalline solids and belong to a class of them. In crystallography, there are 32 crystal classes, 21 of which experience the piezoelectric effect [38]. For a material to be piezoelectric material, it must have an asymmetric crystal lattice structure or a non-centrosymmetric crystalline.

Crystal non-symmetry is what causes the piezoelectric effect. A perovskite structure is any crystal structure material that follows the formula $\mathrm{ABX_3}$. The perovskite structure is named after the mineral called perovskite, composed of calcium titanate $\mathrm{CaTiO_3}$. A typical unit cell for a piezoceramic has a non-symmetric perovskite structure as depicted in Figure 3.1, in which the negative and positive charges forming the unit cell have an asymmetry between them. A dipole is created due to this non-symmetry. This is valid for temperatures below the Curie temperature. If the piezoelectric material temperature goes beyond the Curie temperature, the crystalline struc-

ture loses its non-symmetricity and transforms into a cubic lattice. This is shown in Figure 3.2.

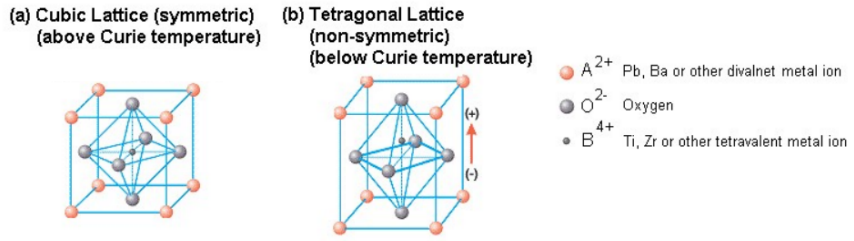

Figure 3.2: Schematics of a) Cubic and b) Tetragonal Lattices [39]

Deforming the material, and thus the crystal structure, changes the distance between the positive and negative charge sites (dipole) in each unit cell, resulting in a net total polarization in the crystal. This is the direct piezoelectric effect. However, in non-piezoelectric crystals, after the applied mechanical stress, despite the displacement in the crystal structure, the distribution of the charges preserves the symmetry, resulting in no net polarization [40]. In Table 3.1, the properties of some popular piezoelectric crystals are tabulated.

Table 3.1: Properties of some piezoelectric crystals at room temperature

Crystal Name	Chemical Formula	Max. piezoelectric coeff. (pC/N)	K_{11}^T	K_{33}^T	Ref
Barium Titanate	$BaTiO_3$	392 (d_{15})	2920	168	[41]
Lead Niobate	$PbNb_2O_6$	45 (d_{33})	–	180	[41]
Quartz	SiO_2	2.3 (d_{11})	4.6	4.7	[41]
Lithium Niobate	$LiNbO_3$	68 (d_{15})	84	30	[42], [43]
Lithium Tantalate	$LiTaO_3$	26 (d_{15})	51	45	[42], [43]
Rochelle Salt	$NaKC_4H_4O_6 \cdot 4H_2O$	2300 (d_{14})	1100	9.2	[41]
Sodium Chlorate	$NaClO_3$	1.7 (d_{14})	5.8		[41]
Tourmaline	$CaAl_3Mn_6(BO_3)_3(SiO_3)_6(OH)_4$	3.6 (d_{15})	8.2	7.5	[41]

When we look at the quartz (the chemical formula is SiO_2) crystal formation, as depicted in Figure 3.3, we see that the oxygen element has negative charges while the silicon element has a positive charge. If the material is under no electrical or mechanical loading, the centers of negative and positive charges overlap, resulting in a net zero dipole moment. However, when there is mechanical or electrical loading, the centers of positive and negative charges are displaced from each other, and a net

dipole moment is generated.

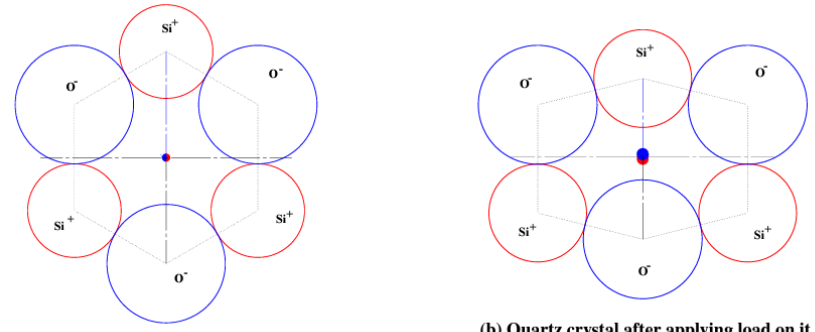

(a) Quartz crystal under no load condition

(b) Quartz crystal after applying load on it

Figure 3.3: Atomic structure of Quartz [44]

Likewise, these charge sites (dipole) extend or contract when they are subjected to an electric field. Whether it extends or contracts, the electric field applied dictates the direction of the straining. Since the crystalline structure is non-symmetric, the applied electric field will cause the positive and negative charges to shift, and this will deform the structure, and mechanical strain will occur. This is called the inverse piezoelectric effect.

Mechanical compressive or tensile stress applied on any piezoelectric ceramic material disrupts the dipole moment of the structure and generates voltage. Compressing the piezoelectric ceramic will cause a voltage generation with the same polarity as poling voltage. However, when pulling in the poling direction or pressing in the transverse direction of the poling direction, the piezoelectric ceramic generates a voltage with a polarity opposite that of the poling voltage, as shown in Figure 3.4c. Moreover, Steinkopff [45] stated that piezoelectric ceramics show a low degree of mechanical tension/compression asymmetry which means that the application of either tension or compression force causes similar force-displacement curves and thus similar values of electric potential.

When the voltage applied to the ceramic in the poling direction has the same polarity as the polarization voltage, the ceramic element elongates, and its diameter decreases (Figure 3.4d). When a voltage with the opposite polarity of the poling voltage is applied, the ceramic element shortens in length and expands from the diameter (Figure 3.4e).

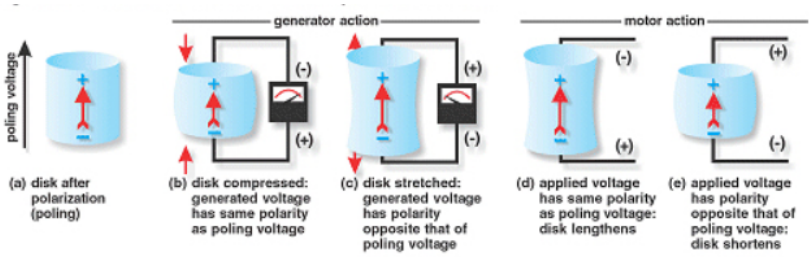

Figure 3.4: Direct and inverse piezoelectric effect. [46]

Piezoceramic materials are aggregates of tiny piezo crystallites. Since usually the dipoles are oriented randomly in the material, movements of these dipoles in response to the applied external electric field will cancel out each other and will yield the net polarization as zero at the macro scale. The dipoles must be aligned to obtain a net polarization, i.e., piezoelectric behavior at the macro scale. The process that makes it happen is called poling.

Piezoelectric composites, or piezocomposites, have been developed in order to improve the properties of pure (monolithic) piezoelectric materials, for instance, lead zirconate titanate (PZT). They can meet the requirements for applications such as underwater sonar, acoustic transducers, medical diagnosis, and non-destructive material evaluation [47]. Piezocomposites usually consist of two phases, one of which is a piezoelectrically active material, and the other is a piezoelectrically passive phase, generally a polymer or air. Piezocomposites are usually described with two numbers beside their names, which designates the architecture of piezoelectric composites [48]. These numbers express how the piezoelectric and polymer phases are interconnected. For instance, a '0–3' piezocomposite implies a piezocomposite whose piezoelectric phase is just some particles distributed in a polymer matrix. Here "0" refers to piezoelectric particles, and "3" refers to a continuous polymer matrix in all directions. Similarly, the '1–3' numbering represents piezoelectric rods embedded in a polymer matrix.

The piezoelectric material's polarization axis is usually considered as x_3 or Z-axis as a convention. This convention will be used in this study.

3.1 Fabrication

As a first step, the piezoceramic should be prepared. In order to prepare a piezoelectric ceramic material, fine powdered metal oxide powders are mixed in specific ratios and then heated up in order to obtain a homogeneous powder mixture. By adding an organic binder to the obtained powder, it can be converted into structural elements in various shapes such as disc, wire, bar, plate, or can be stored as a powder. Piezoceramics, which have been given various forms, are fired by applying for firing programs within certain periods. This firing process is called sintering, and its main purpose is to transform the powder particles into a dense crystalline structure that binds them together. After these processes, the substances are allowed to cool and, if necessary, they are cut to the desired dimensions, or the rough surfaces are smoothened [46].

The 1-3 connectivity configuration is quite ideal for the extrusion process. Piezoceramic rods have to be sintered up to almost their theoretical density (7900 kgm^3); afterward poling process can be applied. For general piezocomposite transducer applications, the rods are manufactured by extrusion of a PZT-organic binder slip [49]. While manufacturing, to align the piezoceramic rods, two fixtures with dozens of holes are used. These fixtures with holes are manufactured according to the pattern and volume fraction of the piezocomposite rods. For instance, a high volume fraction requires dense or larger holes. When the piezoceramics rods are placed into the fixtures, the system is put in a plastic tube filled with epoxy resin [49]. With this process, piezoceramic rods and polymer coalesce, and the excess epoxy is trimmed off.

Lastly, if the piezoceramic rods are not pre-poled, electrodes are applied to the piezocomposite, and the system is poled in a hot oil bath for a couple of minutes under a high electric field.

3.2 Poling

Every piezoelectric material has a Curie temperature, where the material loses its permanent magnetic properties. Below that temperature, the material shows no polarization because the dipoles in the crystal structure are aligned randomly, and the local

polarizations cancel each other. For the piezoelectric material to gain a net polarization, the dipoles must be aligned in one direction. For this purpose, the piezoelectric material is heated above Curie temperature. Thereupon the dipoles can change orientation. A strong electric field is then applied to orient the dipoles in the electric field direction. Heating the material above Curie temperature and applying a strong electric field is called the poling process. While maintaining the electric field present and active, the material is cooled down to under its Curie temperature so that the dipoles can no longer change their orientation. Therefore, the dipoles are oriented permanently, and the material has gained a net polarization. The material that went through the poling process is said to be poled. A schematic that illustrates the poling process is shown in Figure 3.5.

In practice, the Curie temperature changes from material to material. For example, pure $\mathrm{BaTiO_3}$ has a Curie temperature of 123 °C [50], [51], whereas PZT5-H has a Curie temperature of 230 °C [52]. An applied electric field can also have various values depending on the material types and their composition. For example, it varies from 0.1 kV/mm to 4 kV/mm for BZT–BCT ceramics [53].

During the process of poling, a high electric field is created by applying a DC voltage on the material with the help of electrodes placed on the surfaces of the material, and the dipoles are directed parallel to this electric field. During poling, the regions become anisotropic because the dipoles become aligned in the direction of the electric field that is applied. After polarization, a few regions can distort from the polarization direction, but the polarization is permanent in the majority. Thus, the pre-polarization material is isotropic and does not exhibit piezoelectric behavior, but at the end of the polarization, the dipoles are oriented towards the axis with the electric field, and a net electrical dipole moment is formed in the whole structure consisting of polycrystals.

The piezoelectric, elastic, and dielectric properties of ceramics that are poled depend on temperature highly. Thus, heating the material beyond the Curie point kills poling effect because the dipoles will return to be oriented randomly and causes the piezoelectric properties to vanish [55]. For high-temperature applications, piezoceramics with high Curie temperatures are strongly desired. Also, applying a very high electric field can distort the dipoles from their alignment and again end the polarization. In

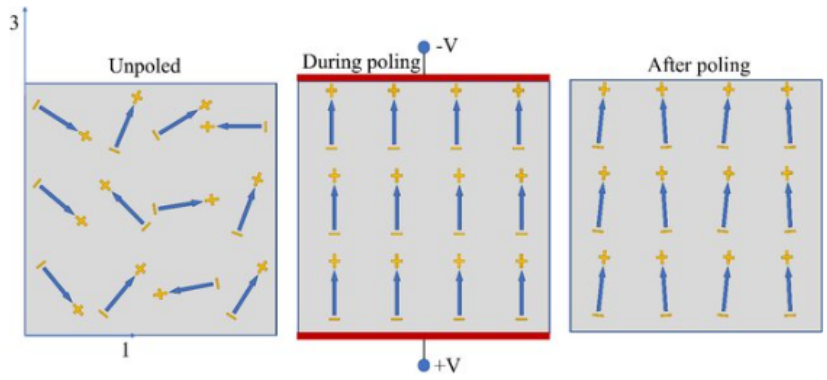

Figure 3.5: Depiction of poling process under an applied electric field [54]

this study, we always assume that the piezoelectric materials are fully poled.

3.3 Properties of Piezoelectric Materials

There are both ceramics and polymers that show piezoelectric effects. Piezoceramics' elastic modulus can vary from 10 GPa to 120 GPa, while piezoelectric polymers can only have elastic moduli of 1-3 GPa [56]. Similar to elastic modulus, dielectric and piezoelectric coefficients of piezoceramics are very high compared to piezopolymers.

3.4 Piezoceramics

One of the, if not the most, frequently used piezoceramic is lead zirconate titanate (PZT), whose chemical formula is $\mathrm{Pb[Zr_xTi_{1-x}]O_3}$ ($0 \leq x \leq 1$). PZT is a ceramic perovskite material because its crystal structure follows the $\mathrm{ABX_3}$ formula, just like barium titanate ($\mathrm{BaTiO_3}$). Great piezoelectric sensitivity, availability and relatively high operating temperatures help PZT ceramic excel among the other piezoceramics and make it the most widely used piezoceramic.

There are different PZT variations. For example, One of the commonly studied chemical compositions is $\mathrm{PbZr_{0.52}Ti_{0.48}O_3}$. Piezoceramics vary according to their hardness. As given in Table 3.2, the properties and characteristics of hard, semi-hard, and soft PZT ceramics are very different.

Table 3.2: Properties of PZT Ceramics Groups [57], [46]

Property	Soft PZT	Semi-hard PZT	Hard PZT
Electromechanical Coupling	High	Medium	Low
Permittivity	High	Medium	Low
Compliance	High	Medium	Low
Density	Low	Medium	Hard
$\mathrm{T_c}$	Low	Medium	Hard
Polarization	Easier	Medium	Harder

Lead titanate ($\mathrm{PbTiO_3}$ or PT) and lead zirconate titanate (PZT) and their variations are known to be toxic piezoelectric materials because they contain lead. They damage the skin, mucous membranes, eyes, and cause harm to unborn babies, and are thought to negatively affect fertility [58]. Therefore, for biological purposes, non-toxic piezoelectric materials, such as $\mathrm{BaTiO_3}$, are used. Properties of common piezoelectric ceramics, which are studied and used in industry, are shown in Table 3.3.

Table 3.3: Properties of common piezoelectric ceramics

Chemical Formula	$\mathrm{T_c}$ (°C)	d_{33} (pC/N)	d_{31} (pC/N)	K_{33}^T	Ref
$\mathrm{BaTiO_3}$	115	190	-78	1700	[41]
$\mathrm{PbTiO_3}$	470	56	–	190	[59]
PZT-5A	365	374	-171	1700	[60]
PZT-5H	195	593	-274	3400	[60]
PZT-7A	350	153	-60	425	[60]
PZT-8	300	225	-97	1000	[60]

European Community started to implement some restrictions on the use of deleterious materials in 2006, which certainly cut the usage of lead (Pb) [37]. Some further restrictions may come in the near future, so the popularity of lead-free piezoelectric ceramics will like to increase.

3.5 Piezopolymers

Many piezoelectric polymers are fluorocarbon-based polymers. Among these polymers, Polyvinylidene difluoride (PVDF) is known as the most studied piezoelectric

polymer. Unlike piezoceramics, PVDF does not have a high piezoelectric strain coefficient, d, but due to its small permittivity, PVDF has a high piezoelectric voltage coefficient, g, making it suitable for sensor applications. A strong piezoelectric effect in PVDF compared to other polymers was discovered in Japan in 1969, and it was observed that the piezoelectric coefficient of its poled thin film could be around 6-7 pC/N [61]. Although polymer piezoelectric materials like PVDF are suited for sensor applications, they are not suited for being an actuator or high-power transducers due to their very small piezoelectric constants and stiffness compared to piezoceramics [1]. For such applications in which piezoelectric polymers fall short, piezocomposites have resorted.

PVDF has a highly crystalline structure; the crystallinity in the structure varies between 50% and 70%. This variation is due to three different phase states called α, β, γ. α and β phases are shown in Figure 3.6. Conversion between these three structures can be accomplished using various chemical and physical techniques. Since there are dipoles perpendicular to the axis of the molecule in the β and γ forms, the material possesses a net polarization and shows a piezoelectric effect. The β phase of PVDF shows the strongest piezoelectricity [62]. Besides PVDF, trifluoro ethylene copolymer poly(vinylidene fluoride-co-trifluoro ethylene) (PVDF-TrFE) has also been studied in the past.

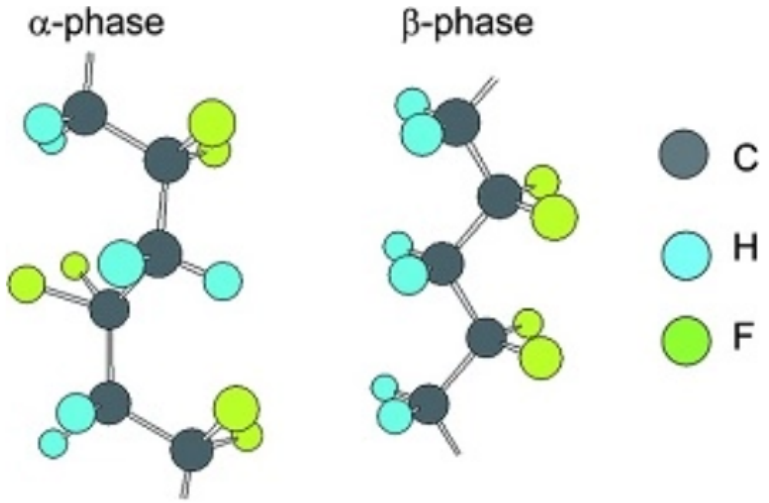

Figure 3.6: Alpha-phase and Beta-phase structure of PVDF [63]

3.6 Doping

Piezoelectric materials' properties can also be improved by adding doping agents called dopants. Dopants are impurities introduced to materials and can change their electrical or optical characteristics. Introducing dopants to PZT can significantly alter its properties [34]. Dopants can be either donors or acceptors.

We can group piezoelectric ceramics into three groups: soft, semi-hard and hard. This grouping was made by considering the compositions and properties of piezoelectric ceramics. Soft ceramics have donor dopants, whereas hard ceramics have acceptor dopants.

Donor dopants create cation (metal) vacancies in the structures of the crystals, resulting in an enhancement in domain reorientation and piezoelectric coefficients. The product of donor dopants is called soft PZTs. Those called 5A and 5H can be examples of soft PZTs. They, in the end, have high piezoelectric coefficients, high electromechanical coupling factors, high permittivity, low coercive field, and low mechanical quality factors [64]. PZT-5A is known for applications of varying and high temperatures. On the other hand, PZT-5H is known to have better piezoelectric properties, but it has a modest Curie temperature, so it has a limited temperature range.

Conversely, acceptor dopants result in oxygen vacancies that attach to the domain walls, inhibiting the dipoles from aligning with the spontaneous polarization inside the domain. That yields hard PZTs, like those designated with 4 and 8 [65]. A hard PZT has characteristics of low piezoelectric properties, low permittivity, high $\mathrm{Q_m}$, and a high coercive field [66].

PZT-based piezoelectric materials show different properties according to their composition ratios. PZT-4, PZT-5, PZT-6, and PZT-7 are generally referred to as PZTs doped with Fe, Nb, Cr, and La, respectively [42]. Properties of different PZT types are shown in Table 3.4.

Table 3.4: Properties of PZT Ceramics

Designation	T_c (°C)	d_{33} (pC/N)	d_{31} (pC/N)	K_{33}^T	Ref
PZT-2	370	152	-60	450	[41]
PZT-4	325	285	-122	1300	[60]
PZT-5A	365	374	-171	1700	[60]
PZT-5H	195	593	-274	3400	[60]
PZT-7A	350	153	-60	425	[60]
PZT-8	300	225	-97	1000	[60]

3.7 Piezocomposites

While designing piezocomposites, it is desired that the best properties of the composite constituents are utilized, and the constituent should cover the weakness of the other constituent. For example, piezoelectric polymer PVDF is good for sensor application due to its high piezoelectric voltage constant, g but, terrible for actuator applications due to its small piezoelectric strain constant, d. On the other hand, piezoelectric ceramic PZT is the opposite, good for actuator applications but bad for sensor applications. However, a piezocomposite made of PZT and polymer has a d value close to PZT and a g value close to PVDF, exhibiting a wide range of piezoelectric responses. Thus, for applications like underwater, in which both actuation and sensing are performed, piezocomposites are considered to be way too better compared to single materials [1].

Table 3.5: Comparison of the Piezoelectric Properties of PZT-Polymer Composites with PVDF and PZT [1]

Connectivity	Material(s)	Density, ρ $(10^{-3}\mathrm{kg/m^{-3}})$	Elas. Coeff., C_{33} (GPa)	Dielectric, ε_3	d_{33} (pC/N)	g_{33} $(10^{-3}mV/N)$	g_h $(10^{-3}mV/N)$
-	Extended PVDF	1.8	3	13	20	160	80
-	PZT(501A)	7.9	81	2000	400	20	3
3-1	PZT - Epoxy	3.0	19	400	300	75	40
3-3	PZT - Silicone (Replica type)	3.3	3	40	110	280	80
3-0	PZT - PVDF	5.5	2.6	120	90	85	-
3-0	PZT - Rubber	6.2	0.08	73	52	140	30

In Table 3.5, particular material and piezoelectric coefficients of Extended PVDF, PZT(501A), and some other PZT-Polymer piezocomposites are compared to see which material is better in which coefficients. Each coefficient actually represents the relevance to a specific application, which will be explained in the next section called Section 3.11. As can be seen from Table 3.5, piezoceramic PZT(501A) has the highest density and dielectric permittivity ε, but this advantage comes at the expense of its piezoelectric voltage coefficients, g_{33} and g_{h}. Extended PVDF offers the lowest density and good piezoelectric voltage coefficients but has very low stiffness and piezoelectric strain coefficient d_{33}. Piezocomposites, on the other hand, offer moderate to high values of coefficients, depending on the constituents and the purpose of the piezocomposite.

3.8 Piezocomposite Design

The major aim in designing a piezocomposite is to maximize its electromechanical energy conversion to give greater responsibility for a unit input. The performance of the piezocomposite can be improved by increasing the volume fraction of the piezoelectric phase, changing the shapes and connections of the inclusions, or using a material with higher piezoelectric coupling properties. However, there are other requirements or constraints, such as stiffness/compliance, flexibility, and weight. The objective in the design of a piezocomposite is to obtain a material that satisfies the requirements and has high properties that are not present in conventional materials.

It is desired that the transducers should have properties such as low-density, large piezoelectric coefficient, compliant and flexible. In applications where piezoelectric materials are used as actuators, piezoelectric materials are usually in the shape of shell patches. Furthermore, there are electrodes on both surfaces that are parallel to the structure to which it is bonded, and the poling axis is usually normal to the patch or structure surface. In such applications, a small electric field applied during the operation will cause the PZT patch to elongate or contract. Since the PZT patch is bonded to the structure perfectly, the structure will bend in the direction of contraction.

A well-design composite should make maximal use of the desired properties of each phase. For that purpose, people usually design a composite that consists of a PZT ceramic and a polymer. PZT ceramic is a must to have because of its high electromechanical coupling factor and high piezoelectric coefficient. Polymer, on the other hand, is useful to increase the elastic compliance and flexibility of the composite and reduce the permittivity (to obtain high g) and density. With the desired properties of each phase, a piezocomposite with high electromechanical coupling capability and yet flexibility can be obtained.

3.9 Product Properties

It is also very interesting to see that, sometimes, apart from the properties of the phases of composite, there become completely new properties (product properties) that are not present in the phases alone.

Assume that applying X to the composite causes a change in Y in phase 1, and a change in Y causes a change in Z in phase 2. If not for the combination of phase 1 and phase 2, the resultant change in quantity Z, would never happen. This new function, which relates input X to output Z is a new product property that the phases as individuals cannot possess. The product effect can be shown in Figure 3.7a. Piezocomposites can show such a product property. The transfer of the quantity Y from 1 to 2 can be accomplished by several different kinds of coupling [49].

Furthermore, sometimes phase 1 or phase 2 alone generates an output less than any combination of phases 1 and 2. This is called the combination effect, as depicted in Figure 3.7b, and it can be seen in certain piezocomposites. Piezoelectric voltage coefficient, g is an example of the combination effect [1].

3.10 Connectivity

Connectivity is one of the most critical subjects in composites. Consider what would happen if the columns of a building were connected in series rather than parallel. In designing a piezoelectric composite, the connectivity of the phases is very important

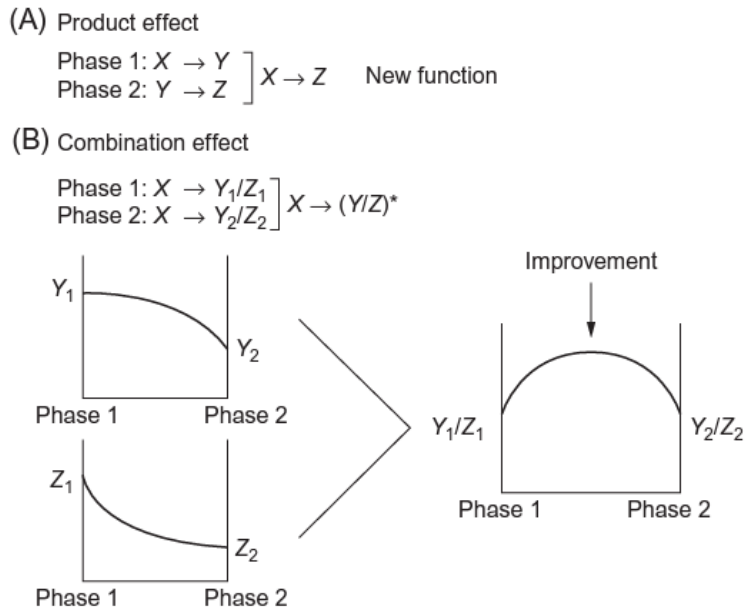

Figure 3.7: a) Product Effect and b) Combination Effect [1]

to care for because connectivity controls the pattern of the electric flux in the material. Of course, it changes mechanical properties as well.

Newnham et al. [48] were the first to introduce the concept of connectivity for piezocomposites that are made of PZT and polymer phases. Since there are three perpendicular axes in nature, a phase can be interconnected in at most three directions and at least zero directions. Therefore, it can have a connection type of 0, 1, 2, or 3. Speaking of diphasic composites, which have two single phases as constituents, the connection type of the composite can be indicated, in general, in ten different configurations, such as 0-0, 0-1, 0-2, 0-3, 1-1, 1-2, 1-3, 2-2, 2-3, 3-3. These combinations are shown in Figure 3.8, in which shaded regions refer to first connectivity number. The first number is used for the connectivity of the active phase, and the second number is used for the connectivity the passive phase. For example, in a 1-3 connectivity pattern, the passive phase is connected in all three directions, whereas the active phase is connected only in one direction. Not surprisingly, usually, shell structures have a connection type of 2, and beam structures have a connection type of 1 if they are not placed perpendicularly interconnected to themselves.

Among all the piezoelectric composite configurations, 1-3 piezocomposites are found

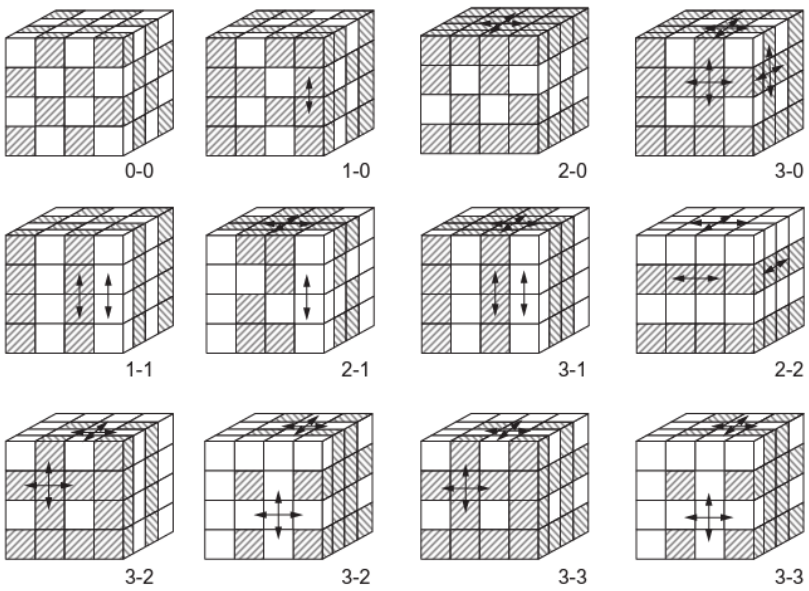

Figure 3.8: Connectivity Patterns of Two-Phase Composites [1]

the most useful and thus have been the focus mostly, although there are studies interested in other important configurations, namely 2-2, 3-3, 0-3. For example, 1-3 and 2-2 piezocomposites are shown in Figure 3.9.

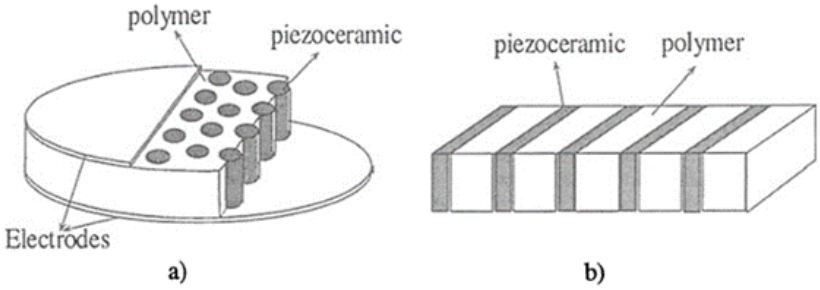

Figure 3.9: a) 1-3 Piezocomposites and b) 2-2 Piezocomposites [67]

For other applications, there might be a need for more phases in a composite. Furthermore, the more phases are present, the more different patterns there can be. For example, there can be 20 three-phase and 35 four-phase connectivity configurations. For n phases, the formula for this is (n+3)!/(3!n!) [49].

3.11 Performance of Piezocomposites

In nature, unfortunately, the desired property coefficients come with undesired ones. For example, piezoelectric ceramics have high piezoelectric coefficients, but they are brittle and lack the flexibility that a transducer needs. On the other hand, polymers can meet the desired mechanical requirements, but they have very little or no piezoelectric effect. Thus, the figures of merit are a concept of trade-off, some of them are high, and some of them are low, depending on the requirements.

Hydrostatic piezoelectric coefficients are the key parameters of the piezocomposites that are as using as hydrostatic transducer materials. They define how effective, and suitable the piezocomposites are for their specific use.

For example, Bennett and Hayward concluded that the best hydrostatic performance of a 1-3 piezoelectric composite is acquired with the piezocomposite that has a low volume fraction of PZT-5H and stiffener plates [6]. Having not too hard a piezoceramic phase and compliant polymer phase helped them to obtain this result. Also, they noted that the polymer phase should have a Poisson's ratio as low as possible [6].

It also should be noted that in design and practice, one should generally stay within the limits of linear response of piezoelectric ceramic in order for the piezoceramic to give a response in proportion to the higher force level [8].

Bennett and Hayward discovered that polymers should have high elastic compliance and low Poisson's ratio. Although these two conditions may be opposing for viscoelastic materials, the results indicated that the effect of Poisson's ratio on hydrostatic performance is significant [6].

Suppose the piezoelectric material is to be used as a hydrophone to detect signals lower than 100 kHz. In that case, the acoustic wavelength dimension will be greater than the hydrophone's, and the stress on the piezocomposite due to the acoustic wave will be hydrostatic [68]. Under such conditions, passive hydrophone sensitivity is specified by the hydrostatic voltage coefficient, g_h [17].

While calculating figures of merit that measure the performance of the piezocompos-

ite, the effects of inertia are neglected; only the constitutive properties are considered in calculations [67].

Since piezoelectric ceramics are not isotropic, the material coefficients depend on the directions of the applied mechanical or electrical force. Therefore, each coefficient has two subscripts to indicate the directions of the two related quantities. Of course, some notations are shown briefly with a single number, thanks to the Voigt notation. The positive polarization direction is specified by the direction Z or 3 in the XYZ or 123 coordinate systems, respectively.

3.11.1 Elastic Compliance

Compliance, the inverse of the stiffness, is the strain that the material observes for unit stress applied. Instead of stiffness, compliance terms are usually used for calculating the figures of merit of piezoelectric materials. $\boldsymbol{s^D}$ is the compliance under constant electrical displacement and, $\boldsymbol{s^E}$ is the compliance under constant electric field. The first subscripts of $\boldsymbol{s^D}$ and $\boldsymbol{s^E}$ indicate the direction of strain, and the second subscripts indicate the direction of stress.

s_{11}^E is the compliance in direction 1 (perpendicular to poling axis) under a constant electric field which means a short circuit. s_{33}^D is the compliance in direction 3 (parallel to poling axis) under constant electrical displacement which means an open circuit.

3.11.2 Permittivity (Dielectric Constant)

Permittivity or dielectric constant, ε, is a material property and, it is the induced dielectric displacement in response to per unit of an electric field. Permittivity also means how much charge a material can store. $\boldsymbol{\varepsilon^S}$ implies the dielectric constant under constant strain, whereas $\boldsymbol{\varepsilon^T}$ implies the dielectric constant under constant stress. The first and the second subindices of ε represent the direction of the dielectric displacement, and the electric field, respectively.

On the other hand, sometimes, the relative dielectric constant is also used and shown by $\boldsymbol{k}$ or $\boldsymbol{K}$. As given in (3.1), it is the ratio of the material permittivity to the absolute

dielectric constant, ε_0, which simply is the amount of charge that the electrodes in a vacuum can store up. It can be said that it is the capability of an electric field to permeate a vacuum. ε_0 is $8.854\text{x}10^{-12}$ farads/meter.

$$\boldsymbol{K^T} = \frac{\boldsymbol{\varepsilon^T}}{\varepsilon_0} \tag{3.1}$$

Depending on the indices $\boldsymbol{\varepsilon}$ takes, different meanings can be understood.

- ε_{11}^T is the permittivity or the polarization in direction 1 (perpendicular to poling axis) in response to an applied electric field in direction 1 under constant stress
- ε_{33}^S is the permittivity or the polarization in direction 3 (parallel to poling axis) in response to an applied electric field in direction 3 under constant strain.

3.11.3 Density

The density of a piezoelectric composite is very critical due to the fact that there might be some weight restrictions depending on the application. Moreover, density affects acoustic impedance matching to the loading. Density differences between the piezocomposite used as a transducer and the surrounding environment, such as water or human tissue, cause a mismatch in their acoustic impedances, causing some waves to reflect off the interface. Therefore, it is crucial to reduce the transducer's density to a value close to that of the surrounding environment to minimize the losses [49]. Whilst densities of piezoceramics vary from 7000 $\mathrm{kg/m^3}$ to 8000 $\mathrm{kg/m^3}$, those of piezoelectric polymers vary from 1000 $\mathrm{kg/m^3}$ to 2000 $\mathrm{kg/m^3}$ [56].

The density of the composite will be between those of its constituents. Therefore can be adjusted depending on the volume fractions. Since PZT has a density of 7900 $\mathrm{kg/m^3}$ and epoxy has a density of 1100 $\mathrm{kg/m^3}$, the density of the composite can have a value near that of epoxy for low PZT volume fractions. That would also make the difference between the densities of the composite and the medium smaller, resulting in a greater acoustic impedance matching capability.

3.11.4 Piezoelectric strain coefficient (d)

The piezoelectric strain constant, designated by $\boldsymbol{d}$, can be defined as the resulting polarization/electric displacement in response to an applied unit mechanical stress ($\boldsymbol{T}$) or the resulting mechanical strain ($\boldsymbol{S}$) in response to an applied unit electric field.

$$\boldsymbol{d} = (\partial \boldsymbol{S}/\partial \boldsymbol{E})_T = (\partial \boldsymbol{D}/\partial \boldsymbol{T})_E \tag{3.2}$$

The first subindex of the piezoelectric charge constant indicates the polarization direction or the direction of the applied electric field. The second subindex of the piezoelectric charge constant indicates the direction of the mechanical stress applied or the resulting mechanical strain. The piezoelectric strain coefficient, $\boldsymbol{d}$ is a very prominent indicator for actuator applications.

Since strain is the product of the piezoelectric charge coefficient and applied electric field, the piezoelectric charge coefficient is a vital coefficient that tests the suitability of the material for strain-dependent actuator application.

Some important piezoelectric coefficients express particular situations:

- d_{31} is the induced polarization (electric displacement) in direction 3 (parallel to poling direction) in response to the applied unit stress in direction 1 (perpendicular to poling direction) or induced strain in direction 1 in response to an applied unit electric field in direction 3.

$$d_{31} = (\partial D_3/\partial T_1)_E = (\partial S_1/\partial E_3)_T \tag{3.3}$$

- d_{33} is the induced polarization (electric displacement) in direction 3 in response to the applied unit stress in direction 3 or induced strain in direction 3 in response to the applied unit electric field in direction 3.

$$d_{33} = (\partial D_3/\partial T_3)_E = (\partial S_3/\partial E_3)_T \tag{3.4}$$

- d_{15} is the induced polarization (electric displacement) in direction 1 in response to the applied unit shear stress in plane 13 or induced shear strain in plane 13

in response to the applied unit electric field in direction 1.

$$d_{15} = (\partial D_1/\partial T_{13})_E = (\partial S_{13}/\partial E_1)_T \tag{3.5}$$

Large $\boldsymbol{d}$ coefficients are desirable in piezoelectric driver applications such as ultrasonic cleaners and sonar.

3.11.5 Hydrostatic strain constant (d_h)

Hydrostatic strain constant or coefficient d_h can be seen as a factor determining the material's performance for active transducer applications. Similar to the piezoelectric strain coefficient, $\boldsymbol{d}$, the hydrostatic strain constant is the resulting hydrostatic strain for a unit electric field (m/V) or the charge induced for a unit hydrostatic force (C/N), see (3.6).

$$\begin{aligned} d_h &= d_{31} + d_{32} + d_{33} \\ &= 2d_{31} + d_{33} \end{aligned} \tag{3.6}$$

3.11.6 Piezoelectric voltage coefficient (g)

The piezoelectric voltage constant, $\boldsymbol{g}$, is the electric field created by the piezoelectric material as a result of the applied unit mechanical stress or the mechanical strain created by the piezoelectric material as a result of the applied unit electrical displacement. The first subindex of the piezoelectric voltage constant indicates the direction of the electric displacement and electric field. The second subscript specifies the direction of the mechanical stress or strain being applied. Since the product of the applied stress and the piezoelectric voltage constant is the strength of the electric field created in a piezoelectric material in response to applied mechanical stress, the piezoelectric voltage constant has a significant role in determining whether the material used for sensor applications is correct.

The piezoelectric voltage constant, $\boldsymbol{g}$ is a highly significant indicator for sensing applications.

$$\boldsymbol{g} = \frac{\boldsymbol{d}}{\boldsymbol{\varepsilon^T}} \tag{3.7}$$

$$\boldsymbol{g} = (-\partial \boldsymbol{E}/\partial \boldsymbol{T})_D = (\partial \boldsymbol{S}/\partial \boldsymbol{D})_T \tag{3.8}$$

Some important piezoelectric voltage coefficients express particular situations:

- g_{31} is the electric field generated in direction 3 (parallel to poling direction) in response to applied unit stress in direction 1 (perpendicular to poling direction) or the resulting strain in direction 1 in response to applied unit electric displacement in direction 3.

- g_{33} is the electric field generated in direction 3 in response to applied unit stress in direction 3 or the resulting strain in direction 3 in response to applied unit electric displacement in direction 3.

- g_{15} is the electric field generated in direction 1 in response to applied unit shear stress in plane 13 or the resulting shear strain in plane 13 in response to applied unit electric displacement in direction 1.

3.11.7 Hydrostatic piezoelectric voltage constant (g_h)

Hydrostatic piezoelectric voltage constant or coefficient is a factor that measures the passive hydrophone sensitivity. It is an electric field generated for a unit of hydrostatic stress (V/mPa), see (3.9).

$$g_h = 2g_{31} + g_{33} = \frac{d_h}{\varepsilon_{33}^T} \tag{3.9}$$

Since for high hydrostatic voltage coefficients, high values of d_h and low permittivity are needed, piezocomposites with small volume fractions of piezoceramics and high values of d_h have substantially high hydrostatic voltage coefficients.

3.11.8 Hydrostatic figure of merit ($d_h g_h$)

The hydrostatic figure of merit, the product of d_h and g_h, designates the piezodevice both as a hydrophone and an actuator (active-passive transducer) and specifies the signal-to-noise ratio [69], [70].

$$HFOM = d_h g_h \tag{3.10}$$

3.11.9 Hydrostatic Compliance (s_h)

Hydrostatic compliance is the elastic compliance that material shows under hydrostatic loads. It can be obtained as follows:

$$s_h^E = s_{11}^E + s_{22}^E + s_{33}^E + 2s_{12}^E + 2s_{13}^E + 2s_{23}^E \tag{3.11}$$

However, since piezoelectric ceramics are mostly transversely isotropic, (3.11) can be reduced to:

$$s_h^E = 2s_{11}^E + s_{33}^E + 2s_{12}^E + 4s_{13}^E \tag{3.12}$$

3.11.10 Hydrostatic Coupling Coefficient (k_h)

The hydrostatic coupling coefficient is the factor that indicates the effectiveness of the conversion between the mechanical and electrical energies for hydrostatic applications. It can be obtained as follows:

$$k_h = \left(\frac{d_h}{\varepsilon_{33}^T s_h^E} \right)^{1/2} = \left(\frac{d_h g_h}{s_h^E} \right)^{1/2} \tag{3.13}$$

3.11.11 Electromechanical Coupling Factor (k)

The electromechanical coupling factor, k, indicates how effective the conversion is between the mechanical and the electrical energies. It measures what fraction of the electrical energy is converted to mechanical energy when an electric field is applied. Vice versa also applies. The first subindex of the electromechanical couple factor indicates the direction the electrodes lie (or the electric field), and the second subindex indicates the direction of the mechanical reaction (e.g. vibration).

$$k^2 = \frac{Output\ mechanical\ energy}{Input\ electrical\ energy} \tag{3.14}$$

Electromechanical coupling factor values in the catalogs of piezoelectric ceramic manufacturers are the theoretical maximum values. A typical piezoelectric ceramic can convert only 30-75% of the energy sent in any form to other energy forms at low input frequencies, depending on its composition and the direction of the applied forces [46]. As expected, the desired thing is usually high electromechanical coupling factor values, and in good designs of piezoelectric systems, this efficiency can reach up to 90% [46].

The electromechanical coupling factor can have various subscripts. For example:

- k_{31} is the coupling factor for the electric field in direction 3 and the mechanical strain (or stress) in direction 1. It is used for piezoceramic plates.

$$k_{31} = \left(\frac{d_{31}}{\varepsilon_{33}^T s_{11}^E} \right)^{1/2} \tag{3.15}$$

- k_{33} is the coupling factor for the electric field in direction 3 and the mechanical strain (or stress) in direction 3. It is used for piezoceramic rods.

$$k_{33} = \left(\frac{d_{33}}{\varepsilon_{33}^T s_{33}^E} \right)^{1/2} \tag{3.16}$$

- k_t, thickness coupling factor, is very similar to k_{33}, but it is used for materials like a disc or a plate whose surface areas are larger than their third dimension, that is, thickness.

Please note that these expressions stated above are valid for low frequency or static cases.

CHAPTER 4

METHODOLOGY

This chapter includes piezoelectricity theory and the methodology used in the study. The piezoelectric constitutive equations are shared and explained, assumptions made through the analysis process are stated, and computational techniques, such as the homogenization method and RVE concept, are introduced.

4.1 Piezoelectric Constitutive Equations

As explained in the previous chapter, piezoelectric materials can respond to both mechanical and electrical changes. Moreover, this interchangeable behavior happens almost linearly, meaning that the coupling between the mechanical action and the electrical reaction can be considered linear. However, this is true under the application of low electric field or low mechanical stress, which is the interest of this thesis [71]. Under high levels of an electric field or mechanical stress, the piezoelectric materials start to show non-linearity and this is due to the polarization switching taking place in the grain domains [72].

The constitutive equations representing the linear piezoelectric coupling behavior are

$$\begin{aligned} T_{ij} &= C^{E}_{ijkl} S_{kl} - e_{kij} E_k, \\ D_i &= e_{ikl} S_{kl} + \varepsilon^{S}_{ik} E_k \end{aligned} \tag{4.1}$$

where $\boldsymbol{T}$ and $\boldsymbol{S}$ are stress and strain tensors, respectively. $\boldsymbol{E}$ and $\boldsymbol{D}$ are the electric field and the electric displacement vectors, respectively. $\boldsymbol{C^E}$ is the fourth-order elasticity tensor at a constant electric field, $\boldsymbol{\varepsilon^S}$ is the second-order dielectric tensor at a

constant strain field, and $\boldsymbol{e}$ is the third-order piezoelectric coupling tensor.

These piezoelectric constitutive equations come from the energy framework and energy conservation equations. The amount of work done on the piezoelectric material is due to an external force applied, electrical work done, or heat entering in. Furthermore, the linear piezoelectric constitutive equations are derived by integrating the differential Gibbs free energy relation [71].

$$\begin{aligned} G &= U - T_{ij}S_{ij} - E_n D_n, \\ dG &= dU - T_{ij}dS_{ij} - S_{ij}dT_{ij} - E_n dD_n - D_n dE_n \end{aligned} \tag{4.2}$$

In 4.2, G and U represent Gibbs free energy and internal energy, respectively. By choosing our independent and dependent variables and taking the derivative of Equation 4.2 with respect to the independent variables, we can get a unique set of constitutive equations. For example, choosing $(\boldsymbol{S}, \boldsymbol{D})$ as independent variables leads to Equation 4.3, whereas choosing $(\boldsymbol{T}, \boldsymbol{E})$ as independent variables can yield such a relation as in Equation 4.4.

$$\begin{aligned} T_{ij} &= C^D_{ijkl}S_{kl} - h_{kij}D_k, \\ E_i &= -h_{ikl}S_{kl} + \beta^S_{ik}D_k \end{aligned} \tag{4.3}$$

$$\begin{aligned} S_{ij} &= s^E_{ijkl}T_{kl} + d_{kij}E_k, \\ D_i &= d_{ikl}T_{kl} + \varepsilon^T_{ik}E_k \end{aligned} \tag{4.4}$$

Each type of constitutive equation might have advantages and disadvantages over the other. For instance, for transducer design, stress $\boldsymbol{T}$ and electric field $\boldsymbol{E}$ are reasonable to choose as independent input variables. Depending on the interest of output variables, any type of piezoelectric constitutive equation set might be selected.

In our study, we preferred to use $(\boldsymbol{S}, \boldsymbol{E})$ as independent variables, but we could have used other combinations such as $(\boldsymbol{S}, \boldsymbol{D})$ or $(\boldsymbol{T}, \boldsymbol{D})$. They are also doable in ABAQUS. For $(\boldsymbol{S}, \boldsymbol{E})$ variable combination, displacement and electric potential boundary conditions are applied, whereas stress and electrical charge loadings should be applied for $(\boldsymbol{T}, \boldsymbol{D})$ variable combination. The reason for our choice is due to the fact that this combination gives piezoelectric coefficient $\boldsymbol{e}$ and dielectric constant $\boldsymbol{\varepsilon^S}$

as in the literature and material data sheets, making comparisons and inferring results easier. We also used $(\boldsymbol{T}, \boldsymbol{E})$ as independent variables calculating the hydrostatic performance coefficients, which will be explained in Chapter 6.

When a piezoelectric material is polarized to a level of polarization with external energy, only some portion of this energy is stored as potential energy because some energy is dissipated as heat [71]. It is shown that heat dissipation is mainly caused by ferroelectric hysteresis and becomes more prominent in high-frequency applications [73]. Since the scope of this thesis is static or low-frequency applications, energy dissipation is not accounted for.

Continuing from Equation 4.1, since the tensors $\boldsymbol{T}$, $\boldsymbol{S}$, $\boldsymbol{C^E}$, $\boldsymbol{\varepsilon^S}$ are symmetric, these constitutive equations can be expressed in matrix notation by Voigt's notation,

$$\begin{Bmatrix} \{\boldsymbol{T}\} \\ \{\boldsymbol{D}\} \end{Bmatrix} = \begin{bmatrix} [\boldsymbol{C^E}] & -[\boldsymbol{e}]^t \\ [\boldsymbol{e}] & [\boldsymbol{\varepsilon^S}] \end{bmatrix} \begin{Bmatrix} \{\boldsymbol{S}\} \\ \{\boldsymbol{E}\} \end{Bmatrix}. \tag{4.5}$$

For anisotropic materials, the material coefficient matrix has 81 (9x9) independent terms. However, since the piezoelectric materials are transversely isotropic, the stiffness, the piezoelectric, and the dielectric matrix get reduced to a total of 11 independent coefficients. Aligning a piezoelectric solid in its axis of symmetry and embedding it into an isotropic matrix yield a piezocomposite that is transversely isotropic. Therefore, Equation 4.5 can be written as:

$$\begin{Bmatrix} T_{11} \\ T_{22} \\ T_{33} \\ T_{12} \\ T_{23} \\ T_{31} \\ D_1 \\ D_2 \\ D_3 \end{Bmatrix} = \begin{bmatrix} C_{11}^E & C_{12}^E & C_{13}^E & 0 & 0 & 0 & 0 & 0 & -e_{13} \\ C_{12}^E & C_{11}^E & C_{13}^E & 0 & 0 & 0 & 0 & 0 & -e_{13} \\ C_{13}^E & C_{13}^E & C_{33}^E & 0 & 0 & 0 & 0 & 0 & -e_{33} \\ 0 & 0 & 0 & C_{66}^E & 0 & 0 & 0 & 0 & 0 \\ 0 & 0 & 0 & 0 & C_{44}^E & 0 & 0 & -e_{15} & 0 \\ 0 & 0 & 0 & 0 & 0 & C_{44}^E & -e_{15} & 0 & 0 \\ 0 & 0 & 0 & 0 & 0 & e_{15} & \varepsilon_{11}^S & 0 & 0 \\ 0 & 0 & 0 & 0 & e_{15} & 0 & 0 & \varepsilon_{11}^S & 0 \\ e_{13} & e_{13} & e_{33} & 0 & 0 & 0 & 0 & 0 & \varepsilon_{33}^S \end{bmatrix} \begin{Bmatrix} S_{11} \\ S_{22} \\ S_{33} \\ S_{12} \\ S_{23} \\ S_{31} \\ E_1 \\ E_2 \\ E_3 \end{Bmatrix} \tag{4.6}$$

Applying a coercive electric field and/or high mechanical stress leads to non-linear behavior for the piezoelectric materials [74]. Moreover, in this non-linear region, the loading rate starts to appear as a factor that affects the electro-mechanical response. At low-loading conditions, rate dependency can be considered negligible, but at high-loading conditions, electrical and mechanical responses of ferroelectric materials are experimentally proven to be time- and frequency-dependent [75]–[78].

Other studies also show that the electrical or mechanical loading rate has an influence on the behavior of piezocomposites [72], [79], [80].

Since the scope of this thesis is piezoelectric materials under low levels of electrical and mechanical loading and low-frequency conditions, rate dependency was not studied.

4.2 Representative Volume Element

A Representative Volume Element (RVE) is said to be the smallest volume element of the composite that is "statistically representative of the composite"[81]. The transition from an RVE to a component is shown in Figure 4.1. Instead of analyzing the whole composite material, we can analyze the representative volume element to obtain the macroscopic behavior of the material.

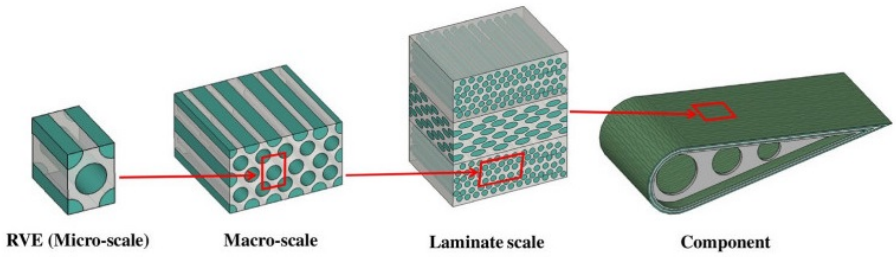

Figure 4.1: Composite built from duplicated RVEs [82]

An example of an RVE model prepared in ABAQUS is shown in 4.2. It consists of a fiber material in the middle and a matrix material surrounding it. For simplicity, the RVE is chosen as a unit cube unit.

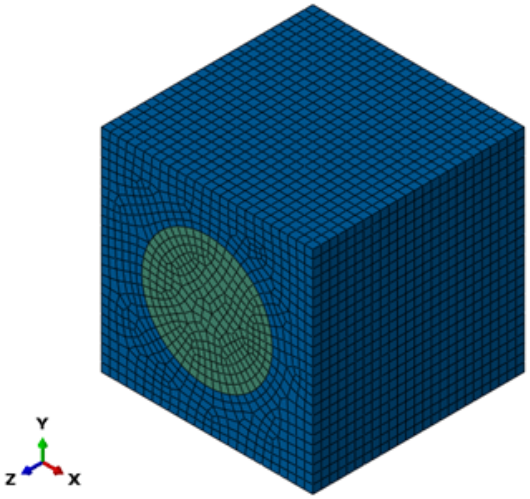

Figure 4.2: An RVE model for 1-3 piezocomposites in ABAQUS

One of the major advantages of the numerical methods is that it provides the user total control over the model, allowing him/her to apply any kind of load and boundary conditions with any material and being able to model any geometry that is meshable and computationally possible. For instance, for complex shapes, unlike circular or square, one has to resort to numerical methods [13].

All the RVE models presented in this thesis comply with the transverse isotropy. However, if an asymmetrical model were used, such as 1-3 piezocomposite which has a fiber with an offset from the center, the transverse isotropy would not be valid anymore. Thus, more terms in Equation 4.6 would be required to capture the deformation of this asymmetrical RVE model correctly.

4.3 Homogenization

The main idea of homogenization is to develop an equivalent and homogenized continuum which has average piezomechanical properties the same as the original heterogeneous material. For that purpose, we will calculate the effective properties of heterogeneous materials by solving the boundary value problem. In order to do that, one should define proper boundary conditions on the representative volume element (RVE).

By mechanics of material, we aim to predict and understand the behavior of the material. Although this can be done quickly for homogeneous materials, it is arguably more cumbersome for heterogeneous materials. Therefore, by estimating the effective (averaged or overall) properties of the heterogeneous material, the homogenization technique makes predicting the material behavior much easier.

For instance, if we were to analyze a brick wall (see Figure 4.3), the smallest part of the brick wall that consists of a couple of bricks and filler between them can reproduce the whole brick wall by periodicity and thus would be enough for us to predict the whole brick wall behavior.

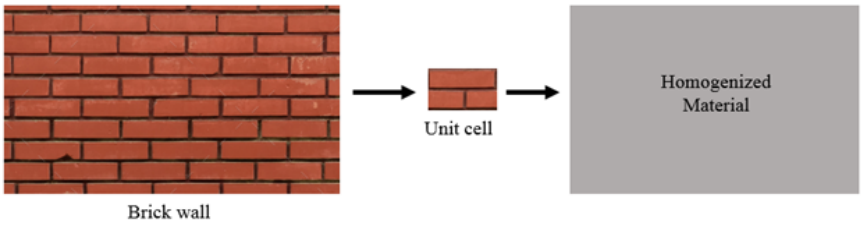

Figure 4.3: Illustration of homogenization example

In this study, we focus on the numerical homogenization method using finite element analysis whereas there are also analytical methods. Of these analytical methods, mixture rule models do not consider the interaction between the phases, while self-consistent methods consider some interaction, but they are limited to simple geometries.

When conducting computational homogenization, the effective properties will be computed by the finite element method. For that purpose, the finite element analysis program ABAQUS will be used.

The scale at which the homogenization method is applied is very important. It should be noted that the composite material that we deal with must be periodic or almost periodic and the size of the unit cell must be very small compared to the whole model's size and larger than the material grain size or fiber diameter [67].

Another assumption is that the operational wavelength is larger than the dimensions of the unit cell, which means that the problem is static. If the operational wavelength

happens to be smaller than the dimensions of the unit cell, then wave reflections inside the unit cell will take place and they will have to be considered when doing the math [67].

One of the benefits of the homogenization method is that we only need information about the RVE. Therefore, the RVE can have any complex shape and can be solved with the help of FEM.

The main aim of homogenization is to get a homogenous model that is equivalent to the original composite. In both models, the stored strain energies are required to be the same [12]. The whole domain can be reduced to a single cell, which is called a unit cell or representative volume element (RVE).

An RVE is the smallest part that can be modeled, and it contains all the required and sufficient information like geometrical and material parameters at the microscale to obtain the effective (overall) material properties of the composite.

Composite materials can be simulated with RVEs placed periodically, meaning that by merging these RVEs periodically in all directions together, the macroscopic behavior of the original model can be obtained. Therefore, to ensure that these RVEs can add up while their matching faces fit together perfectly, it is necessary to apply periodic boundary conditions (PBC) to the RVEs. These periodic boundary conditions on the boundary of the unit cell are given in [83]. These PBC ensure that every RVE that makes up the composite model has the same exact deformation mode and no RVE surfaces penetrate each other, or no gap exists between the adjacent RVEs.

To obtain certain effective coefficients, certain load cases or boundary conditions must be given to the RVE model. These load cases are such that only one component of the macroscopic strain is prescribed as non-zero while all others are zero.

As for the mesh convergence, Bergel et al. [13] stated that for accurate results, the mesh density on the surfaces parallel to the fiber cross-section should be such that the average element size is around 5% of the RVE width.

The selection of proper microscopic boundary conditions is a crucial step in any numerical homogenization approach. Since the RVE is subjected to these boundary

conditions, the effective properties are ascertained from the RVE's averaged response.

However, the boundary conditions must satisfy some mathematical conditions. As Hill [84] suggested in his Hill-Mandel macro homogeneity condition (or Hill condition), the equivalence of elastic materials' energetically and mechanically determined properties is ensured along with some required conditions. Hill-condition can be satisfied by the following three boundary conditions for heterogeneous medium [85], [86], [87]:

(1) linear displacement boundary condition (Dirichlet condition)
(2) constant traction boundary condition (Neumann condition) and
(3) periodic boundary condition.

Hill's energy principle suggests that:

$$\overline{\boldsymbol{\sigma} : \boldsymbol{\epsilon}} = \bar{\boldsymbol{\sigma}} : \bar{\boldsymbol{\epsilon}} \tag{4.7}$$

where bar denotes the volume average.

The above condition states that the average of the double contraction of the stress and strain tensors is equal to the double contraction of their average values.

In an RVE, the average stresses and strains are described by

$$\bar{\varepsilon}_{ij} = \frac{1}{V} \int_V \varepsilon_{ij} \, dV \tag{4.8}$$

$$\bar{\sigma}_{ij} = \frac{1}{V} \int_V \sigma_{ij} \, dV \tag{4.9}$$

$$\overline{\sigma_{ij} \, \varepsilon_{ij}} = \frac{1}{V} \int_V \sigma_{ij} \varepsilon_{ij} \, dV \tag{4.10}$$

where V is the volume of the representative volume element.

With the use of the divergence theorem and with the assumption of no body forces, skipping the intermediate steps, we can have

$$\oint_{\delta V} (t_i - \bar{\sigma}_{ij} n_j)(u_i - \bar{\varepsilon}_{ik} x_k)\, dS = 0 \tag{4.11}$$

From the equation, we can make either the first or second term zero, and that provides us displacement boundary condition and traction boundary condition, respectively. Alternatively, we can get periodic boundary conditions, which will be explained in the PBC section.

4.3.1 Linear Displacement Boundary Condition (DBC)

Linear displacement boundary condition requires defining uniform displacement values on the surfaces of the RVE, which is also called Kinematic Uniform Boundary Conditions (KUBC) or Dirichlet Condition.

The displacement field in the form of macroscopic strain is enforced on the RVE boundaries:

$$u_i - \bar{\varepsilon}_{ij} x_j = 0 \qquad \forall\, x \;\in\; \delta V \tag{4.12}$$

where $\bar{\varepsilon}_{\mathrm{ij}}$ is the average strain. This equation satisfies Hill's energy principle.

4.3.2 Constant Traction Boundary Condition (TBC)

Constant traction boundary condition requires defining uniform traction values on the surfaces of the RVE, which is also called Static Uniform Boundary Conditions (SUBC) or Neumann Condition.

The traction field in the form of macroscopic stress is enforced on the RVE boundaries:

$$t_i = \bar{\sigma}_{ij} n_j \qquad \forall\, x \;\in\; \delta V \tag{4.13}$$

where $\bar{\sigma}_{\mathrm{ij}}$ is the average strain. This equation satisfies Hill's energy principle.

4.3.3 Periodic Boundary Condition (PBC)

In application, the periodic boundary condition imposes the anti-periodicity of the traction field over the RVE border and the periodicity of fluctuations [88]. To achieve this, we divide the RVE boundary δV into positive δV^+ and negative δV^- components, see Figure 4.4.

Noting that fluctuation term is:

$$u_i = \bar{u}_i + \widetilde{u}_i = \bar{\varepsilon}_{ij} x_j + \widetilde{u}_i \tag{4.14}$$

$$\widetilde{\boldsymbol{u}}(x^+) = \widetilde{\boldsymbol{u}}(x^-) \quad \forall\, x^+ \in \delta V^+ \quad \text{and} \quad \forall\, x^- \in \delta V^- \tag{4.15}$$

$$\boldsymbol{t}(x^+) = -\boldsymbol{t}(x^-) \quad \forall\, x^+ \in \delta V^+ \quad \text{and} \quad \forall\, x^- \in \delta V^- \tag{4.16}$$

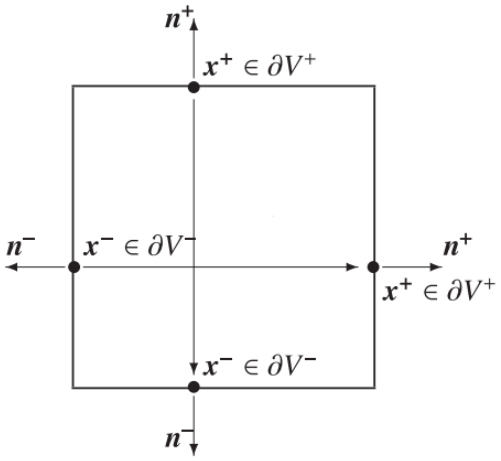

Figure 4.4: Positive and negative boundary discretization [88]

4.3.4 Comparison of Boundary Conditions

Many studies in the literature show that the PBC is considered to be the most efficient method, even for arrangements that are not periodic [89]–[91]. Furthermore, as presented in Figure 4.5, the periodic boundary condition offers a more accurate estimate

for a given RVE size than the linear displacement and the constant traction boundary conditions.

Although the periodic boundary condition is suitable for periodic structures, as the name suggests, the aforementioned conclusion is also valid, provided the micro-structure does not show geometrical periodicity [88].

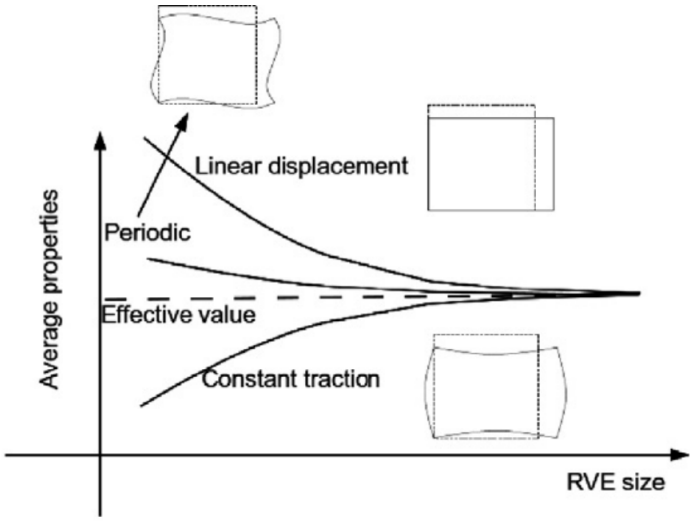

Figure 4.5: Convergence comparison of the boundary conditions in a RVE [88]

As seen from Figure 4.5, as the RVE size gets bigger, the average properties for all BC types converge to each other.

4.4 Application of PBCs

A composite material can be represented by periodically arrayed RVEs. This brings simplicity to modeling. For this periodicity, periodic boundary conditions must be applied to the modeled RVE. Boundary conditions to be applied in this context are critical for the success of the modeling [92]. Thus, each neighboring RVE in the structure should have the same deformation shape and should not be separated or overlapped. The general periodic boundary condition given by Havner [93] has been accepted as one of the foundations of the representative volume element concept.

Periodicity condition means that the shapes of opposite boundaries, such as positive and negative X, Y, and Z surfaces, remain identical. Moreover, these surfaces will

have traction values that are equal in magnitude but of the opposite sign.

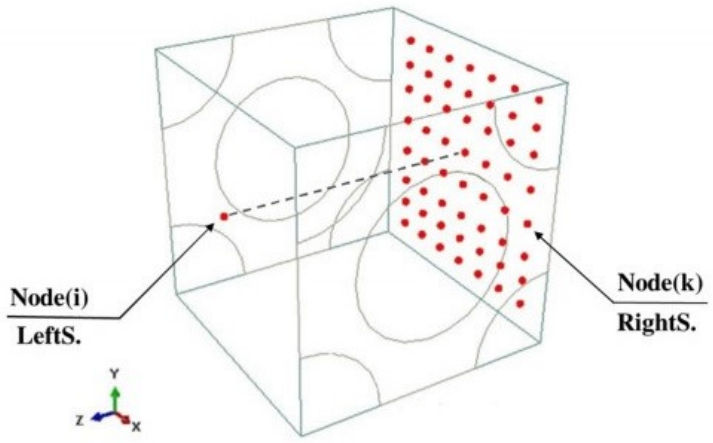

Figure 4.6: Schematic of a matching pair of nodes on opposite faces of an RVE [82]

To be able to apply the PBC, the meshes of the opposing surfaces must be identical. Afterward, the classical application enforces the same degree of freedom value to the nodes on two opposing RVE surfaces. The opposing nodes are shown in Figure 4.6.

A Python script is developed to apply the periodic boundary condition. The periodic boundary condition (PBC) script made the process very simple and time-efficient. Applying PBC to RVE would be a very time-consuming and challenging operation without the script. Selecting each and every node on the opposing faces by hand and binding them to each other with a constraint equation would be required. For a very fine mesh, it may take much too long time if not impossible.

Depending on the loading case, certain constraints are used to set the strain values between each matching node's displacement values.

In Figure 4.7, the names of the surfaces of the representative volume element ($X+$, $X-$, $Y+$, $Y-$, $Z+$, and $Z-$) and the reference systems (X-Y-Z and 1-2-3) are shown.

The periodicity in the representative volume element requires conformation conditions with respect to opposite edges on the surfaces. According to the periodicity rule, the displacement, which is related to the mean unit cell strain can be expressed as the following expression:

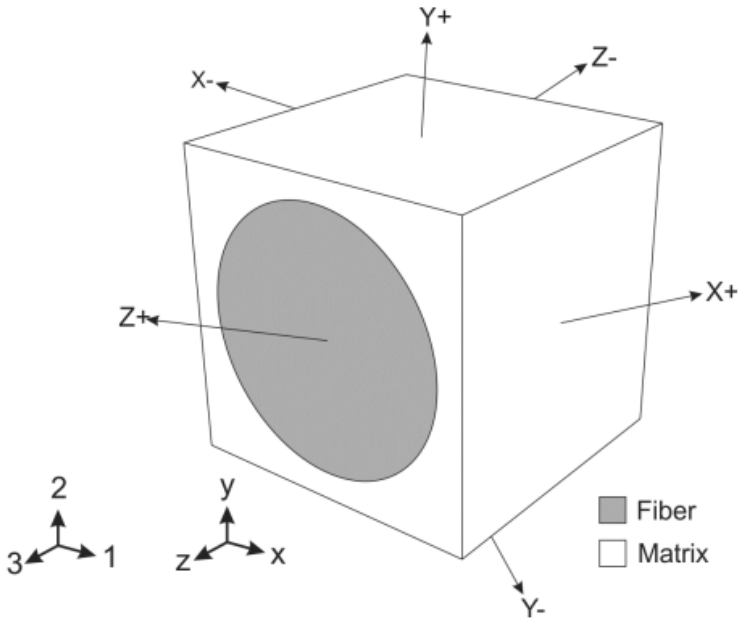

Figure 4.7: Part and Surface Designations in a Representative Volume Element [94]

$$u_i{}^{K^+} - u_i{}^{K^-} = \bar{S}_{ij}(x_j{}^{K^+} - x_j{}^{K^-}) \tag{4.17}$$

where u_i refers to the displacement value of the nodes, $\bar{S}_{ij}$ is the mean strain value and x_j denotes the coordinates of the node. The '$K+$' and '$K-$' indices refer to the nodes on positive x_j and negative x_j faces, respectively, of the surfaces $X+$, $X-$, $Y+$, $Y-$, $Z+$, and $Z-$, as depicted in Figure 4.7.

A similar equation can also be written for the electrical degrees of freedom, as shown in Equation 4.18. ϕ stands for electric potential, and $\boldsymbol{E}$ stands for the electric field vector.

$$\phi^{K^+} - \phi^{K^-} = \bar{E}_i(x_i{}^{K^+} - x_i{}^{K^-}) \tag{4.18}$$

These conditions stated above must be applied for each pair of nodes on opposite sides of the unit cell. Provided that the structure is symmetric, i.e. its inclusion does not have offset, it is not a must to specify these conditions on the nodes of the unit cell for some of the loading cases. Because, in these loading cases, displacement and electrical boundary conditions already satisfy the parallelism constraint. In fact, all

electrical boundary conditions can be given as surface boundary conditions and do not require the application of PBC.

Automatic procedures for searching for mutual nodes and applying constraints provide great convenience. Scripts can be written in Python both for this purpose and to avoid mistakes when choosing nodes. Python is an embedded programming language in ABAQUS, and every command done on GUI can be done with Python codes.

Because only the volume percentage and fiber distribution affect the numerical estimation of the effective coefficients, not the absolute size, the unit cell size can be selected to have a unit length. Choosing a unit cube in the dimension of unity can help in both pre and post-process.

The right mesh size needs to be determined to get results that are accurate enough. It is recommended that the average element size in the x_1-x_2 plane (perpendicular to the fiber axis) is about 5% of the width of the unit cell [13]. Also, unit cells can be modeled in the x_3 direction with just one element since the expected infinite fiber length makes the effective material properties independent of that direction. However, depending on the researcher's preference, it can be preferable to visualize the typical cell element as a cube.

Table 4.1: Load cases and relevant material coefficient groups

No.	1	2	3	4	5	6
Group	C_{11}^{eff},C_{12}^{eff}	C_{13}^{eff}, C_{33}^{eff}	C_{44}^{eff}, e_{15}^{eff}	C_{66}^{eff}	e_{13}^{eff}, e_{33}^{eff}, ε_{33}^{eff}	ε_{11}^{eff}

4.5 Loadings and Boundary Conditions

Several load cases are required to obtain effective material properties. All 11 active coefficients can be computed with 6 different load cases. These are shown in Table 4.1. In these loadings, the displacement and electric potential are applied in such a way that only the relevant (to be calculated) strain and electric field components are non-zero.

The boundary conditions are shown in Table 4.2. For each effective coefficient, certain displacements or electric potentials must be applied to certain surfaces. The displacement and electric potential values to be unset are shown by "$-$". Moreover, the formula to obtain the effective coefficient is given in the last column.

Table 4.2: Boundary conditions on the RVE surfaces and corresponding effective coefficients

Effective Properties	$X-$ u_i/ϕ	$X+$ u_i/ϕ	$Y-$ u_i/ϕ	$Y+$ u_i/ϕ	$Z-$ u_i/ϕ	$Z+$ u_i/ϕ	Formula
C_{11}^{eff}	0/0	$\widetilde{u}_1$/0	0/0	0/0	0/0	0/0	$\bar{T}_{11}$ / $\bar{S}_{11}$
C_{12}^{eff}	0/0	$\widetilde{u}_1$/0	0/0	0/0	0/0	0/0	$\bar{T}_{22}$ / $\bar{S}_{11}$
C_{13}^{eff}	0/0	0/0	0/0	0/0	0/0	$\widetilde{u}_3$/0	$\bar{T}_{11}$ / $\bar{S}_{33}$
C_{33}^{eff}	0/0	0/0	0/0	0/0	0/0	$\widetilde{u}_3$/0	$\bar{T}_{33}$ / $\bar{S}_{33}$
C_{44}^{eff}	$\widetilde{u}_3$/0	$\widetilde{u}_3$/0	0/–	0/–	$\widetilde{u}_1$/–	$\widetilde{u}_1$/–	$\bar{T}_{13}$ / $\bar{S}_{31}$
C_{66}^{eff}	$\widetilde{u}_2$/–	$\widetilde{u}_2$/–	$\widetilde{u}_1$/–	$\widetilde{u}_1$/–	0/0	0/0	$\bar{T}_{12}$ / $\bar{S}_{12}$
e_{13}^{eff}	0/–	0/–	0/–	0/–	0/0	0/$\widetilde{\varphi}$	$-\bar{T}_{11}$ / $\bar{E}_3$
e_{33}^{eff}	0/–	0/–	0/–	0/–	0/0	0/$\widetilde{\varphi}$	$-\bar{T}_{33}$ / $\bar{E}_3$
e_{15}^{eff}	$\widetilde{u}_3$/0	$\widetilde{u}_3$/0	0/–	0/–	$\widetilde{u}_1$/–	$\widetilde{u}_1$/–	$\bar{D}_1$ / $\bar{S}_{31}$
ε_{11}^{eff}	0/0	0/$\widetilde{\varphi}$	0/–	0/–	0/–	0/–	$\bar{D}_1$ / $\bar{E}_1$
ε_{33}^{eff}	0/–	0/–	0/–	0/–	0/0	0/$\widetilde{\varphi}$	$\bar{D}_3$ / $\bar{E}_3$

Another important point is that while obtaining the coefficients in the axial direction, the boundary conditions in the table above can be applied directly without PBC and the desired results can be obtained. These values are C_{11}^{eff}, C_{12}^{eff}, C_{13}^{eff}, C_{33}^{eff}, e_{13}^{eff}, e_{33}^{eff}, ε_{11}^{eff} and ε_{33}^{eff}. In other words, these displacement and electrical boundary conditions already satisfy the parallelism condition [19]. However, for the coefficients C_{44}^{eff}, e_{15}^{eff}, C_{66}^{eff} related with shear, a connection must be established between the nodes that will create the periodic boundary condition. A script was written in the Python scripting language for this periodic boundary condition generation, which is embedded in ABAQUS.

The loadings can be divided into two types: axial and simple shear loadings. In the following sections, detailed explanations and representations of these loadings are shown.

4.5.1 Axial Load

As an example of axial mechanical loading, consider loading for C_{13}^{eff} and C_{33}^{eff}. Boundary conditions should be applied such that all strain components and electrical fields are zero, except for the normal strain in the x_3 direction. Therefore, the normal displacements on all surfaces except the positive Z surface are set to zero. An arbitrary normal displacement value is assigned on the $Z+$ surface of the model, i.e., $u_z = \widetilde{u}_3$, while keeping the $Z-$ surface fixed, i.e., $u_z = 0$. On the $X-$ and $X+$ surfaces, the boundary conditions to fix the displacements in the x direction should be applied so that $u_x = 0$. Similarly, in the $Y-$ and $Y+$ directions, the boundary conditions to fix the displacements in the y direction should be applied so that $u_y = 0$.

In addition, electric potential (voltage) boundary conditions should also be defined. On $Z-$ and $Z+$ surfaces, the electric potential (voltage) boundary condition should be defined so that $\phi = 0$. Electric potential boundary conditions for $X-$, $X+$, $Y-$, and $Y+$ surfaces might be defined depending on the electric potential gradient presence across these surfaces. If there is an electrical field induced in the normal directions of these surfaces zero electric potential boundary conditions must be defined, otherwise not. Applied boundary conditions are shown in Figure 4.8.

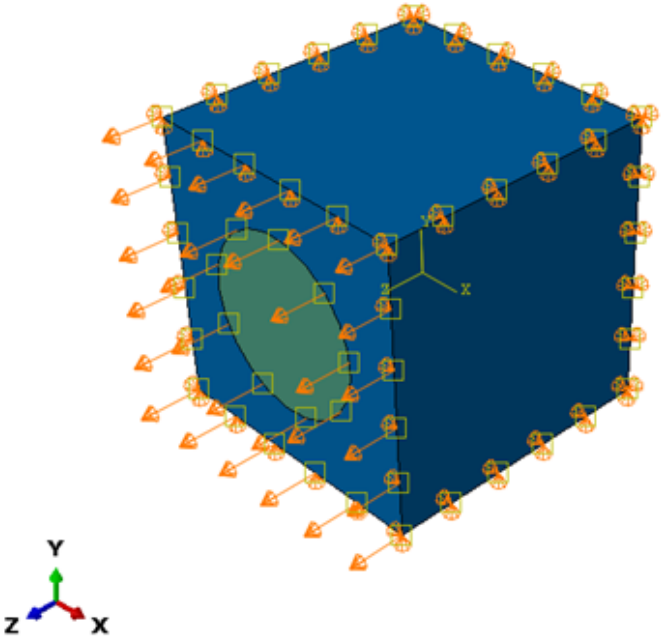

Figure 4.8: Mechanical Loading applied in Z to calculate C_{13}^{eff} and C_{33}^{eff}

Then, C_{13}^{eff} can be found by dividing the mean normal stress value in the X direction, $\bar{T}_{11}$ obtained from the model by the mean normal strain value in the Z direction, $\bar{S}_{33}$. Similarly, C_{33}^{eff} can be found by dividing the mean normal stress value in the Z direction, $\bar{T}_{33}$ obtained from the model by the mean normal strain value in the Z direction, $\bar{S}_{33}$. Other coefficients can be found in this way using the boundary conditions and equations in the table.

Similarly, boundary conditions in other directions created by normal strain or electrical boundary conditions can also be given.

4.5.2 Simple Shear

Obtaining the coefficients based on the mean shear strain is more complicated and requires more attention. For example, for C_{44}^{eff} with a pure in-plane state on the x_1-x_3 plane, the constraint equations must be written for the nodal points on surfaces X and Z. In this equation for opposite nodes, an arbitrary value is written to the difference of displacements of these two nodes. However, the constraint equations consist of the arbitrary values only in the in-plane directions, which are 1 and 3 for C_{44}^{eff} case. On the X surfaces, displacement in x_3 direction (u_3) must be involved. Alike, on the Z surfaces, displacement in x_1 direction (u_1) must be involved.

$$\begin{aligned} {u_3}^{X+} - {u_3}^{X-} &= \widetilde{u}_3, \\ {u_1}^{Z+} - {u_1}^{Z-} &= \widetilde{u}_1 \end{aligned} \tag{4.19}$$

In ABAQUS, a single constraint equation contains a single pair of nodes. So, for each opposite pair of nodes, there should be a constraint equation, and it is almost impossible to do it by hand unless the model is very small. Therefore, these constraints are enforced in ABAQUS using Python script. These constraint equations must be written in a parametric form so that the arbitrary value can be changed later if needed.

After the script is run, all the opposite nodes are linked to each other. For the computation of C_{44}^{eff}, degrees of freedom of opposite X and Z surface nodes are enforced to have a difference of the arbitrary value. However, opposite Y surface nodes will have zero displacement in the Y direction. These arbitrary values are assigned to reference

points RP-1, RP-2, and RP-3 so that anytime the user can change the arbitrary value in a single move. The constraint equations can be written as follows:

$$\begin{aligned} {u_3}^{X+} - {u_3}^{X-} - {u_3}^{RP-3} &= 0, \\ {u_1}^{Z+} - {u_1}^{Z-} - {u_1}^{RP-1} &= 0 \end{aligned} \tag{4.20}$$

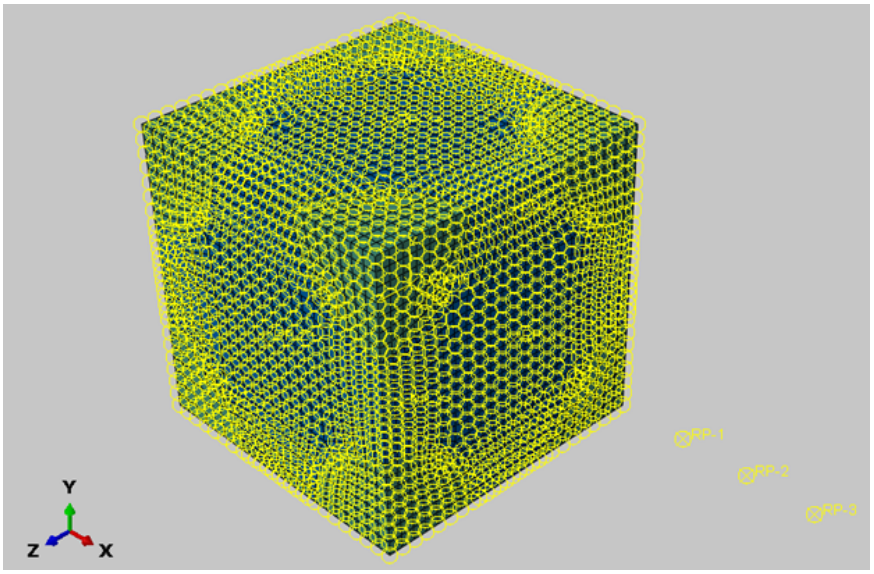

Figure 4.9: An example of an RVE with the constraint equations which are depicted with yellow circles.

While applying the mechanical boundary conditions, some restrictions must be made in order to make only the field values (stress, strain, electric field, etc.) related to the material coefficients be calculated non-zero. Therefore, for C_{44}^{eff} case, as stated in the table, the electrical degrees of freedom on both positive and negative X surfaces should be enforced to be zero.

Shear loadings cannot be depicted visually because all the displacement loadings occur in the constraint definitions in ABAQUS. However, all pairs of nodes matched are shown in Figure 4.9. Each yellow circle refers to a constraint definition. The constraint equations are defined in ABAQUS as given in Equation 4.20. Constraint and boundary conditions for C_{66}^{eff} can be done with a similar procedure.

4.6 Calculation of Effective Properties

In this section, the calculation of the effective properties is explained.

Here we assume that the average mechanical and electrical properties of our RVE are equivalent to those of piezocomposite, as shown in Equation 4.21.

$$\langle T_{ij} \rangle = \overline{T_{ij}}, \quad \langle D_k \rangle = \overline{D_k}, \quad \langle S_{ij} \rangle = \overline{S_{ij}}, \quad \langle E_k \rangle = \overline{E_k}, \tag{4.21}$$

The average stresses (T_{ij}), strains (S_{ij}), electric fields (E_i), and electrical displacements (D_i) in the RVE can be defined as in Equation 4.22.

$$\begin{aligned} \overline{T_{ij}} &= \frac{1}{|V|}\left(\int_V T_{ij}\, dV\right), \quad \overline{S_{ij}} = \frac{1}{|V|}\left(\int_V S_{ij}\, dV\right) \\ \overline{D_i} &= \frac{1}{|V|}\left(\int_V D_i\, dV\right), \quad \overline{E_i} = \frac{1}{|V|}\left(\int_V E_i\, dV\right) \end{aligned} \tag{4.22}$$

where $\overline{|V|}$ denotes the RVE volume.

In FEM, similar to the equations above that define the average properties of the RVE, the average properties can be calculated by the following relations in 4.23.

$$\begin{aligned} \overline{T_{ij}} &= \frac{1}{V_{tot}}\left(\sum_{n=1}^{nel} T_{ij}^n\, V^n\right), \quad \overline{S_{ij}} = \frac{1}{V_{tot}}\left(\sum_{n=1}^{nel} S_{ij}^n\, V^n\right) \\ \overline{D_i} &= \frac{1}{V_{tot}}\left(\sum_{n=1}^{nel} D_i^n\, V^n\right), \quad \overline{E_i} = \frac{1}{V_{tot}}\left(\sum_{n=1}^{nel} E_i^n\, V^n\right) \end{aligned} \tag{4.23}$$

These calculations repeat for every element or integration point in the FE model. In ABAQUS, the volume of the integration points can be requested. Thus, by multiplying the values of the field of interest at the integration points with the volume of that integration point and summing them up, the total value is obtained. Then, these total values are divided by the total volume resulting in the average value of the RVE.

CHAPTER 5

TWO PHASE PIEZOCOMPOSITES

This chapter aims to obtain the complete set of material parameters, which consists of the effective elastic, dielectric and piezoelectric tensors. In this chapter, except for the macro-scale application, only unidirectional periodic 1-3 piezoelectric composites with cylindrical fibers are studied and analyzed. Different loading cases and boundary conditions are applied to obtain the 11 effective coefficients of transversely isotropic 1-3 piezoelectric composites.

First, the necessary steps in the finite element model will be explained, and some information about the analysis, method, and ABAQUS will be given. Afterward, the results obtained will be shown and discussed.

In the results section, extracting all 11 effective material coefficients is exemplified, and the difference between Periodic Boundary Condition (PBC) and Displacement Boundary Condition (DBC) is shown with analyses. Also, four similar studies from the literature will be compared with this study. Each two of the four studies investigated the same case. Therefore, two different 1-3 piezocomposite models are analyzed, and each is compared with two studies. Later, a study containing experimental data will be compared to our results. Lastly, a macro-scale analysis is conducted to see if the homogenization method works and offers a real advantage.

The first model is compared with the studies carried out by Tita et al. [19] and Berger et al. [12]. The second model is compared with the studies of Berger et al. [13] and Pettermann et al. [95].

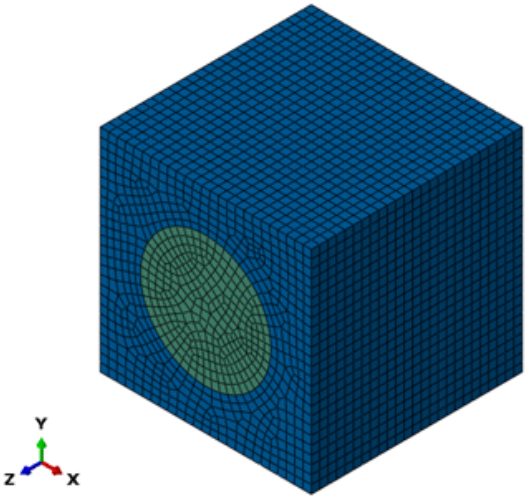

Figure 5.1: An RVE model for 1-3 piezocomposites in ABAQUS

5.1 An analysis of 1-3 piezocomposite

In this section, the fundamentals of the analysis of 1-3 piezocomposites in ABAQUS will be explained.

5.1.1 FEM Model

An example of an RVE for 1-3 piezocomposites prepared in ABAQUS is shown in Figure 5.1. As can be seen, the cylindrical section in the middle represents the piezoelectric fiber, and the other section is the matrix phase.

There are a couple of assumptions that should be stated for the upcoming analyses:

- Fiber and matrix phases are assumed to be perfectly bonded.
- The fiber is aligned and poled along the Z or x_3 axis.

5.1.1.1 Material

Notations for representing higher-order tensors as matrices can change from program to program. ABAQUS uses the notations 1, 2, 3, 4, 5, and 6 for 11, 22, 33, 12, 13, and 23 to map higher-order tensors to matrices. This applies to all material coefficients.

Elastic Properties: The whole fourth-order tensor of elastic material coefficients is given into ABAQUS. The reduced form of the elastic material coefficients for transversely isotropic materials is given in Equation 4.6.

Piezoelectric Properties: For piezoelectric coefficients, ABAQUS uses triple index notation, whereas piezoelectric data supplied by manufacturers usually have double index notation. Therefore, a conversion between the two must be made. Correspondence between tensor and vector notations is as follows, the 11, 22, 33, 12, 13, and 23 components of the tensor correspond to the 1, 2, 3, 4, 5, and 6 components, respectively, of the corresponding vector [2].

The piezoelectric material properties can be defined by giving the stress coefficients ($\boldsymbol{e}$) or strain coefficients ($\boldsymbol{d}$). In either case, a complete tensor is made of 18 components, and its order is given in Table 5.1.

Table 5.1: Piezoelectric tensor format in ABAQUS [2]

$e_{1\,11}$	$e_{1\,22}$	$e_{1\,33}$	$e_{1\,12}$	$e_{1\,13}$	$e_{1\,23}$
$e_{2\,11}$	$e_{2\,22}$	$e_{2\,33}$	$e_{2\,12}$	$e_{2\,13}$	$e_{2\,23}$
$e_{3\,11}$	$e_{3\,22}$	$e_{3\,33}$	$e_{3\,12}$	$e_{3\,13}$	$e_{3\,23}$

While the first index on the piezoelectric coefficients refers to the component of electric displacement, the next pair of indices refer to the component of mechanical stress or strain [2].

Hence, the piezoelectric components causing electrical displacement in the 1-direction are all given in the first row and the other directions in the other rows.

Dielectric Properties: The dielectric property of a material allows it to have a potential gradient (also known as an electric field). Because of this, although non-piezoelectric materials have no piezoelectric coefficient, they still show an electrical potential gradient because they have dielectric properties.

5.1.1.2 Mesh

In order to conduct the piezoelectric analysis, the "Piezoelectric" option must be selected in the element type family. By selecting "Piezoelectric", the electric potential degree of freedom (DOF) is added to three mechanical DOFs (components of the displacement vector). Electric potential degree of freedom is indicated with the 9th DOF in ABAQUS.

The piezoelectric element type is only available for solid elements. Depending on the shape of the solid element and the order of the interpolation function, the following elements are mostly used: C3D8E (8-node linear piezoelectric brick), C3D10E (10-node quadratic piezoelectric tetrahedron), C3D20E (20-node quadratic piezoelectric brick), C3D20RE (20-node quadratic piezoelectric brick, reduced integration).

In ABAQUS, the electric field is called the electrical potential gradient (EPG), and the electrical displacement is called the electrical flux vector (EFLX).

For the fidelity of the results, a mesh convergence study was done and all analyses are conducted with a mesh size fine enough.

5.1.1.3 Loadings and BCs

Loading and boundary conditions are applied as explained in Section 4.5.

5.1.2 Results and Discussion

In this section, the results of an RVE model are shown and discussed. First, extracting all 11 effective material coefficients is presented, and later, the difference between Periodic Boundary Condition (PBC) and Displacement Boundary Condition (DBC) is studied with different RVE models.

In this section, the subject 1-3 piezoelectric composite is made of circular piezoelectric fiber, PZT-5A, and Epoxy matrix. The model can be seen in Figure 5.2. The material properties are taken from Berger et al. [12] and tabulated in Table 5.2.

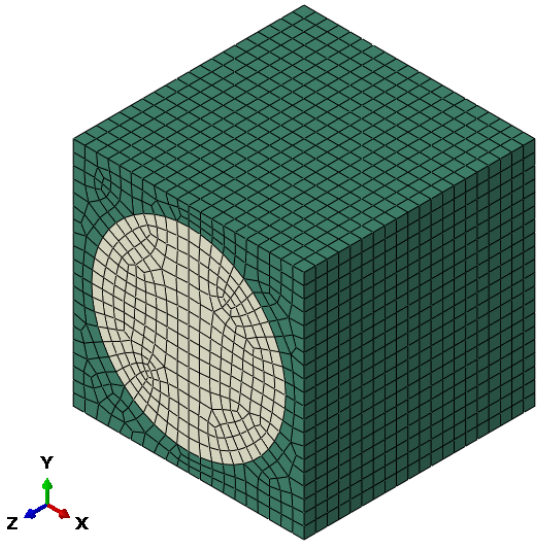

Figure 5.2: The subject RVE model with fiber volume fraction of 55.5%

Table 5.2: Material Properties of PZT-5A and Epoxy. Note that elastic, piezoelectric and dielectric coefficients are given in $\mathrm{GPa}, \mathrm{C/m^2}$ and $\mathrm{nF/m}$, respectively.

	C_{11}	C_{12}	C_{13}	C_{33}	C_{44}	C_{66}	e_{13}	e_{33}	e_{15}	ε_{11}	ε_{33}
PZT-5A	121.00	75.40	75.20	111.00	21.10	22.80	-5.40	15.80	12.30	8.11	7.35
Epoxy	3.86	2.57	2.57	3.86	0.64	0.64	–	–	–	7.97×10^{-2}	7.97×10^{-2}

5.1.2.1 Extraction of 11 Effective Coefficients

A 1-3 piezocomposite made of PZT-5A with 55.5% fiber content and an epoxy matrix is investigated. Boundary conditions are applied according to Table 4.2.

Obtained effective properties and pure constituent material properties are shown in Table 5.3. It can be seen that the effective material coefficients are always between the values of the constituents, namely PZT-5A and Epoxy. Pure constituent material coefficients determine the range of the effective coefficients. However, while some coefficients stand in the middle of this range, some stand close to values of PZT-5A or epoxy. This can be explained by the effect of connectivity. Since the fiber is placed along the Z axis, the coefficients directly related to the Z axis, such as C_{33}^{eff}, e_{33}^{eff}, and ε_{33}^{eff}, are quite high. However, other coefficients related to the X or/and Y axes are found lower and close to those of epoxy.

Table 5.3: Effective and constituent material properties of PZT-5A/Epoxy piezocomposite for 55.5% volume fraction. Note that elastic, piezoelectric and dielectric coefficients are given in GPa, $\mathrm{C/m^2}$ and $\mathrm{nF/m}$, respectively.

	C_{11}	C_{12}	C_{13}	C_{33}	C_{44}	C_{66}	e_{13}	e_{33}	e_{15}	ε_{11}	ε_{33}
PZT-5A	121.00	75.40	75.20	111.00	21.10	22.80	-5.40	15.80	12.30	8.11	7.35
Epoxy	3.86	2.57	2.57	3.86	0.64	0.64	–	–	–	7.97×10^{-2}	7.97×10^{-2}
Eff. Props.	10.84	4.64	6.03	35.07	2.21	1.54	-0.26	10.84	0.02	0.29	4.26

Coefficients C_{11}^{eff} and C_{12}^{eff}: First, the result of mechanical loading in the X-axis is examined. According to the first two rows of Equation 4.6, by applying pure axial strain in the X-direction, we can obtain the effective coefficients C_{11}^{eff} and C_{12}^{eff} by $C_{11} = T_{11}/S_{11}$ and $C_{12} = T_{22}/S_{11}$.

In Figure 5.3, von Mises distribution in the deformed shape and stress distributions in X and Y directions in undeformed shape are shown. As can be seen, although PBC is applied, the deformation shape does not have wavy shape because the RVE is symmetric.

Please note that stress components are designated with T_{ij} in the equations and table; however, it is designated with S_{ij} in ABAQUS. Similarly, strain components are designated with S_{ij} in the thesis, with E_{ij} in ABAQUS.

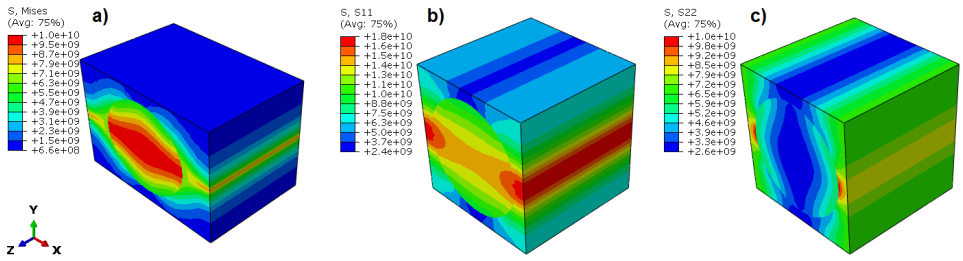

Figure 5.3: Under mechanical loading in X, a) von Mises distribution in the deformed shape, b) stress distribution in X and c) stress distribution in Y in undeformed shapes

Coefficients C_{13}^{eff} and C_{33}^{eff}: Similarly, by applying pure axial strain in the Z-direction, we can obtain the effective coefficients C_{13}^{eff} and C_{33}^{eff} by $C_{13} = T_{11}/S_{33}$ and $C_{33} = T_{33}/S_{33}$.

In Figure 5.4, von Mises distribution in the deformed shape and stress distributions in the X and Z directions in the undeformed shape are shown. Similar to C_{11}^{eff} and C_{12}^{eff} case, the deformation shape does not have wavy shape because the RVE is symmetric.

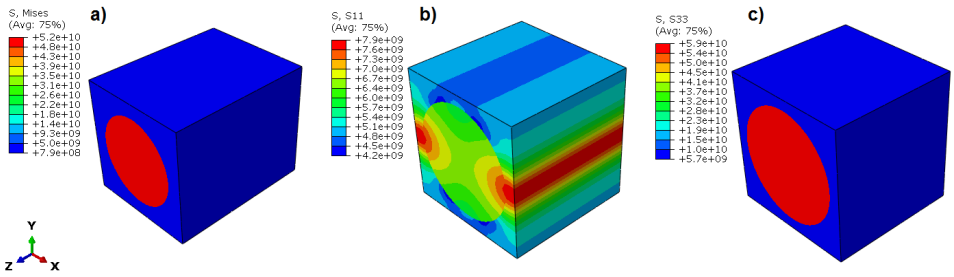

Figure 5.4: Under mechanical loading in Z, a) von Mises distribution in the deformed shape, b) stress distribution in X and c) stress distribution in Z in undeformed shapes

Coefficient ε_{11}^{eff}: According to the 7th row of Equation 4.6, by applying an electrical field in the X-axis, we cause the RVE to possess electrical charges and we can obtain ε_{11}^{eff} by $\varepsilon_{11} = D_1/E_1$.

In Figure 5.5, von Mises distribution in the deformed shape, electric displacement, and electric field in the X-direction in the undeformed shape are shown.

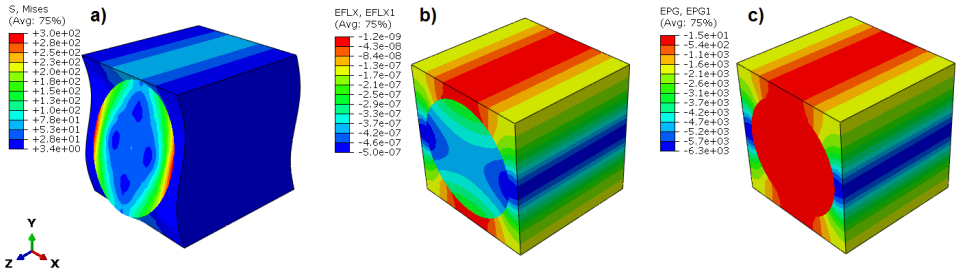

Figure 5.5: Under electrical loading in X, a) von Mises distribution in the deformed shape, b) electric displacement in X and c) electric field in X in undeformed shapes

Coefficients e_{13}^{eff}, e_{33}^{eff} and ε_{33}^{eff}: By applying an electrical field in the Z-axis, we can obtain e_{13}^{eff}, e_{33}^{eff} and ε_{33}^{eff} by $e_{13} = T_{11}/E_3$, $e_{33} = T_{33}/E_3$, and $\varepsilon_{33} = D_3/E_3$.

Figure 5.6 shows electric displacement in the Z direction in the deformed shape and stress distributions in the X and Z directions in the undeformed shapes.

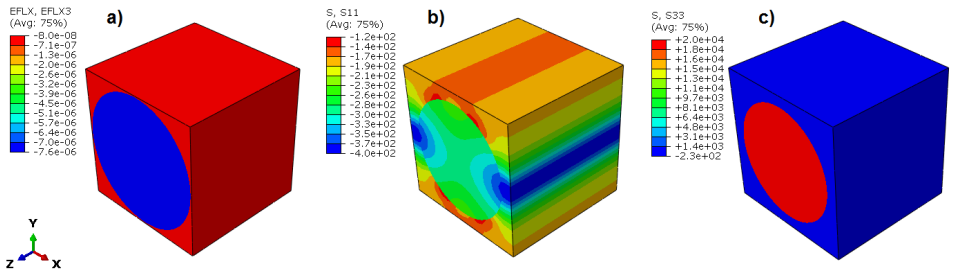

Figure 5.6: Under electrical loading in Z, a) electric displacement in Z distribution in the deformed shape, b) stress distribution in X and c) stress distribution in Z in undeformed shapes

Coefficient C_{66}^{eff}: To obtain C_{66}^{eff} , a pure shear state in X-Y must be enforced on the RVE, and by $C_{66} = T_{12}/S_{12}$, it can be obtained.

Figure 5.7 shows the distributions of 12 components of stress and strain in the deformed shape. It should be noticed that the shapes of the surfaces of the RVE are repeatable. If this RVE cell were merged with its identical twin in any direction, their surfaces would match perfectly, which is a requirement of periodicity condition and a result of PBC.

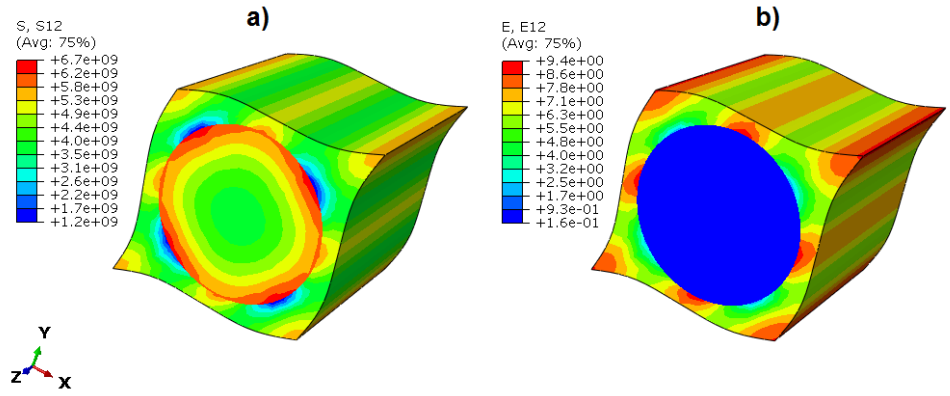

Figure 5.7: Under shear loading in X-Y, a) stress distribution in X-Y and b) strain distribution in X-Y in the deformed shapes

Coefficients C_{44}^{eff} and e_{15}^{eff}: According to the fourth and eighth rows of Equation 4.6, a pure shear state in Y-Z-plane is enforced on the RVE and C_{44}^{eff} and e_{15}^{eff} can be obtained by $C_{44} = T_{23}/S_{23}$ and $e_{15} = D_2/S_{23}$. Instead of creating a simple shear state in Y-Z-plane, we could create a simple shear state in X-Z-plane and obtain the same coefficients because the fourth and eighth rows and fifth and seventh rows of Equation 4.6 have the same coefficients.

In Figure 5.8, the distributions of 23 components of stress and strain in the deformed shape are shown.

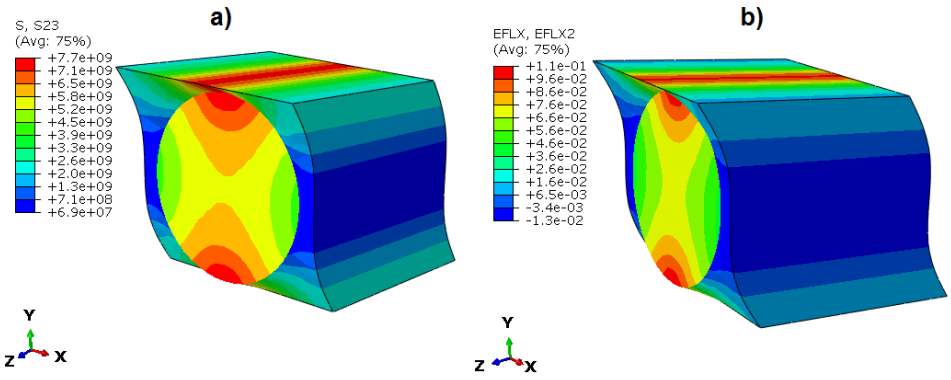

Figure 5.8: Under shear loading in Y-Z, a) stress distribution in Y-Z and b) electric displacement distribution in Y in the deformed shapes

Coefficients C_{44}^{eff} and e_{15}^{eff} are known to be the most difficult coefficients to get, and most discrepancies are found in these coefficients when compared with other studies from the literature. Because they depend on the boundary conditions greatly, any little non-zero parameter except S_{13} or S_{23} can yield wrong calculation of C_{44}^{eff} and e_{15}^{eff}.

Also, similar to the loading to determine C_{66}^{eff}, the wavy displacement field on the Z surfaces is the result of applying periodic boundary conditions. PBCs guarantee the periodicity requirement. Therefore, for shear loadings, PBCs have to be used, and displacement boundary conditions are not suitable. However, for axial loadings, either DBC or PBC can be used.

5.1.2.2 PBC vs. DBC

In this subsection, boundary conditions PBC and DBC are investigated. DBC is applicable only for non-shear loadings. It can be used for axial loadings because DBC complies with the periodicity requirement of RVE.

For comparison, we take the case in which electrical loading in Z is applied to the RVE. With this loading, we make use of the effective stress and electrical displacement values to calculate the effective material coefficients. Therefore, this loading type covers both the mechanical and the electrical output parameters, which are stress and electric displacement, respectively.

Table 5.4: Comparison of mechanical and electrical parameter results of PBC and DBC

Parameter	Unit	PBC	DBC	Difference of DBC w.r.t. PBC
S_{11}	m/m	order of 10^{-17}	order of 10^{-19}	0%
S_{22}	m/m	order of 10^{-18}	order of 10^{-18}	0%
S_{33}	m/m	order of 10^{-19}	order of 10^{-18}	0%
T_{11}	Pa	-257.128	-257.127	-3$\times10^{-4}$%
T_{22}	Pa	-257.002	-257.002	+1$\times10^{-4}$%
T_{33}	Pa	10837.189	10837.189	+1$\times10^{-6}$%
E_1	V/m	order of 10^{-13}	order of 10^{-13}	0%
E_2	V/m	order of 10^{-13}	order of 10^{-13}	0%
E_3	V/m	-1000	-1000	0%
D_1	$\mathrm{C/m^2}$	order of 10^{-21}	order of 10^{-21}	0%
D_2	$\mathrm{C/m^2}$	order of 10^{-21}	order of 10^{-21}	0%
D_3	$\mathrm{C/m^2}$	-4.260$\times10^{-6}$	-4.260$\times10^{-6}$	+3$\times10^{-7}$%

The results are tabulated in Table 5.4. Generally, DBC is known to be stiffer than PBC and yields effective coefficients higher than PBC does. For most of the coefficients, it does so. T_{22}, T_{33} and D_3 are greater in DBC result; however T_{11} is found to be greater in PBC results. In fact, for this analysis, T_{11} and T_{22} should be equal because PZT-5A's piezoelectric material coefficients e_{13} and e_{32} are equal to each other. The

effective stresses T_{11} and T_{22} are slightly different due to the discretization errors.

Therefore, except for one coefficient, DBC results were found to be greater than PBC. However, in our case, the mesh size effect is greater than the effect of the difference between PBC and DBC. For that reason, for axial loading, either PBC or DBC can be used. Meshing the model fine enough is found to be more critical than the choice of BC.

5.2 Comparison with literature

In this section, the studies found in the literature will be reproduced, and our modeling technique will be verified. Our results will be compared to a total of five studies, four of which are numerical and one experimental.

5.2.1 Comparison with Tita et al. [19] and Berger et al. [12]

This section compares the results of the current study to the works of Berger et al. [12] and Tita et al. [19].

The study of Berger et al. [12] includes both analytical and numerical solutions. The analytical solution is based on the method called Asymptotic Homogenization Method (AHM), and the numerical solution utilized FEM. On the other, in Tita et al. [19], only a numerical solution is present.

This comparison is performed with a 1-3 piezocomposite model made of PZT-5A and Epoxy. Only one fiber volume fraction value is studied, which is 55.5%. Material properties are taken from Tita et al. [19] and Berger et al. [12] and shown in Table 5.2.

The model can be seen in Figure 5.2. It has cylindrical piezoelectric fiber in the middle and epoxy around it.

This model is analyzed in ABAQUS and has 9860 linear 8-noded piezoelectric solid elements (C3D8E). In the study of Berger et al. [12], FEM calculations were made with ANSYS. . Similarly, the RVE model has 8-noded brick elements with three

mechanical and one electrical potential DOFs. The study of Tita et al. [19] used ABAQUS for calculations, and for meshing the RVE model, approximately 4000 quadratic piezoelectric brick elements (C3D20E) were used.

All loadings and BCs are applied according to the explanation in Section 4.5. For the computation of C_{44} and e_{15}, a shear loading is applied in the Y-Z-plane, unlike the X-Z-plane as explained before. This only changes the deformation, not the coefficients, because the material and the model are transversely isotropic, and the axis of isotropy is the Z-axis.

Table 5.5: Comparison for 55.5% volume fraction. Note that elastic, piezoelectric and dielectric coefficients are given in $\mathrm{GPa}, \mathrm{C/m^2}$ and $\mathrm{nF/m}$, respectively.

	C_{11}^{eff}	C_{12}^{eff}	C_{13}^{eff}	C_{33}^{eff}	C_{44}^{eff}	C_{66}^{eff}	e_{13}^{eff}	e_{33}^{eff}	e_{15}^{eff}	ε_{11}^{eff}	ε_{33}^{eff}
Berger et al. AHM [12]	9.739	5.590	6.079	35.071	2.146	2.085	-0.250	10.861	0.022	0.278	4.209
Berger et al. FEM [12]	10.917	4.652	6.079	35.351	1.890	1.557	-0.255	10.889	0.018	0.288	4.249
Tita et al. [19]	10.856	4.666	6.043	35.127	2.205	1.528	-0.258	10.864	0.025	0.287	4.270
Current study	10.835	4.641	6.028	35.074	2.214	1.537	-0.257	10.837	0.023	0.286	4.260

All results are tabulated in Table 5.5. Axial coefficients, C_{13}^{eff}, C_{33}^{eff}, e_{13}^{eff}, e_{33}^{eff}, ε_{11}^{eff}, ε_{33}^{eff} present excellent agreement and they are very close for each type of analysis. Coefficients C_{11}^{eff}, C_{12}^{eff} and C_{66}^{eff} are found very close in numerical results. Analytical results for these coefficients deviate from the other three results. However, for C_{44}^{eff} and e_{15}^{eff}, analytical results are in close agreement with this study and Tita et al. [19]. FEM results of Berger et al. [12] underpredicted these coefficients. Some discrepancies usually come across with coefficients C_{44}^{eff} and e_{15}^{eff}. Because shear loadings, unlike axial loadings, are more complicated, leading to more heterogeneous fields, and these coefficients are affected significantly by BCs.

5.2.2 Comparison with Berger et al. [13] and Pettermann et al. [95]

This section compares the results of this study and the studies of Berger et al. [13] and Pettermann et al. [95]. The results of both Berger et al. [13] and Pettermann et al. [95] are FEM-based numerical solutions.

The subject model is a 1-3 piezocomposite model made of PZT-7A and Epoxy. How-

ever, this epoxy is different from the epoxy in the previous section. Material properties are shown in Table 5.6 and can be found in Berger et al. [13].

Table 5.6: Material Properties of PZT-7A and Epoxy. Note that elastic, piezoelectric and dielectric coefficients are given in GPa, $\mathrm{C/m^2}$ and $\mathrm{nF/m}$, respectively.

	C_{11}	C_{12}	C_{13}	C_{33}	C_{44}	C_{66}	e_{13}	e_{33}	e_{15}	ε_{11}	ε_{33}
PZT-7A	154.837	83.237	82.712	131.390	25.696	35.800	-2.120	9.521	9.349	4.065	2.079
Epoxy	8.000	4.400	4.400	8.000	1.800	1.800	–	–	–	0.037	0.037

In the study of Berger et al. [13], effective material coefficients are transformed into a set of new coefficients. Transformation formulae are shown in Equation 5.1. They are derived from the piezoelectric constitutive equations written in the form of ($\boldsymbol{S}$,$\boldsymbol{D}$) as independent variables (see Equation 4.3). $\boldsymbol{C^D}$ is the elasticity tensor at a constant electric displacement, $\boldsymbol{\beta}$ is the dielectric tensor, and $\boldsymbol{h^D}$ is the piezoelectric coupling tensor at a constant electric displacement.

$$
\begin{gathered}
\beta_{11}^{eff} = 1/\varepsilon_{11}^{eff}, \qquad \beta_{33}^{eff} = 1/\varepsilon_{33}^{eff}, \\
C_{11}^{effD} = C_{11}^{eff} + {e_{13}^{eff}}^2 \beta_{33}^{eff}, \qquad C_{12}^{effD} = C_{12}^{eff} + {e_{13}^{eff}}^2 \beta_{33}^{eff}, \\
C_{13}^{effD} = C_{13}^{eff} + e_{13}^{eff} e_{33}^{eff} \beta_{33}^{eff}, \\
C_{33}^{effD} = C_{33}^{eff} + {e_{33}^{eff}}^2 \beta_{33}^{eff}, \\
C_{44}^{effD} = C_{44}^{eff} + {e_{15}^{eff}}^2 \beta_{11}^{eff}, \\
C_{66}^{effD} = C_{66}^{eff}, \qquad h_{31}^{effD} = e_{13}^{eff} \beta_{33}^{eff}, \\
h_{33}^{effD} = e_{33}^{eff} \beta_{33}^{eff} \qquad h_{15}^{effD} = e_{15}^{eff} \beta_{11}^{eff}
\end{gathered}
\tag{5.1}
$$

In this section, fiber volume fraction values of 20%, 40%, and 60% are studied. RVE models for these fiber volume fraction values are shown in Figure 5.9. Trends and variations of the effective material coefficients are plotted. However, since the result of Pettermann et al. [95] is available only for 60% volume fraction, the plots do not include the results of Pettermann et al. [95]. A comparison of the three studies is made only for a 60% volume fraction and tabulated in Table 5.7.

For different fiber volume fractions, different effective material coefficients are obtained. These results are compared with Berger et al. [13] and can be seen in Figures

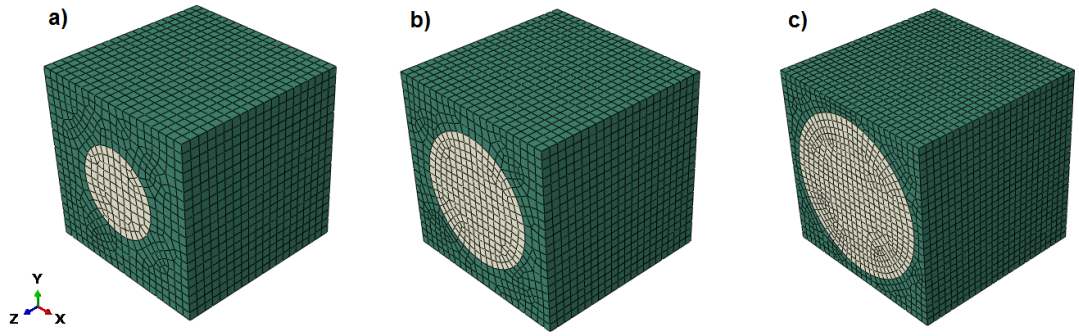

Figure 5.9: Investigated fiber volume fraction ratios: a) 20%, b) 40%, c) 60%

Table 5.7: Comparison for 60% volume fraction. Note that the units are in GPa, $10^9\,\mathrm{Vm/C}$ and $10^9\,\mathrm{V/m}$, respectively.

	C_{11}^{effD}	C_{12}^{effD}	C_{13}^{effD}	C_{33}^{effD}	C_{44}^{effD}	C_{66}^{effD}	β_{11}^{eff}	β_{33}^{eff}	h_{31}^{effD}	h_{33}^{effD}	h_{51}^{effD}
Current study	25.13	8.75	10.82	86.99	6.68	4.63	6.359	0.781	-0.157	5.034	0.329
Berger et al. [13]	25.17	8.71	10.82	86.97	6.66	4.64	6.364	0.781	-0.157	5.034	0.328
Difference	-0.14%	0.45%	0.00%	0.02%	0.29%	-0.13%	-0.07%	-0.02%	0.10%	0.01%	0.35%
Pettermann et al. [95]	25.19	8.76	10.84	87.10	6.70	4.64	6.341	0.780	-0.157	5.034	0.330
Difference	-0.08%	-0.57%	-0.18%	-0.15%	-0.60%	0.00%	0.36%	0.13%	0.00%	0.00%	-0.61%

5.10, 5.11 and, 5.12. The agreement is good, but e_{15}^{eff} shows a greater deviation in higher fiber volume fractions.

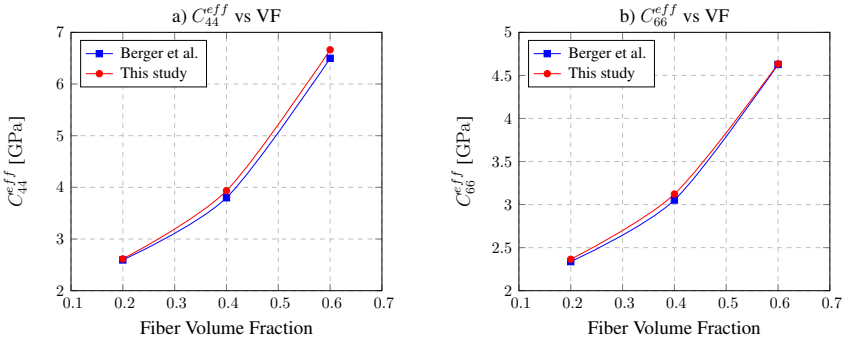

Figure 5.10: a) C_{44}^{eff} and b) C_{66}^{eff} versus fiber volume fraction

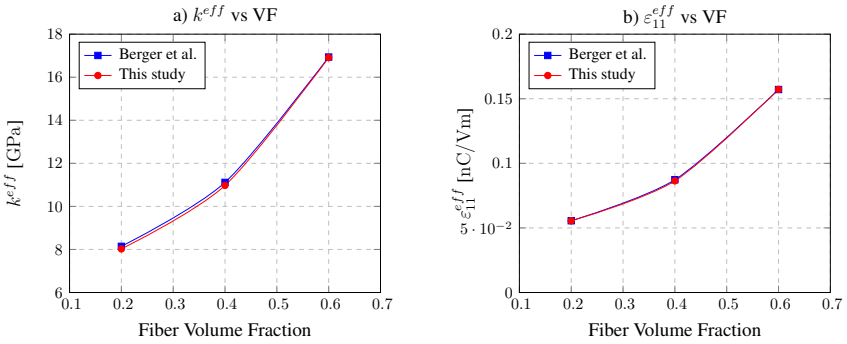

Figure 5.11: a) k^{eff} $(= (C_{11}^{eff} + C_{22}^{eff})/2)$ and b) ε_{11}^{eff} versus fiber volume fraction

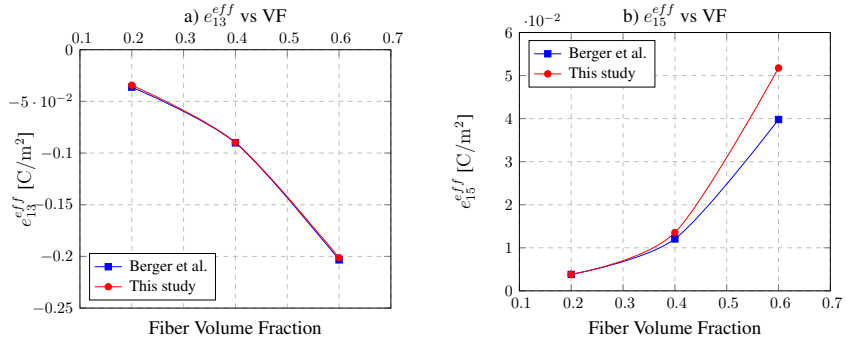

Figure 5.12: a) e_{13}^{eff} and b) e_{15}^{eff} versus fiber volume fraction

5.2.3 Comparison with experimental data

In this section, in order to verify our modeling technique, experimental data is found from the literature and compared with the FEM results obtained in this study.

Experimental data are taken from the studies of Dunn and Taya [11] and Chan and Unsworth [9]. The verification model is a 1-3 piezocomposite that is made of PZT-7A and epoxy, and both references used the same material. Material coefficients are taken from these studies and tabulated in Table 5.8.

The 1-3 piezocomposite was experimented by Chan and Unsworth [9] for various volumes of fiber fractions. Volume fractions up to 70% are modeled in FEM, and the results are compared for effective coefficients d_{33}^{eff}, $\varepsilon_{33}^{T,eff}$, and $s_{11}^{eff} + s_{12}^{eff}$. These values are plotted and compared in Figure 5.13.

As the PZT-7A volume fraction converges to 1, meaning that the whole part is made

Table 5.8: Material properties of PZT-7A and Epoxy. Note that elastic, piezoelectric and dielectric coefficients are given in GPa, $10^{-12}\ \mathrm{m/V}$ and $\mathrm{nF/m}$, respectively.

	C_{11}	C_{12}	C_{13}	C_{33}	C_{44}	C_{66}	d_{31}	d_{33}	d_{15}	ε_{11}^{S}	ε_{33}^{S}
PZT-7A	148.0	76.2	74.2	131.0	25.4	35.9	-60	150	362	4.0728	2.0807
Epoxy	8.0	4.4	4.4	8.0	1.8	1.8	–	–	–	0.0372	0.0372

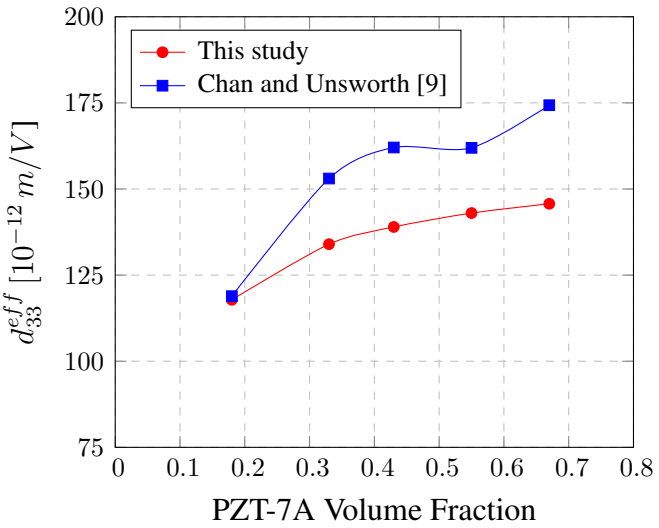

Figure 5.13: d_{33}^{eff} vs. PZT-7A volume fraction

of PZT-7A, the effective d_{33} value should converge to $150\times10^{-12}\ \mathrm{m/V}$ because this is the material property. However, as it seems in Figure 5.13, the effective d_{33} goes beyond $150\times10^{-12}\ \mathrm{m/V}$ around 30% of fiber volume. After measuring the d_{33} value for a randomly chosen PZT-7A sample and finding d_{33} out to be $163\text{-}167\times10^{-12}\ \mathrm{m/V}$, Chan and Unsworth [9] decided to take material property d_{33} as $167\times10^{-12}\ \mathrm{m/V}$ in their numerical model to verify with their experimental data. Thus, we follow the same procedure and re-run our FEM models.

As can be seen in Figure 5.14, the numerical results are now closer to the experimental data, and now it can be said that the numerical results are in agreement with the experiment. Besides d_{33}^{eff}, other effective material coefficients $\varepsilon_{33}^{T,eff}$, and $s_{11}^{eff} + s_{12}^{eff}$ are also compared with the experimental data in Figures 5.15 and 5.16.

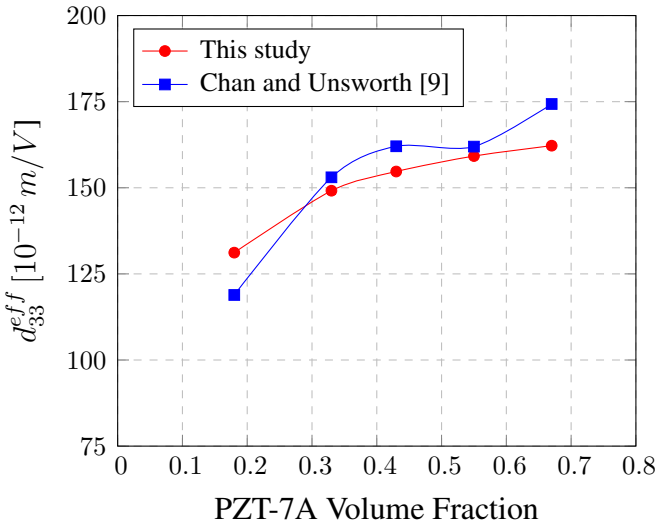

Figure 5.14: d_{33}^{eff} vs. PZT-7A volume fraction ($d_{33} = 167{\times}10^{-12}\,\mathrm{m/V}$ for PZT-7A)

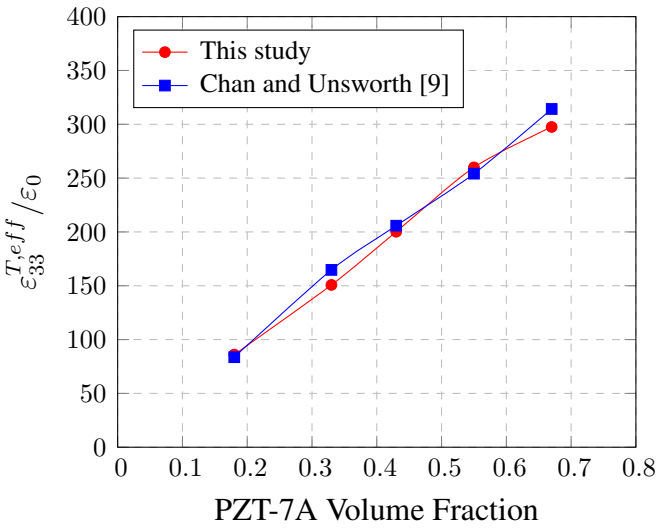

Figure 5.15: $\varepsilon_{33}^{T,eff}/\varepsilon_0$ vs. PZT-7A volume fraction ($d_{33} = 167{\times}10^{-12}\,\mathrm{m/V}$ for PZT-7A)

Looking at the figures, it can be said that the numerical results obtained in this study are generally in agreement with the experimental data presented by Chan and Unsworth [9] although there are some slight deviations. In Figure 5.14, d_{33}^{eff} values obtained by FEM followed the trend of the experimental data. Except for the first one, other values underestimated the experimental data, and the percentage of error

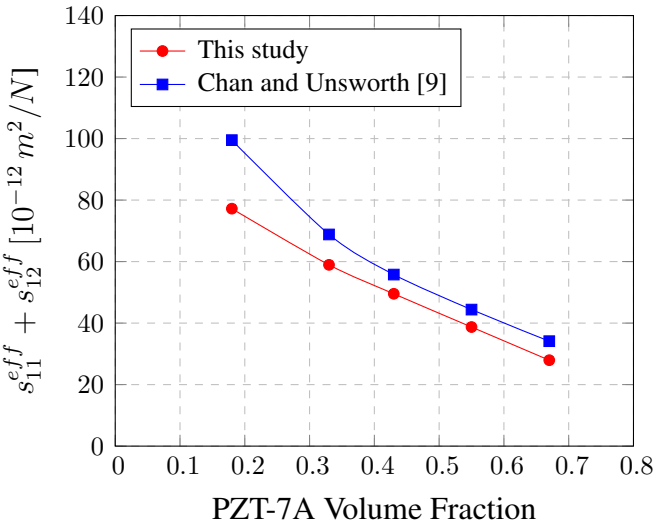

Figure 5.16: $s_{11}^{eff} + s_{12}^{eff}$ vs. PZT-7A volume fraction ($d_{33} = 167{\times}10^{-12}\,\mathrm{m/V}$ for PZT-7A)

remained below 10%. In Figure 5.15, ratios of $\varepsilon_{33}^{T,eff}$ to absolute dielectric constant, ε_0 are shown. As can be seen, the results are found to be very close, and they change almost linearly with the PZT-7A volume fraction. In Figure 5.16, effective compliance coefficients $s_{11}^{eff} + s_{12}^{eff}$ are compared. The numerical results obtained by this study are in agreement with the experimental data and have a similar trend. The minimum and the maximum percentages of error are found to be around 11% and 22%, respectively.

5.3 Application to a Macro-Scale Boundary Value Problem

So far, only homogenized material coefficients obtained by RVE are presented in this study. In this section, on the other hand, an example of a macroscale piezocomposite structure with the homogenized material properties obtained by prior RVE analyses is studied, which is actually the main purpose of the homogenization method.

In this section, we aim to reproduce a macro-scale piezocomposite model with the help of the homogenization method and treat it like a uniform homogeneous material. For this purpose, an appropriate RVE model will be prepared and analyzed to obtain

the complete set of material moduli. Then these homogenized material properties are given into the macro-scale model with the single material section. It is expected that both homogeneous and heterogeneous macro-scale give very similar results. An arbitrary model could be developed to validate the application of the homogenization method to macro-scale BVPs, but we did prefer to compare our results to a literature study. Therefore, the model presented by Prasad et al. [96] is chosen and studied. This model is made of a circular shim plate at the bottom and a circular piezoelectric plate on top, as shown in Figure 5.17. For computational efficiency, only a quarter model with symmetric BCs is analyzed.

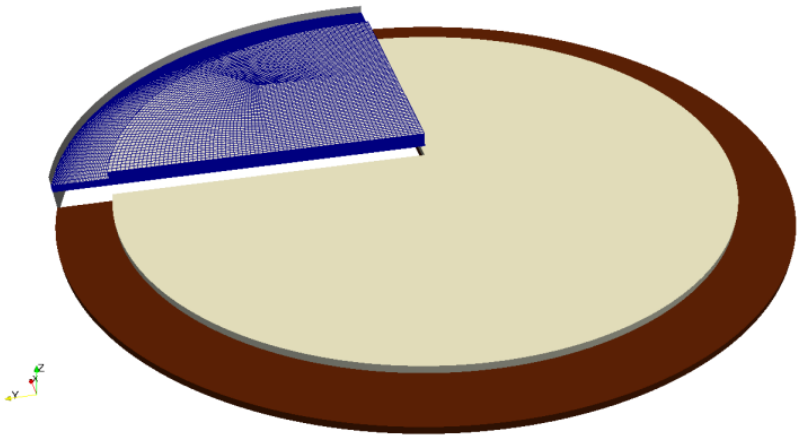

Figure 5.17: Full scale of macroscale model and its quarter computational domain [97]

Material properties of piezoelectric material APC850 are taken from the study of Prasad et al. [96] but some material coefficients were missing because their loading requires not all terms of the material moduli. Therefore, the remaining missing coefficients are obtained from the manufacturer's data sheet [98]. The material properties of APC850 and shim are tabulated in Table 5.9. The dielectric material properties ε_{11} and ε_{33} are taken the same, as 1750.

In all analyses, the ratio of piezoelectric plate height to shim plate height, which is a parameter, remained constant at 0.4. In fact, the radius of the shim plate was fixed, too. Only the radius of the piezoelectric plate is changed. Ratios of radii of the piezoelectric plate to shim plate studied in this chapter are as follows: 0.2, 0.4, 0.55, 0.65, 0.75, 0.85, and 0.9.

Table 5.9: Material properties of APC850 and shim. Note that elastic, piezoelectric and dielectric coefficients are given in $\mathrm{GPa}, 10^{-12}\,\mathrm{m/V}$ and $\mathrm{nF/m}$, respectively.

	Elastic Modulus, E	Poisson's ratio, v	d_{31}	d_{33}	d_{15}	$\varepsilon/\varepsilon_0$
APC850	63	0.31	-175	400	590	1750
Shim	90	0.32	–	–	–	1

First, the heterogeneous macro-scale model is analyzed as it is; piezoelectric plate on top, shim plate on the bottom. Then, a homogeneous macro-scale model is developed, and its homogenized material properties are obtained by RVE models, as explained in Chapter 4. The RVE model is prepared as shown in Figure 5.18 because this model represents the macro-scale model better than a cylindrical RVE model and gives better results. Since the height ratio is fixed at 0.4, only one RVE model is needed. Mechanical and electrical loadings are applied to this RVE model to get the complete set of material coefficients. Then, these homogenized material properties are set into the homogeneous macro-scale model.

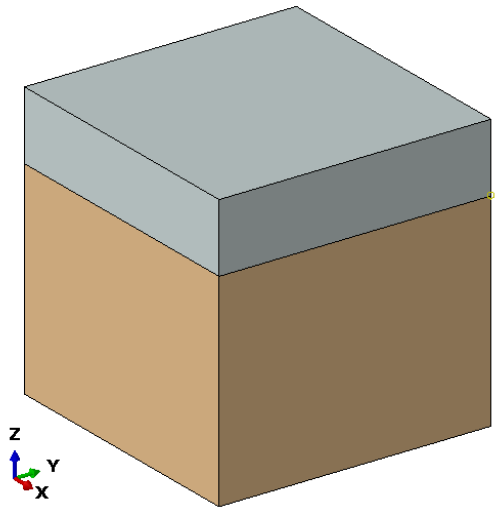

Figure 5.18: RVE model prepared for macro-scale problem

The model is fixed on the outer surface of the shim plate, and a positive voltage is applied on the upper surface of the piezoelectric plate while fixing the voltage on the lower surface of the shim plate to zero. The fixed outer surface, material regions, and mesh are shown in Figure 5.19. Since the outer portion of the models consists of only

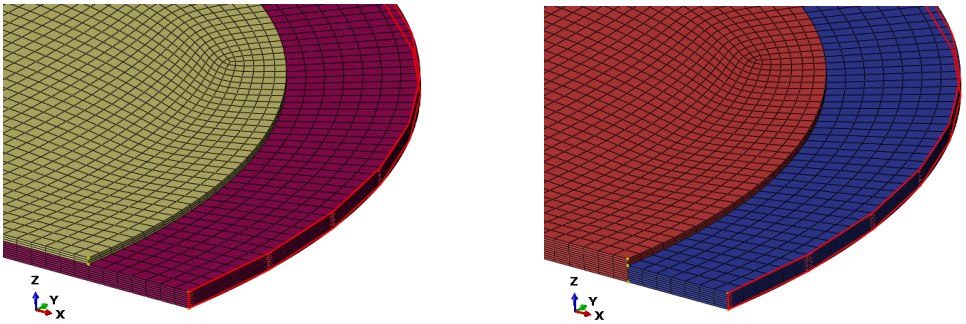

(a) Heterogeneous Macro-Scale Model (b) Homogeneous Macro-Scale Model

Figure 5.19: Material regions, mesh and mechanical BC surface of a) the heterogeneous and b) the homogeneous macro-scale models

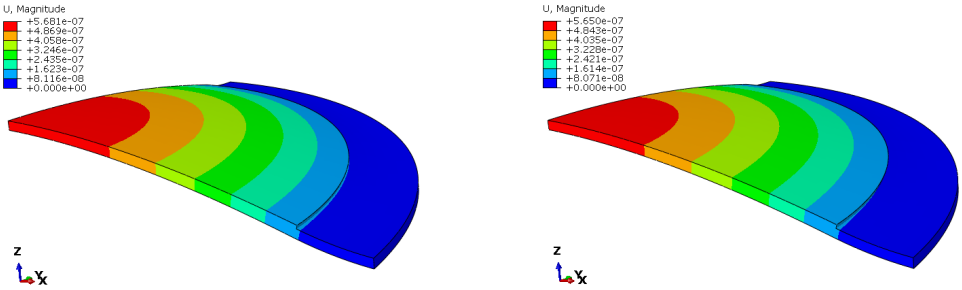

(a) Heterogeneous Macro-Scale Model (b) Homogeneous Macro-Scale Model

Figure 5.20: Displacement contour of a) the heterogeneous and b) the homogeneous macro-scale models under 5 V electrical load.

shim, homogenization is only applied to the interior portion of the model. In Figure 5.19a, yellow and red regions correspond to the APC850 piezoelectric material and shim, while in 5.19b, red and blue regions correspond to the homogenized piezocomposite and shim, respectively. The following model has a radius ratio of 0.85, and 5 V is applied between its surfaces.

The overall displacement distribution of the macro-scale models is shown in Figure 5.20, and it is seen that both models yield almost the same result, which proves the validity of the homogenization method.

Also, to compare our results to Prasad et al. [96], different radii of the piezoelectric

plate are analyzed, and the deflection of the middle point on the piezoelectric plate vs. ratio of the radii of the piezoelectric plate to the shim plate curve is drawn as shown in Figure 5.21. There is some discrepancy between these two results, but they show the same trend. Nonetheless, the primary purpose of this section, showing the validity of the homogenization method and proving that the macro-model with the homogenized properties gives similar results as the original heterogeneous model, is demonstrated.

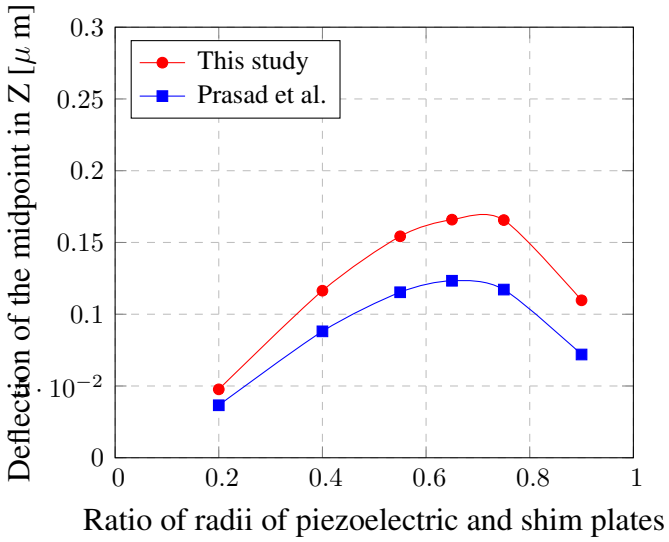

Figure 5.21: Deflection of the middle point for various radii of the piezoelectric plate

CHAPTER 6

POROUS PIEZOCOMPOSITES

Porosity is generally considered as a defect in materials; however, a well-designed porosity in piezoelectric materials can enhance the performance of the piezoelectric material. The pores inside the material actually lower the mechanical and piezoelectric material properties. Nevertheless, figures of merit calculated for piezoelectric materials increase as the porosity increases. This behavior is due to a partial coupling between the longitudinal and transverse effects [99]. Porosity leads to higher values of FOMs and lowers acoustic impedance values, causing an improved acoustic performance in ultrasonic applications.

In this chapter, the generation of porosity and its effects on the effective coefficients and the figures of merit are explained. Later, analyses of porous piezoceramics and porous piezocomposites are conducted.

6.1 Generation of Porosity

Pores usually are generated by some external post-treatments after the piezoelectric material is manufactured. The space that pores will replace, is usually filled with other materials in preprocessing. These materials are then removed by thermal treatment. This method is the most resorted method, and it is called the "Sacrificial Template Method" or the "BurPS (Burn out Polymer Sphere) Process". There are also other techniques, namely the "Replica Technique" or "Direct Foaming" [28], [99]. These techniques are shown in Figure 6.1.

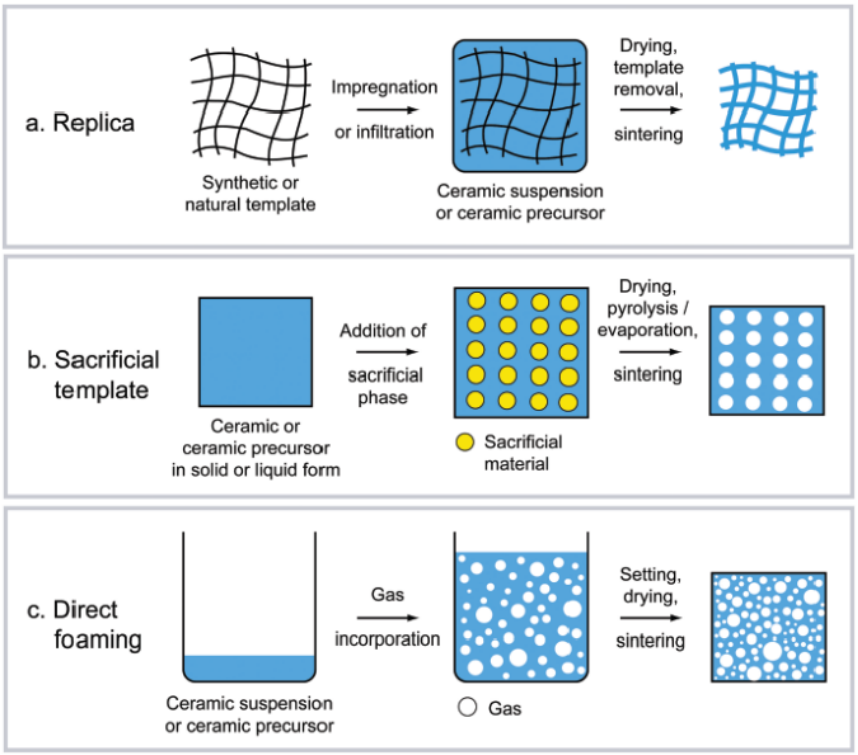

Figure 6.1: Porosity Manufacturing Techniques [100]

6.1.1 Sacrificial Template Method

In this method, simply put, pre-filled materials are evaporated with heat from the piezoelectric material. The most common sacrifice materials are polyethylene oxide (PEO) and poly(methyl methacrylate) (PMMA), polyvinyl chloride (PVC), the polystyrene (PS). [99], [101]. Organic sacrifice materials can be removed with thermal treatments, but some chemical treatments must be applied to remove inorganic sacrifice materials. However, this technique is applicable only for inclusion percentages lower than 70% [102]. The size of the pores depends on the size of the sacrificial materials, usually varying from 2 to 100 micrometers [100].

In this method, overlapping of the pores is minimized; pores can only barely touch each other at their boundaries.

6.1.2 Replica Technique

In this method, a prepared template is impregnated into a ceramic suspension and then removed, resulting in a macro-porous ceramic. However, a drawback of this method is that the minimum cell size is limited to around 200 micrometers [100].

6.1.3 Direct Foaming

This method, on the other hand, uses the incorporation of air bubbles into the ceramic material. The more amount of gas incorporated into the ceramic suspension, the higher level of porosity is obtained. However, the pore size is depended on the stability of the wet foam, which is known before the setting process occurs. With controlled foam stability and setting kinetics, pore sizes ranging from 35 micrometers to 1.2 mm have been achieved [100].

Unlike the sacrificial templated method, direct foaming can cause overlapping of the pores because, during the process, air bubbles can intersect each other and merge [28].

6.2 Calculation of Hydrostatic Performance Coefficients

Hydrostatic performance coefficients were mentioned in Section 3.11 in Chapter 3. However, for completeness, the equations are explicitly shown here, too.

Piezoelectric equations can be written in the stress-electric displacement form as shown in (4.1), or can be written as shown in the following form:

$$\begin{aligned} \boldsymbol{\epsilon} &= \boldsymbol{s^E} \cdot \boldsymbol{\sigma} + \boldsymbol{d}^T \cdot \boldsymbol{E}, \\ \boldsymbol{D} &= \boldsymbol{d} \cdot \boldsymbol{\sigma} + \boldsymbol{\varepsilon^\sigma} \cdot \boldsymbol{E} \end{aligned} \tag{6.1}$$

where $\boldsymbol{\sigma}$ and $\boldsymbol{\epsilon}$ are stress and strain vectors, respectively. $\boldsymbol{E}$ and $\boldsymbol{D}$ are the electric field and the electric displacement vectors, respectively. $\boldsymbol{s^E}$ is the compliance matrix at a constant electric field, $\boldsymbol{d}$ is the piezoelectric strain coefficient, $\boldsymbol{\varepsilon^\sigma}$ is the dielectric

matrix at a constant stress. In order to get this set of equations, we need to have the following necessary relationship:

$$\begin{aligned} \boldsymbol{s^E} &= \boldsymbol{C^{E^{-1}}}, \\ \boldsymbol{d} &= \boldsymbol{e} \cdot \boldsymbol{s^E}, \\ \boldsymbol{\varepsilon^\sigma} &= \boldsymbol{\varepsilon^S} + \boldsymbol{d} \cdot \boldsymbol{C^{E^{-1}}} \cdot \boldsymbol{d^T} \end{aligned} \tag{6.2}$$

By using the relations given in (6.2), we can calculate the hydrostatic performance coefficients d_h and g_h as shown in (6.3).

$$\begin{aligned} d_h &= 2d_{31} + d_{33} \\ g_h &= 2g_{31} + g_{33} = \frac{d_h}{\varepsilon_{33}^\sigma} \end{aligned} \tag{6.3}$$

6.3 Analysis of Porous Piezoceramics

Porous piezoceramic materials possess high hydrostatic figures of merit, lower acoustic impedance mismatch with respect to the medium, and low mechanical quality factor, which is a subject of vibration.

By controlling the porosity density/size or the morphology of the pores, desired characteristics can be achieved.

The grade of anisotropy of a composite is determined by its constituents. Moreover, since the piezoelectric material is transversely isotropic, air inclusion must be isotropic or transversely isotropic at most not to violate the assumptions that already been made. The air itself is isotropic, but the shape and distribution of pores can affect the overall anisotropy of the piezoceramic. Therefore, air inclusion the shape of perfect spheres or in the shapes of ellipses or cylinders elongated along the normal direction of the plane of isotropy, which is direction 3, comply the assumptions of the transversely isotropic analysis.

The analysis procedure of porous piezoceramics is very similar to that of two-phase piezocomposites. The extraction of effective coefficients is the same, but the postpro-

cessing calculations differ.

Porosity can be in any shape in FEM however, in reality, pores generally are produced in the shape of a sphere or cylinder. Therefore, only spherical or cylindrical pores will be examined.

6.3.1 Modelling

The finite element model can include the pore geometry as a solid domain or not. The example RVE models are shown in Figure 6.2, where the pores are indicated with the white region and piezoceramics with grey. By treating pores as empty spaces, we do not have meshes in pore domains and we simulate the real case; however, this brings complexity to the RVE model. The more straightforward method is to model the pore geometry with appropriately chosen material properties. For phases modeled as pores, very low elastic properties ($E = 100\,Pa$), zero piezoelectric properties, and relative permittivity of vacuum ($\varepsilon = 1$) can be used.

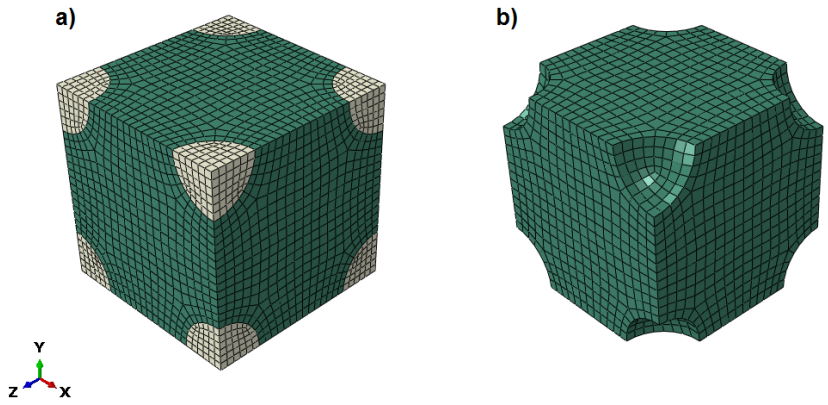

Figure 6.2: Two modeling examples, in which a) pore is modeled and b) pore is not modeled

Since the purpose is to obtain hydrostatic performance coefficients, we only need to get coefficients C_{11}^{eff}, C_{12}^{eff}, C_{13}^{eff}, C_{33}^{eff}, e_{13}^{eff}, e_{33}^{eff}, and ε_{33}^{eff} because other coefficients did not affect the hydrostatic coefficients d_h and g_h.

Since these effective coefficients can be obtained properly with displacement boundary conditions (DBC), either DBC or periodic boundary conditions (PBC) can be

used.

To see the effects of modeling pores or not and boundary conditions, the following three cases under mechanical loading in X are compared:

- Modeling pores as solid domains and using DBC
- Modeling pores as solid domains using PBC
- Modeling pores as empty domains and using DBC

The RVE model consists of 90% PZT-5A content and 10% pore content. Pores are modeled as two spheres, one of which is a full sphere at the center of the cube, and the other is divided into eight and located at the corners.

The von Mises stress distribution results for mechanical loading in X-direction are shown in Figure 6.3. It can be seen that the contours and the deformation state of the piezoceramic phase are very similar. The deformed shape of the pores differ depending on the BC but it is not of interest.

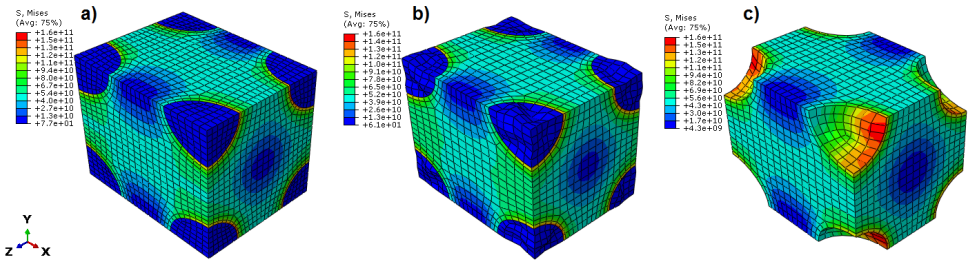

Figure 6.3: Under mechanical loading in X-direction, von Mises stress distribution in deformed shape of a) BC with pore geometry, b) PBC with pore geometry and c) PBC without pore geometry

As seen in Table 6.1, all three results are in close agreement and there is an insignificant difference between the three. Therefore, instead of modeling pores as vacancies in the mesh domain, we can model the pore phase with appropriate material parameters.

Moreover, either DBC or PBC yields close results. Although DBC is known to be stiffer than PBC, when the second phase is air, this is not valid anymore. If some

Table 6.1: Comparison of pore modeling techniques for 10% pore volume fraction. The units are in GPa, $\mathrm{C/m^2}$ and $\mathrm{nF/m}$, respectively.

Modelling	C_{11}^{eff}	C_{12}^{eff}	e_{13}^{eff}	e_{33}^{eff}	ε_{33}^{eff}
DBC with pore geometry	91.503	53.705	-3.179	14.123	6.627
PBC with pore geometry	91.672	53.805	-3.205	14.132	6.605
PBC without pore geometry	91.635	53.756	-3.207	14.130	6.599

other materials not too soft compared to PZT-5A were used as the second phase, the DBC result would be greater.

6.3.2 Comparison with literature data

In this section, the analyses conducted in the study of Martinez et al. [28] are reproduced. In their study, both the numerical FEA solution and analytical Mori-Tanaka solution are presented.

PZT-5A is used as piezoceramic, and the material properties are shown in Table 5.2. Analyses are conducted for three different pore volume fractions 10%, 30%, and 50%. For each pore volume fraction value, effective coefficients are tabulated and compared. These are shown in Tables 6.2, 6.3, and 6.4. The results indicate that this study agrees with the numerical and analytical resultd of Martinez et al[28]. and the analytical result, with a slight increase in higher pore volume fractions. ε_{33}^{eff} values in the article seemed incorrect and inconsistent with the material value. In [28] the effective ε_{33}^{eff} values for various pore volume ratios were found greater than the ε_{33} of PZT-5A, which is not possible.

Also, the hydrostatic performance coefficients for each volume fraction are evaluated and plotted in Figures 6.4 and 6.5. As can be seen, the difference between this study and Martinez's numerical study is minimal for both d_h and g_h. All three solutions gave close results for d_h. However, Mori-Tanaka's solution overpredicts g_h compared to numerical methods. This might be due to the difference in ε_{33}^{eff} values obtained with Mori-Tanaka's solution.

Table 6.2: Comparison for 10% pore volume fraction. Note that the units are in GPa, $\mathrm{C/m^2}$ and $\mathrm{nF/m}$, respectively.

	C_{11}^{eff}	C_{12}^{eff}	C_{13}^{eff}	C_{33}^{eff}	e_{13}^{eff}	e_{33}^{eff}	ε_{33}^{eff}
This study	91.490	53.692	52.649	82.184	-3.179	14.123	6.627
Martinez et al. [28]	90.321	52.833	51.902	81.406	-3.050	14.084	13.214**
Difference	1.3 %	1.6 %	1.4 %	1.0 %	4.2 %	0.3 %	-49.8 %
Mori-Tanaka [28]	91.955	54.693	53.091	82.355	-3.099	14.168	12.517**
Difference	-0.5 %	-1.8 %	-0.8 %	-0.2 %	2.6 %	-0.3 %	-47.1 %

** Plotted values of ε_{33}^{eff} seemed incorrect and inconsistent in the paper [28].

Table 6.3: Comparison for 30% pore volume fraction. Note that the units are in GPa, $\mathrm{C/m^2}$ and $\mathrm{nF/m}$, respectively.

	C_{11}^{eff}	C_{12}^{eff}	C_{13}^{eff}	C_{33}^{eff}	e_{13}^{eff}	e_{33}^{eff}	ε_{33}^{eff}
This study	53.686	29.289	28.055	47.231	-0.618	10.536	5.157
Martinez et al. [28]	52.353	28.357	27.120	46.484	-0.631	10.103	9.713**
Difference	2.5 %	3.3 %	3.4 %	1.6 %	-2.1 %	4.3 %	-46.9 %
Mori-Tanaka [28]	55.504	30.263	27.987	47.736	-0.792	10.415	8.420**
Difference	-3.3 %	-3.2 %	0.2 %	-1.1 %	-22.0 %	1.2 %	-38.7 %

** Plotted values of ε_{33}^{eff} seemed incorrect and inconsistent in the paper [28].

Table 6.4: Comparison for 50% pore volume fraction. Note that the units are in GPa, $\mathrm{C/m^2}$ and $\mathrm{nF/m}$, respectively.

	C_{11}^{eff}	C_{12}^{eff}	C_{13}^{eff}	C_{33}^{eff}	e_{13}^{eff}	e_{33}^{eff}	ε_{33}^{eff}
This study	29.697	15.569	14.801	26.188	0.302	6.607	3.463
Martinez et al. [28]	28.556	14.759	13.913	25.625	0.277	6.458	6.449**
Difference	4.0 %	5.5 %	6.4 %	2.2 %	9.0 %	2.3 %	-46.3 %
Mori-Tanaka [28]	32.179	16.360	14.500	27.106	0.060	6.869	5.275**
Difference	-7.7 %	-4.8 %	2.1 %	-3.4 %	401.2* %	-3.8 %	-34.4 %

* e_{13}^{eff} values nearing zero cause large percent differences.

** Plotted values of ε_{33}^{eff} seemed incorrect and inconsistent in the paper [28].

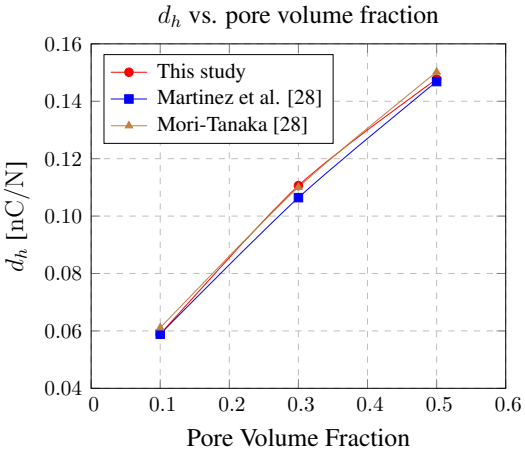

Figure 6.4: d_h versus pore volume fraction

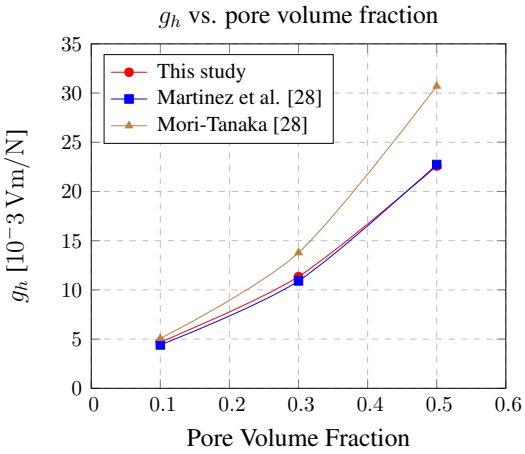

Figure 6.5: g_h versus pore volume fraction

6.3.3 Effect of Pore Shapes

In this section, the effects of pore shapes are investigated. Since the air itself is isotropic, the shape of the pore geometry can cause anisotropy overall. As the transverse isotropy must be preserved in the RVE models, air inclusions can be modeled as perfect spheres or as ellipses and cylinders elongated along the normal direction of the plane of isotropy.

For comparison, while keeping the pore volume fraction at 10 %, we model the pore shape as follows:

- Perfect sphere
- Ellipse having aspect ratio of 1.53 aligned with the Z axis (axis of isotropy)
- Cylinder aligned with the Z axis

Models with three distinct pore shapes are shown in Figure 6.6.

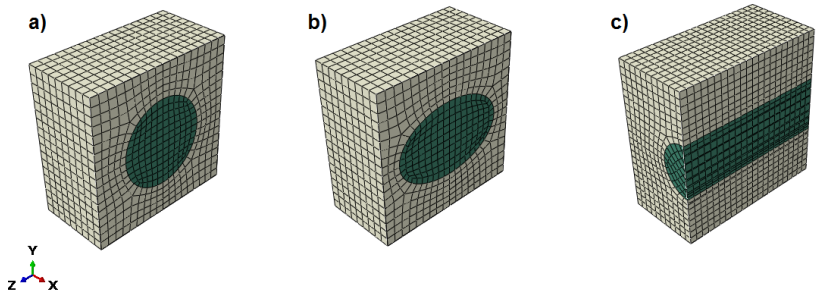

Figure 6.6: Cut-views of the RVEs that contain 10 $\%$ pore in the shape of a) perfect sphere, b) ellipse aligned with Z axis c) cylinder aligned with Z axis

Table 6.5: Effective properties comparison of different pore shapes at the same volume fraction 10 $\%$. Note that the units are in GPa, $\mathrm{C/m^2}$ and $\mathrm{nF/m}$, respectively.

Pore Shape	C_{11}^{eff}	C_{12}^{eff}	C_{13}^{eff}	C_{33}^{eff}	e_{13}^{eff}	e_{33}^{eff}	ε_{33}^{eff}
Perfect Sphere	93.529	54.704	53.176	83.157	-3.403	14.262	6.531
Ellipse aligned with Z	89.505	51.295	52.106	85.023	-3.369	14.794	6.615
Cylinder aligned with Z	80.618	43.625	47.572	84.550	-3.416	15.344	6.702

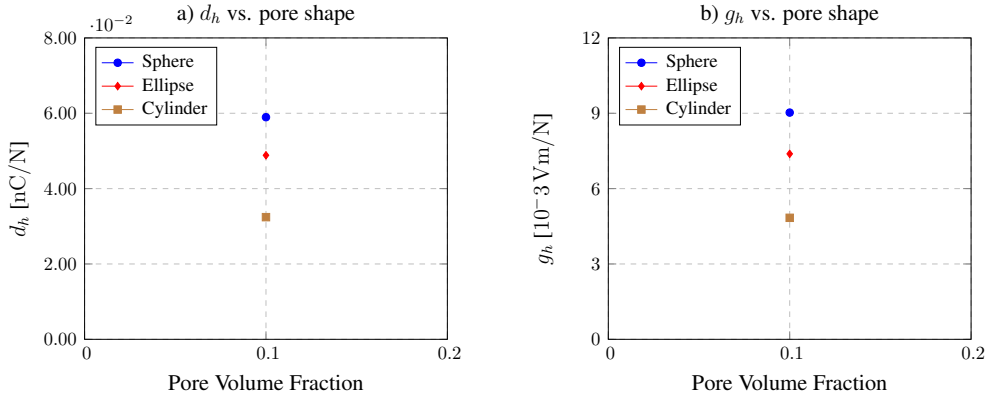

Figure 6.7: a) d_h and b) g_h versus pore shape

The effective coefficients are tabulated in Table 6.5, and the hydrostatic performance coefficients are shown in Figure 6.7. It can be seen that the spherical sphere yields the highest d_h and g_h values. This might be attributed to the lowest C_{33}^{eff} value it has because C_{33}^{eff} is known to be dominant in d_h and g_h calculation, and smaller C_{33}^{eff} yields higher d_h and g_h values.

6.3.4 Effect of Pore Size

In this section, the effect of pore size will be investigated. For this purpose, RVEs having a single spherical central pore with pore fractions of 0%, 10%, 20%, and 30% are analyzed.

Table 6.6: Effective properties of porous piezoceramics with spherical pores at varying volume fractions. Note that the units are in GPa, $\mathrm{C/m^2}$ and $\mathrm{nF/m}$, respectively.

Pore Fraction	C_{11}^{eff}	C_{12}^{eff}	C_{13}^{eff}	C_{33}^{eff}	e_{13}^{eff}	e_{33}^{eff}	ε_{33}^{eff}
0* %	121.000	75.400	75.200	111.000	-5.400	15.800	7.349
10 %	93.529	54.704	53.176	83.157	-3.403	14.262	6.531
20 %	72.996	39.535	37.552	63.284	-2.222	12.549	5.625
30 %	56.864	28.134	26.106	48.293	-1.400	10.737	4.704

* (Pure PZT-5A)

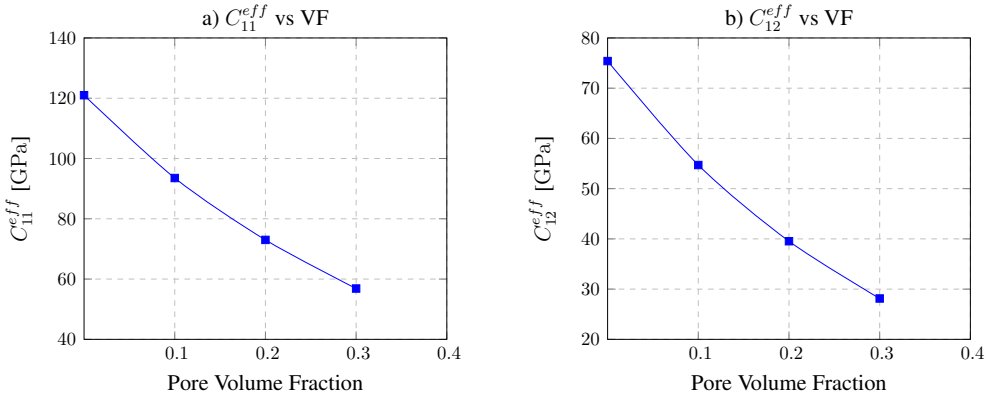

Figure 6.8: a) C_{11}^{eff} and b) C_{12}^{eff} versus pore volume fraction

As can be seen from Table 6.6 and Figures 6.8-6.11, more pore content means lower effective material coefficients as expected because the material content decreases.

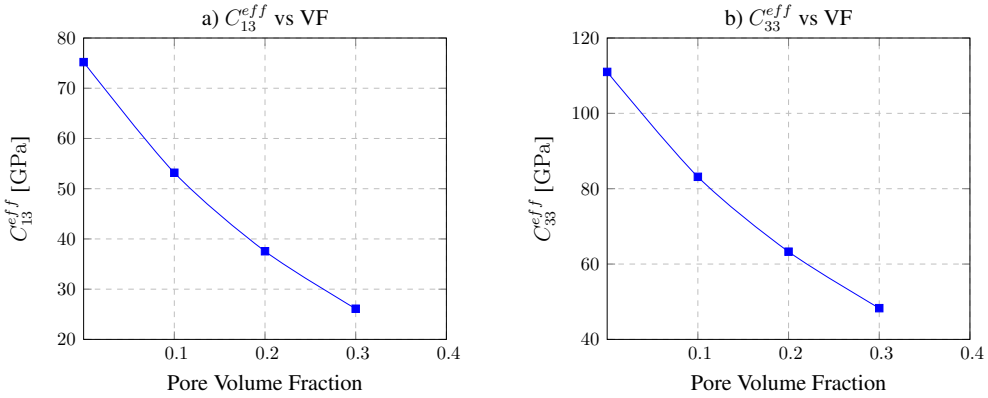

Figure 6.9: a) C_{13}^{eff} and b) C_{33}^{eff} versus pore volume fraction

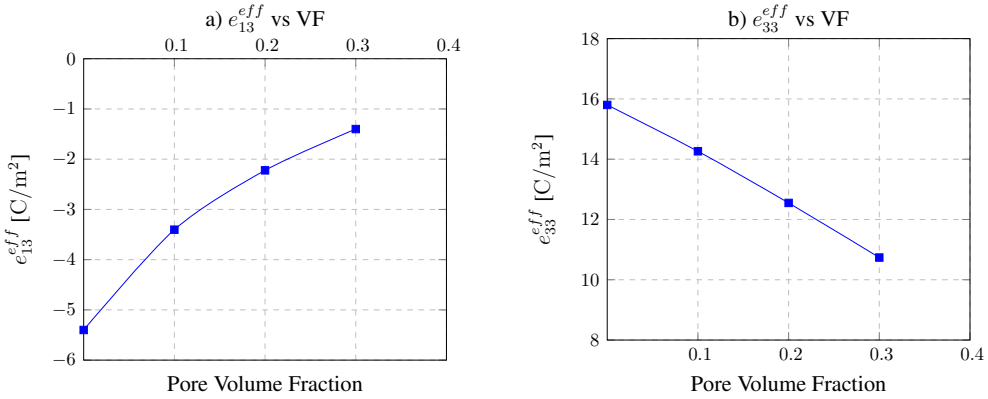

Figure 6.10: a) e_{13}^{eff} and b) e_{33}^{eff} versus pore volume fraction

However, as the pore volume ratio increases, hydrostatic performance coefficients d_h and g_h increase, as shown in Figure 6.12, which is a beneficial result of the addition of pores.

6.3.5 Effect of Spherical Pore Configuration

In this section, different configurations of spherical pores are investigated. While keeping the pore volume fraction constant, the location of the spheres and/or the number of pores are altered to see the effect of the distribution of the spherical pores.

For comparison, the following three configurations are analyzed:

- Model a: Single spherical pore at the center of the RVE

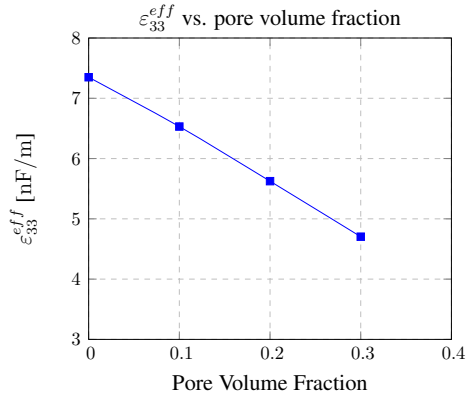

Figure 6.11: ε_{33}^{eff} versus pore volume fraction

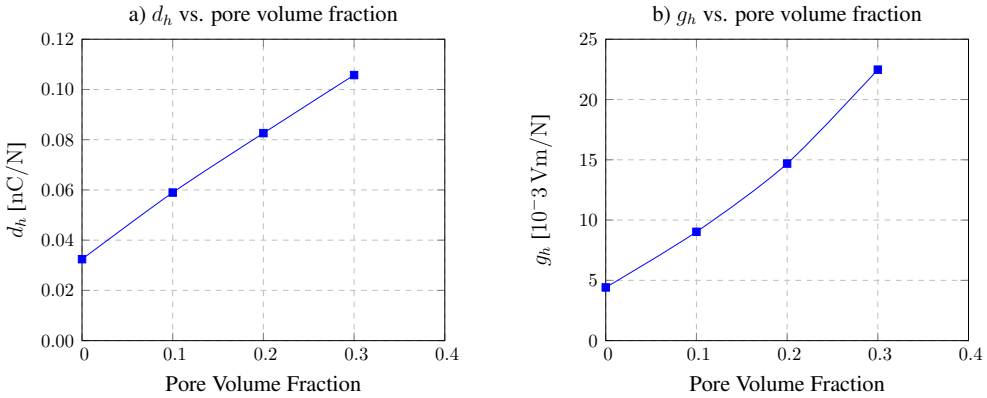

Figure 6.12: a) d_h and b) g_h versus pore volume fraction

- Model b: Two spherical pores; one at the center and the other is divided into 1/8 spheres located at the corners
- Model c: Two spherical pores aligned in the axis of isotropy

Three spherical pore models are shown in Figure 6.13.

Table 6.7: Effective properties of piezoceramics with spherical pores at varying volume fractions. Note that the units are in GPa, $\mathrm{C/m^2}$ and $\mathrm{nF/m}$, respectively.

Sphere Configuration	C_{11}^{eff}	C_{12}^{eff}	C_{13}^{eff}	C_{33}^{eff}	e_{13}^{eff}	e_{33}^{eff}	ε_{33}^{eff}
Model a	93.529	54.704	53.176	83.157	-3.403	14.262	6.531
Model b	91.503	53.705	52.649	82.184	-3.179	14.123	6.627
Model c	90.387	52.063	52.061	84.820	-3.524	14.746	6.598

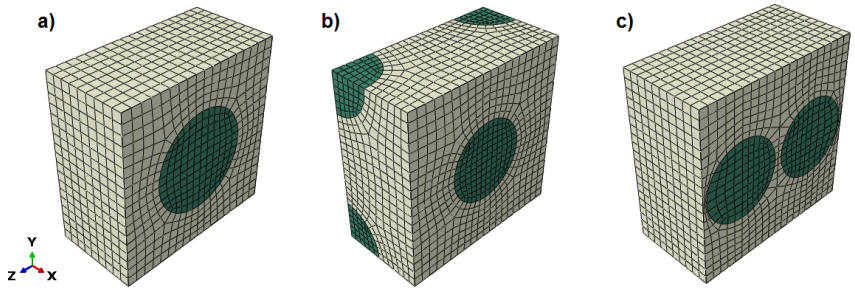

Figure 6.13: Cut-views of the RVEs that contain 10 % pore in the shape of a) single sphere, b) two spheres, one in the middle and the other divided into 1/8 located at the corners, and c) two spheres aligned in the axis of isotropy

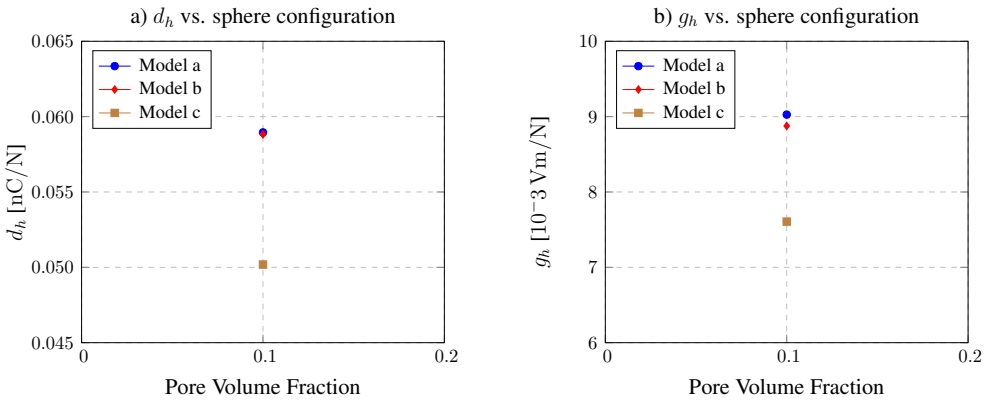

Figure 6.14: a) d_h and b) g_h versus spherical pore configuration

The effective coefficients are tabulated in Table 6.7, and the hydrostatic performance coefficients are shown in Figure 6.14. It can be seen that Model a and Model b are very close to each other, as expected. On the other hand, Model c is found to be the worst configuration of all when hydrostatic performance coefficients are considered.

6.3.6 Effect of Cylindrical Pore Configuration

In this section, different configurations of cylindrical pores are investigated. While keeping the pore volume fraction constant, the location and/or the number of cylinders are altered to see the effect of the distribution of the cylindrical pores.

For comparison, the following three configurations are analyzed:

- Model a: Single cylindrical pore at the center of the RVE
- Model b: Two cylindrical pores, one at the center and the other divided into 1/4 located at the edges
- Model c: Two cylindrical pores aligned in the axis of isotropy

Three spherical pore models are shown in Figure 6.15.

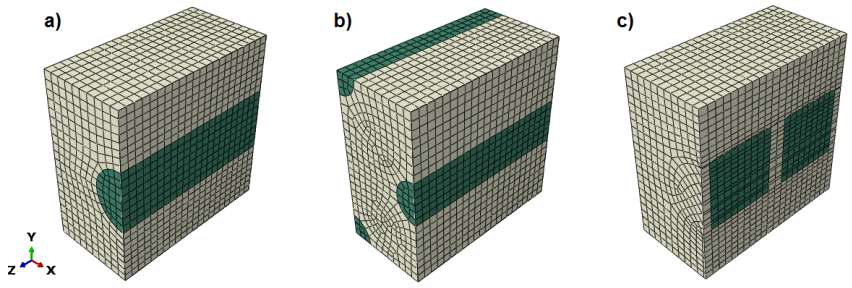

Figure 6.15: Cut-views of the RVEs that contain 10 $\%$ pore in the shape of a) a single cylinder, b) two cylinders, one at the center and the other divided into 1/4 located at the edges, and c) two cylinders aligned in the axis of isotropy

Table 6.8: Effective properties of piezoceramics with cylindrical pores at varying volume fractions. Note that the units are in GPa, $\mathrm{C/m^2}$ and $\mathrm{nF/m}$, respectively.

Cylinder Configuration	C_{11}^{eff}	C_{12}^{eff}	C_{13}^{eff}	C_{33}^{eff}	e_{13}^{eff}	e_{33}^{eff}	ε_{33}^{eff}
Model a	80.723	43.690	47.639	84.616	-3.421	15.345	6.704
Model b	80.284	45.291	48.082	85.032	-3.453	15.348	6.713
Model c	87.261	49.223	49.995	83.924	-3.548	14.890	6.559

The effective coefficients are tabulated in Table 6.8, and the hydrostatic performance coefficients are shown in Figure 6.16. It can be seen that Model a and Model b yielded the same result, as expected. These two configurations were also found similar in the spherical configuration section. On the other hand, Model c is found to be the best configuration of all when hydrostatic performance coefficients are considered. This might be due to the low C_{33}^{eff} and low ε_{33}^{eff} values.

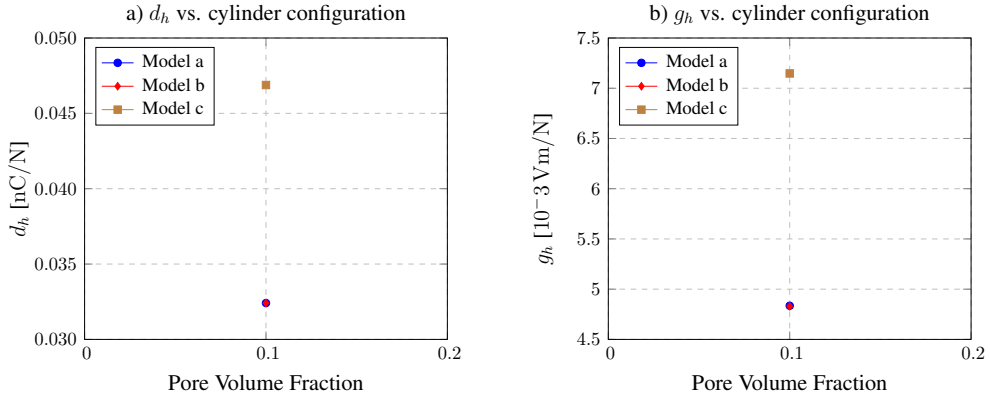

Figure 6.16: a) d_h and b) g_h versus cylindrical pore configuration

6.4 Analysis of Porous Piezocomposites

This section combines porous piezoceramics and matrix materials to get the porous piezocomposites. To this end, the piezoelectric phase of the 1-3 piezocomposites is substituted with porous ceramics. Homogenized properties of the porous piezoceramics are inserted into the piezoelectric phase, and the porous piezocomposites are analyzed. Finally, the effective coefficients and performance coefficients are calculated.

The studied 1-3 piezocomposite is made of cylindrical PZT-5A fiber and epoxy, whose material properties are given in Table 5.3. In this section, a two-step homogenization method is followed. First, piezoceramics with spherical pores will be analyzed, as shown if Figure 6.17a. The reason why the pores are taken as spherical is that the pores in piezoceramics are usually manufactured spherical in practice, and consequently, most studies modeled the pores as spherical, too. After calculating the complete set of homogenized material properties of porous piezoceramics, we insert them into the piezoelectric fiber region of the two-phase 1-3 piezocomposite (see Figure 6.17b) and calculate the final material properties.

In all analyses, the epoxy volume fraction was fixed at 40%. The addition of pore causes a reduction in fiber volume fraction. Therefore, volume fractions of pore and PZT-5A always add up to 60%.

The effective material properties of piezocomposite for varying pore volume frac-

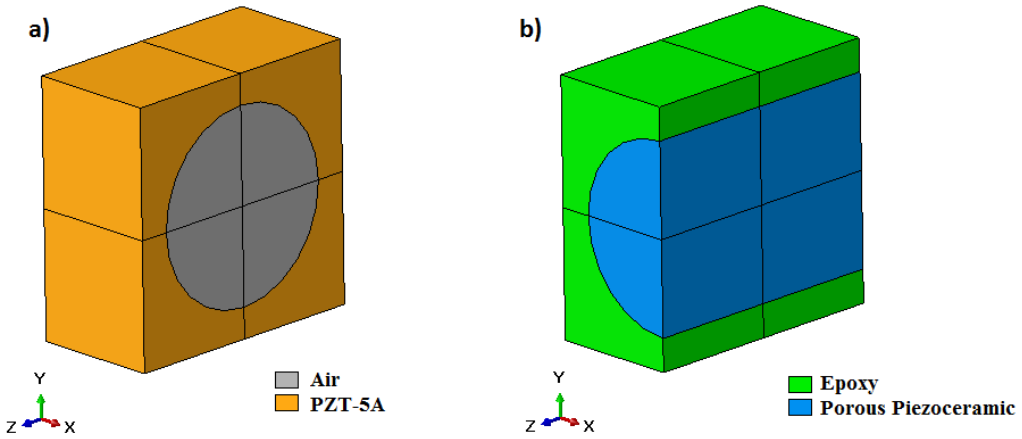

Figure 6.17: Cut-views of the RVE models of a) the porous piezoceramic and b) the porous piezocomposite

tions are tabulated in Table 6.9. As expected, the addition of pore degrades the effective material properties because adding an amount of pore means removing the same amount of piezoceramic. Some material coefficients were affected more than the loss of the piezoceramic material. For example, increasing pore content from 0% to 30% halved the PZT-5A content; however, material coefficients like C_{33}^{eff}, e_{13}^{eff}, e_{33}^{eff}, and ε_{33}^{eff} decreased more than two times. Only mechanical coefficients, except C_{33}^{eff}, decreased less than two times. These observations conclude that the addition of pore substantially affects the piezoelectric, dielectric, and axial mechanical coefficient in fiber direction negatively. Therefore, there might be a limit to the addition of pores regarding the composite requirements determined according to the operating conditions.

Table 6.9: Effective properties of porous piezocomposites with varying pore volume fraction and with fixed 40% epoxy content. Note that the units are in GPa, $\mathrm{C/m^2}$ and $\mathrm{nF/m}$, respectively.

Pore Fraction	PZT-5A Fraction	C_{11}^{eff}	C_{12}^{eff}	C_{13}^{eff}	C_{33}^{eff}	e_{13}^{eff}	e_{33}^{eff}	ε_{33}^{eff}
0* %	60 %	12.480	4.975	6.785	37.993	-0.313	11.697	4.601
10 %	50 %	11.919	4.871	6.081	29.314	-0.227	8.751	3.639
20 %	40 %	11.208	4.659	5.298	22.348	-0.172	6.426	2.707
30 %	30 %	9.966	4.175	4.215	15.434	-0.113	4.232	1.813

* (Nonporous PZT-5A-Epoxy piezocomposite)

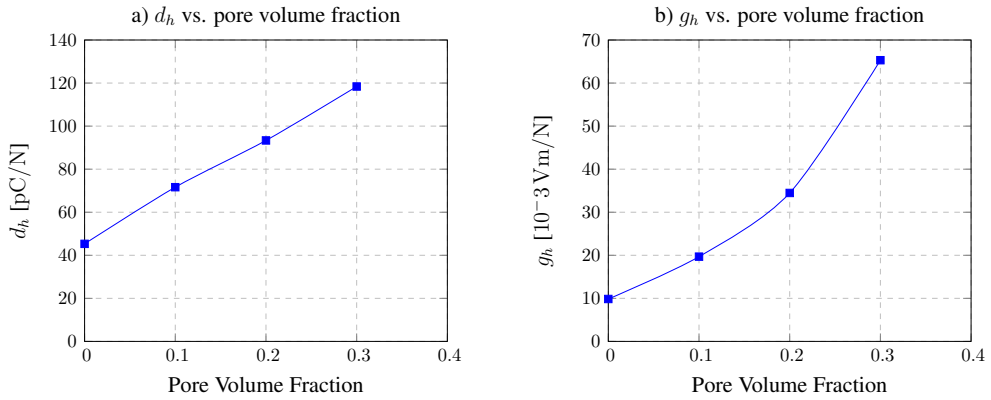

Figure 6.18: a) d_h and b) g_h versus pore volume fraction in piezocomposite made of PZT-5A and epoxy

After obtaining the homogenized properties, we can calculate the hydrostatic performance coefficients, plotted in Figure 6.18. As can be seen, any amount of pore increases the hydrostatic performance coefficients. These increases occur linearly for d_h but quadratically for g_h. This behavior was already observed in Section 6.3 while studying porous piezoceramics. While adding 20% pore doubles d_h, it increases g_h more than three times. At higher pore content, this difference will be much higher. Therefore, for higher hydrostatic performance coefficients, depending on the performance coefficient requirement, some amount of pore content can be added to the piezoelectric fiber of the piezocomposites. However, it should be noted that higher pore content means degraded effective material coefficients for piezocomposites. Therefore, the effective mechanical coefficients should also be checked. Insufficient stiffness can spoil the operation of the piezocomposite, no matter how high its hydrostatic performance coefficients are.

CHAPTER 7

CONCLUSION

In this chapter, comments about the results will be made and the conclusions drawn will be mentioned.

The ability of piezoelectric materials to convert energy between mechanical and electrical interactions makes them useful for sensing and actuation applications. However, because of their brittleness, the need for more compliant piezoelectric structures emerged, leading to the development of piezocomposites (or piezoelectric composites). The behavior of piezocomposites can be estimated using analytical or numerical micromechanical approaches. In this thesis, the latter is studied.

The homogenization method is used to estimate the effective material coefficients of the piezocomposites. In the commercial FE software program ABAQUS, a unit cell model of a piezocomposite is created and analyzed with appropriate loading and boundary conditions. After post-processing, the effective material coefficients and figure of merits are calculated.

The results are compared to experimental, analytical, and numerical results from the literature to verify the method used in this thesis. In addition, to prove the usability and advantage of the homogenization method, a macro-scale model is created with the effective material properties previously calculated using the homogenization method. The macro-scale model is also analyzed with the original heterogeneous material properties, and these two analyses yielded similar results, proving the validity of the homogenization method.

Overall, some of the effective material coefficients were found to be very sensitive to boundary conditions. Therefore, the appropriate application of boundary conditions is

crucial. The ground rule is that the boundary conditions should be applied so that only the field values (stress, strain, electric field, etc.) related to the material coefficients to be calculated should be non-zero. For example, to calculate C_{11}^{eff} and C_{12}^{eff}, the unit cell should have non-zero stress/strain values only in directions 1 and 2. Moreover, these boundary conditions can be applied more than a single way. It is shown that both PBC and DBC can be used depending on the loading. PBC can be used for any load case, whereas DBC can be used only for axial loadings.

In Chapter 5, two-phase piezocomposites that consist of a piezoelectric fiber and a non-piezoelectric compliant matrix are studied. It is found that the effective material coefficients in the direction of the piezoelectric phase (C_{33}^{eff}, e_{33}^{eff}, and ε_{33}^{eff}) increase linearly with piezoelectric volume fraction for 1-3 piezocomposites. However, for transverse and shear material coefficients, this behavior is nonlinear. Also, the coefficients C_{44}^{eff} and e_{15}^{eff} have notoriety for being the most difficult ones to verify with other methods. In comparison plots of the different methods, C_{44}^{eff} and e_{15}^{eff} have the biggest scatter. This is attributed to the fact that the material values involved in these calculations have significant differences in order, and sometimes it is hard to get a pure shear state mathematically, meaning having exact zero values at other coefficients.

Porous piezoceramics and piezocomposites made of porous piezoceramics are investigated in Chapter 6. It is shown that although porosity decreases the effective material coefficients, the resultant hydrostatic performance coefficients are found to be greater than those of non-porous materials. This behavior is valid for both piezoceramics and piezocomposites with porous piezoelectric fibers. Even high amounts of porosity, such as 30% or 50%, lead to further increases in hydrostatic performance coefficients. Most effective material coefficients are affected more than the predictions of simple rule of mixtures. For example, C_{11}^{eff} decreased from 121 GPa to 93.529 GPa with the addition of 10% porosity to a non-porous piezoceramic. It is seen that the 93.529 GPa is far less than 90% of the material property 121 GPa. On the other hand, e_{33}^{eff} and ε_{33}^{eff} are found in linear proportion to the material content, meaning that 20% porosity yielded 80% of the piezoelectric phase's material properties.

The hydrostatic performance coefficients d_h and g_h for both piezoceramics and piezo-

composites with porous piezoelectric fibers always increase with porosity. These increases happen linearly for d_h and quadratically for g_h. Large percentages of porosity can yield very high g_h values for piezocomposites. Of course, higher hydrostatic performance coefficients may not always mean better, because, at high pore volume fractions, the effective material coefficients decrease significantly. This might be undesirable for some applications that have some stiffness requirements.

Finally, the effects of pore shape and configuration are investigated. The pore volume fraction is always kept at 10%. A single spherical, ellipsoidal, and cylindrical pore is investigated. Both d_h and g_h are found to be greater for spherical pore shape, followed by the ellipsoidal and the cylindrical pore in descending order. Finally, the effects of different pore configurations on hydrostatic performance coefficients are studied for spherical and cylindrical pores.

REFERENCES

[1]K. Uchino, "Piezoelectric composite materials", *Advanced Piezoelectric Materials*, Elsevier, 2017, pp. 353–382.

[2]M. Smith, *ABAQUS/Standard User's Manual, Version 6.9*, English. United States: Dassault Systèmes Simulia Corp, 2009.

[3]R. Pramanik and A. Arockiarajan, "Effective properties and nonlinearities in 1-3 piezocomposites: A comprehensive review", *Smart Materials and Structures*, vol. 28, no. 10, p. 103 001, 2019.

[4]W. A. Smith, "Optimizing electromechanical coupling in piezocomposites using polymers with negative poisson's ratio", *IEEE 1991 Ultrasonics Symposium,*, IEEE, 1991, pp. 661–666.

[5]P. J. Swart and M. Avellaneda, "Role of matrix porosity and poisson's ratio in the design of high-sensitivity piezocomposite transducers", *American Society of Mechanical Engineers, Aerospace Division (Publication) AD*, vol. 45, pp. 59–66, 1994.

[6]J. Bennett and G. Hayward, "Design of 1-3 piezocomposite hydrostatic transducers using finite element analysis", *1994 Proceedings of IEEE Ultrasonics Symposium*, IEEE, vol. 2, 1994, pp. 979–982.

[7]W. A. Smith and B. A. Auld, "Modeling 1-3 composite piezoelectrics: Thickness-mode oscillations", *IEEE transactions on ultrasonics, ferroelectrics, and frequency control*, vol. 38, no. 1, pp. 40–47, 1991.

[8]W. A. Smith, "Modeling 1-3 composite piezoelectrics: Hydrostatic response", *IEEE transactions on ultrasonics, ferroelectrics, and frequency control*, vol. 40, no. 1, pp. 41–49, 1993.

[9]H. L. W. Chan and J. Unsworth, "Simple model for piezoelectric ceramic/polymer 1-3 composites used in ultrasonic transducer applications", *IEEE Transactions on Ultrasonics, Ferroelectrics, and Frequency Control*, vol. 36, no. 4, pp. 434–441, 1989.

[10]R. Guinovart-Dıaz, J. Bravo-Castillero, R. Rodrıguez-Ramos, F. Sabina, and R. Martınez-Rosado, "Overall properties of piezocomposite materials 1–3", *Materials Letters*, vol. 48, no. 2, pp. 93–98, 2001.

[11]M. Dunn and M. Taya, "Micromechanics predictions of the effective electroelastic moduli of piezoelectric composites", *International Journal of Solids and Structures*, vol. 30, no. 2, pp. 161–175, 1993.

[12]H. Berger, S. Kari, U. Gabbert, R. Rodriguez-Ramos, R. Guinovart, J. A. Otero, *et al.*, "An analytical and numerical approach for calculating effective material coefficients of piezoelectric fiber composites", *International Journal of Solids and Structures*, vol. 42, no. 21-22, pp. 5692–5714, 2005.

[13]H. Berger, S. Kari, U. Gabbert, R. Rodriguez-Ramos, J. Bravo-Castillero, R. Guinovart-Diaz, *et al.*, "Unit cell models of piezoelectric fiber composites for numerical and analytical calculation of effective properties", *Smart Materials and Structures*, vol. 15, no. 2, p. 451, 2006.

[14]R. Kar-Gupta and T. Venkatesh, "Electromechanical response of 1–3 piezoelectric composites: An analytical model", *Acta Materialia*, vol. 55, no. 3, pp. 1093–1108, 2007.

[15]——, "Electromechanical response of 1-3 piezoelectric composites: Effect of poling characteristics", *Journal of Applied Physics*, vol. 98, no. 5, p. 054 102, 2005.

[16]——, "Electromechanical response of 1–3 piezoelectric composites: A numerical model to assess the effects of fiber distribution", *Acta Materialia*, vol. 55, no. 4, pp. 1275–1292, 2007.

[17]C. Bowen and H. Kara, "Pore anisotropy in 3–3 piezoelectric composites", *Materials chemistry and physics*, vol. 75, no. 1-3, pp. 45–49, 2002.

[18]M. E. Moreno, V. Tita, and F. D. Marques, "Influence of boundary conditions on the determination of effective material properties for active fiber composites", *Proceedings of the 11th Pan-American congress of applied mechanics*, 2010.

[19]V. Tita, R. de Medeiros, F. D. Marques, and M. E. Moreno, "Effective properties evaluation for smart composite materials with imperfect fiber–matrix adhesion", *Journal of Composite Materials*, vol. 49, no. 29, pp. 3683–3701, 2015.

[20]N. Mishra, B. Krishna, R. Singh, and K. Das, "Evaluation of effective elastic, piezoelectric, and dielectric properties of su8/zno nanocomposite for vertically

integrated nanogenerators using finite element method", *Journal of Nanomaterials*, vol. 2017, 2017.

[21]J. Heiber, F. J. Clemens, T. Graule, and D. Hülsenberg, "Influence of fibre diameter on the microstructure and the piezoelectric properties of pzt-fibres", *Advances in Science and Technology*, Trans Tech Publ, vol. 45, 2006, pp. 2459–2463.

[22]C. N. Della and D. Shu, "On the performance of 1–3 piezoelectric composites with a passive and active matrix", *Sensors and Actuators A: Physical*, vol. 140, no. 2, pp. 200–206, 2007.

[23]L. Li, S. Zhang, Z. Xu, F. Wen, X. Geng, H. J. Lee, *et al.*, "1–3 piezoelectric composites for high-temperature transducer applications", *Journal of physics D: Applied physics*, vol. 46, no. 16, p. 165 306, 2013.

[24]C. N. Della and D. Shu, "Performance of 1–3 piezoelectric composites with porous piezoelectric matrix", *Applied Physics Letters*, vol. 103, no. 13, p. 132 905, 2013.

[25]T. Mori and K. Tanaka, "Average stress in matrix and average elastic energy of materials with misfitting inclusions", *Acta metallurgica*, vol. 21, no. 5, pp. 571–574, 1973.

[26]H. Khanbareh, K. de Boom, B. Schelen, R. Scharff, C. Wang, S. van der Zwaag, *et al.*, "Large area and flexible micro-porous piezoelectric materials for soft robotic skin", *Sensors and Actuators A: Physical*, vol. 263, pp. 554–562, 2017.

[27]A. N. Isaeva and V. Y. Topolov, "Comparative study on the performance of piezo-active 1–3-type composites with lead-free components", *Journal of Advanced Dielectrics*, vol. 11, no. 05, p. 2 160 003, 2021.

[28]G. Martınez-Ayuso, M. I. Friswell, S. Adhikari, H. H. Khodaparast, and H. Berger, "Homogenization of porous piezoelectric materials", *International Journal of solids and Structures*, vol. 113, pp. 218–229, 2017.

[29]H. G. Liddell and R. Scott, *A greek-english lexicon. perseus digital library*, 1940.

[30]G. Gautschi, *Piezoelectric Sensorics: Force Strain Pressure Acceleration and Acoustic Emission Sensors Materials and Amplifiers*. Springer Science & Business Media, 2006.

[31]B. C. Sekhar, B. Dhanalakshmi, B. S. Rao, S. Ramesh, K. V. Prasad, P. S. Rao, *et al.*, "Piezoelectricity and its applications", *Multifunctional Ferroelectric Materials*, p. 71, 2021.

[32]J. Curie and P. Curie, "Sur l'électricité polaire dans les cristaux hémièdres à faces inclinées", *CR Acad Sci Gen*, vol. 91, pp. 383–6, 1880.

[33]A. Manbachi and R. S. Cobbold, "Development and application of piezoelectric materials for ultrasound generation and detection", *Ultrasound*, vol. 19, no. 4, pp. 187–196, 2011.

[34]J. F. Tressler, S. Alkoy, and R. E. Newnham, "Piezoelectric sensors and sensor materials", *Journal of electroceramics*, vol. 2, no. 4, pp. 257–272, 1998.

[35]K. Uchino, *Advanced piezoelectric materials: Science and technology*. Woodhead Publishing, 2017.

[36]V. Buscaglia, M. T. Buscaglia, and G. Canu, "Batio3-based ceramics: Fundamentals, properties and applications", *Journal: Encyclopedia of Materials: Technical Ceramics and Glasses*, pp. 311–344, 2021.

[37]K. Uchino, *Ferroelectric devices, second edition*. Jan. 2009, pp. 1–349.

[38]D. Berlincourt, "Piezoelectric crystals and ceramics", *Ultrasonic transducer materials*, Springer, 1971, pp. 63–124.

[39]J. Waanders, *Piezoelectric ceramics: properties and applications*. Philips Components, 1991.

[40]J. Geusic, H. J. Levinstein, J. Rubin, S. Singh, and L. Van Uitert, "The nonlinear optical properties of ba2nanb5o15", *Applied Physics Letters*, vol. 11, no. 9, pp. 269–271, 1967.

[41]M. Choy, K. Hellwege, W. Cook, A. Hellwege, R. Hearmon, H. Jaffe, *et al.*, *Elastic, Piezoelectric, Pyroelectric, Piezooptic, Electrooptic Constant, and Nonlinear Dielectric Susceptibilities of Crystals / Elastische, piezoelektrische, pyroelektrische, piezooptische, elektrooptische Konstantenund nichtlineare dielektrische Suszept*, ser. Landolt-Börnstein: Numerical Data and Functional Relationships in Science and Technology - New Series. Springer Berlin Heidelberg, 1978, ISBN: 9783540085065.

[42]T. Ikeda, "Fundamentals of piezoelectricity (oxford university press, 1990).",

[43]Y. Xu, *Ferroelectric materials and their applications*. Elsevier, 2013.

[44]M. Shabara, A. Rahman Badawi, and T.-B. Xu, "Comprehensive piezoelectric material application issues on energy harvesting for artificial intelligence systems", *AIAA Scitech 2020 Forum*, 2020, p. 1862.

[45]T. Steinkopff, "Finite-element modelling of ferroic domain switching in piezoelectric ceramics", *Journal of the European Ceramic Society*, vol. 19, no. 6-7, pp. 1247–1249, 1999.

[46]L. APC International, *Piezoelectric Ceramics: Principles and Applications*. APC International, 2011, ISBN: 9780615565033. [Online]. Available: `https://books.google.com.tr/books?id=nUafpwAACAAJ`.

[47]V. F. Janas and A. Safari, "Overview of fine-scale piezoelectric ceramic/polymer composite processing", *Journal of the American Ceramic Society*, vol. 78, no. 11, pp. 2945–2955, 1995.

[48]R. Newnham, D. Skinner, and L. Cross, "Connectivity and piezoelectric-pyroelectric composites", *Materials Research Bulletin*, vol. 13, no. 5, pp. 525–536, 1978.

[49]R. E. Newnham, L. Bowen, K. Klicker, and L. Cross, "Composite piezoelectric transducers", *Materials & Design*, vol. 2, no. 2, pp. 93–106, 1980.

[50]K.-i. Sakayori, Y. Matsui, H. Abe, E. Nakamura, M. Kenmoku, T. Hara, *et al.*, "Curie temperature of batio3", *Japanese journal of applied physics*, vol. 34, no. 9S, p. 5443, 1995.

[51]P. V. Balachandran, D. Xue, and T. Lookman, "Structure–curie temperature relationships in batio 3-based ferroelectric perovskites: Anomalous behavior of (ba, cd) tio 3 from dft, statistical inference, and experiments", *Physical Review B*, vol. 93, no. 14, p. 144 111, 2016.

[52]PEP Products, *PZT5H Materials (Soft PZT) Technical Data (Typical Values)*, `https://ctscorp.com/wp-content/uploads/2015/11/PEP_PZT5H_DATA.pdf`, [Online; accessed 29-November-2022], 2004.

[53]J. P. Praveen, T. Karthik, A. James, E. Chandrakala, S. Asthana, and D. Das, "Effect of poling process on piezoelectric properties of sol–gel derived bzt–bct ceramics", *Journal of the European Ceramic Society*, vol. 35, no. 6, pp. 1785–1798, 2015.

[54]S. Sharma, R. Kumar, M. Talha, and R. Vaish, "Design of spatially varying electrical poling for enhanced piezoelectricity in pb (mg1/3nb2/3) o3–0.35 pbtio3",

International Journal of Mechanics and Materials in Design, vol. 17, no. 1, pp. 99–118, 2021.

[55]B. Jaffe, W. Cook, and H. Jaffe, "The piezoelectric effect in ceramics", *Piezoelectric Ceramics*, pp. 7–21, 1971.

[56]D. J. Leo, *Engineering analysis of smart material systems*. John Wiley & Sons, 2007.

[57]K. Uchino, *Ferroelectric devices*. CRC press, 2018.

[58]Alfa Aesar, *Material Safety Data Sheet*, https://web.archive.org/web/20110719173104/http://www.alfa.com/content/msds/USA/35671.pdf, [Online; accessed 29-November-2022], 2011.

[59]R. Turner, P. A. Fuierer, R. Newnham, and T. R. Shrout, "Materials for high temperature acoustic and vibration sensors: A review", *Applied acoustics*, vol. 41, no. 4, pp. 299–324, 1994.

[60]M. M. company product literature.

[61]H. Kawai, "Japan "the piezoelectricity of poly (vinylidene fluoride)"", *J. appl. Phys*, vol. 8, pp. 975–976, 1969.

[62]C. Ku and R. Liepins, *Electrical Properties of Polymers: Chemical Principles*. Hanser Publishers, 1987, ISBN: 9783446842809. [Online]. Available: https://books.google.com.tr/books?id=GiSszQEACAAJ.

[63]Omnexus, *Polyvinylidene Fluoride (PVDF): Complete Guide*, https://omnexus.specialchem.com/selection-guide/polyvinylidene-fluoride-pvdf-plastic, [Online; accessed 29-November-2022].

[64]H. Jaffe and D. Berlincourt, "Piezoelectric transducer materials", *Proceedings of the IEEE*, vol. 53, no. 10, pp. 1372–1386, 1965.

[65]D. Damjanovic and R. Newnham, "Electrostrictive and piezoelectric materials for actuator applications", *Journal of intelligent material systems and structures*, vol. 3, no. 2, pp. 190–208, 1992.

[66]R. C. Buchanan, *Ceramic materials for electronics: processing, properties, and applications*. Marcel Dekker Ltd, 1986.

[67]E. C. N. Silva, "Synthesis of piezocomposites", *Optimal Synthesis Methods for MEMS*, Springer, 2003, pp. 155–191.

[68]P. Guillaussier, C. Audoly, and D. Boucher, "Porous lead zirconate titanate ceramics for hydrophones", *Ferroelectrics*, vol. 187, no. 1, pp. 121–128, 1996.

[69]J. Bennett and G. Hayward, “Design of 1-3 piezocomposite hydrophones using finite element analysis”, *IEEE transactions on ultrasonics, ferroelectrics, and frequency control*, vol. 44, no. 3, pp. 565–574, 1997.

[70]H. Gallantree, “Piezoelectric ceramic/polymer composites”, *Br. Ceram. Proc.*, vol. 41, pp. 161–169, Jan. 1989.

[71]R. C. Smith, *Smart material systems: model development*. SIAM, 2005.

[72]A. Arockiarajan, B. Delibas, A. Menzel, and W. Seemann, “Studies on rate-dependent switching effects of piezoelectric materials using a finite element model”, *Computational Materials Science*, vol. 37, no. 3, pp. 306–317, 2006.

[73]J. Zheng, S. Takahashi, S. Yoshikawa, K. Uchino, and J. De Vries, “Heat generation in multilayer piezoelectric actuators”, *Journal of the American Ceramic Society*, vol. 79, no. 12, pp. 3193–3198, 1996.

[74]A. Sohrabi and A. Muliana, “Rate-dependent electro-mechanical coupling response of ferroelectric materials: A finite element formulation”, *Mechanics of Materials*, vol. 62, pp. 44–59, 2013.

[75]T. Fett and G. Thun, “Determination of room-temperature tensile creep of pzt”, *Journal of Materials Science Letters*, vol. 17, no. 22, pp. 1929–1931, 1998.

[76]A. B. Schäufele and K. Heinz Härdtl, “Ferroelastic properties of lead zirconate titanate ceramics”, *Journal of the American Ceramic Society*, vol. 79, no. 10, pp. 2637–2640, 1996.

[77]D. Zhou and M. Kamlah, “Room-temperature creep of soft pzt under static electrical and compressive stress loading”, *Acta materialia*, vol. 54, no. 5, pp. 1389–1396, 2006.

[78]H. Ben Atitallah, Z. Ounaies, and A. Muliana, “Temperature and time effects in the electro-mechanical coupling behavior in active fiber composite”, *Proceedings of 16th US National Congress on Theoretical and Applied Mechanics US-NCTAM, State College, Pennsylvania*, 2010.

[79]R. Jayendiran and A. Arockiarajan, “Nonlinear modeling on rate dependent ferroelectric and ferroelastic response of 1-3 piezocomposites”, *Smart Materials and Structures*, vol. 25, no. 6, p. 065 017, 2016.

[80]S. Maniprakash, R. Jayendiran, A. Menzel, and A. Arockiarajan, “Experimental investigation, modelling and simulation of rate-dependent response of 1–3 ferroelectric composites”, *Mechanics of Materials*, vol. 94, pp. 91–105, 2016.

[81]W. J. Drugan and J. R. Willis, "A micromechanics-based nonlocal constitutive equation and estimates of representative volume element size for elastic composites", *Journal of the Mechanics and Physics of Solids*, vol. 44, no. 4, pp. 497–524, 1996.

[82]S. L. Omairey, P. D. Dunning, and S. Sriramula, "Development of an abaqus plugin tool for periodic rve homogenisation", *Engineering with Computers*, vol. 35, no. 2, pp. 567–577, 2019.

[83]P. Suquet, *Elements of homogenization theory for inelastic solid mechanics. sanchez-palencia e, zaoui a. homogenization techniques for composite media*, 1987.

[84]R. Hill, "Elastic properties of reinforced solids: Some theoretical principles", *Journal of the Mechanics and Physics of Solids*, vol. 11, no. 5, pp. 357–372, 1963.

[85]S. Hazanov and M. Amieur, "On overall properties of elastic heterogeneous bodies smaller than the representative volume", *International Journal of Engineering Science*, vol. 33, no. 9, pp. 1289–1301, 1995.

[86]M. Ostoja-Starzewski, "Material spatial randomness: From statistical to representative volume element", *Probabilistic engineering mechanics*, vol. 21, no. 2, pp. 112–132, 2006.

[87]D. Pahr and H. Böhm, "Assessment of mixed uniform boundary conditions for predicting the mechanical behavior of elastic and inelastic discontinuously reinforced composites", *Comput. Model. Engng. Sci*, vol. 34, pp. 117–136, 2008.

[88]V.-D. Nguyen, E. Béchet, C. Geuzaine, and L. Noels, "Imposing periodic boundary condition on arbitrary meshes by polynomial interpolation", *Computational Materials Science*, vol. 55, pp. 390–406, 2012.

[89]T. Kanit, S. Forest, I. Galliet, V. Mounoury, and D. Jeulin, "Determination of the size of the representative volume element for random composites: Statistical and numerical approach", *International Journal of solids and structures*, vol. 40, no. 13-14, pp. 3647–3679, 2003.

[90]K. Terada, M. Hori, T. Kyoya, and N. Kikuchi, "Simulation of the multi-scale convergence in computational homogenization approaches", *International Journal of Solids and Structures*, vol. 37, no. 16, pp. 2285–2311, 2000.

[91]F. Larsson, K. Runesson, S. Saroukhani, and R. Vafadari, "Computational homogenization based on a weak format of micro-periodicity for rve-problems", *Computer Methods in Applied Mechanics and Engineering*, vol. 200, no. 1-4, pp. 11–26, 2011.

[92]R.-S. Qin, Y. Xiao, and H. Lan, "Numerical simulation of effective properties of 3d piezoelectric composites", *Journal of Engineering*, vol. 2014, 2014.

[93]K. S. Havner, "A discrete model for the prediction of subsequent yield surfaces in polycrystalline plasticity", *International Journal of Solids and Structures*, vol. 7, no. 7, pp. 719–730, 1971.

[94]R. d. Medeiros, M. E. Moreno, F. D. Marques, and V. Tita, "Effective properties evaluation for smart composite materials", *Journal of the Brazilian Society of Mechanical Sciences and Engineering*, vol. 34, pp. 362–370, 2012.

[95]H. E. Pettermann and S. Suresh, "A comprehensive unit cell model: A study of coupled effects in piezoelectric 1–3 composites", *International Journal of Solids and Structures*, vol. 37, no. 39, pp. 5447–5464, 2000.

[96]S. A. Prasad, B. V. Sankar, L. N. Cattafesta, S. Horowitz, Q. Gallas, and M. Sheplak, "Two-port electroacoustic model of an axisymmetric piezoelectric composite plate", *43 rd AIAA/ASME/ASCE/AHS/ASC Structures, Structural Dynamics, and Materials Conference, Denver, CO*, 2002.

[97]V.-T. Nguyen, P. Kumar, and J. Y. C. Leong, "Finite element modellingand simulations of piezoelectric actuators responses with uncertainty quantification", *Computation*, vol. 6, no. 4, p. 60, 2018.

[98]A. I. Ltd., *PHYSICAL AND PIEZOELECTRIC PROPERTIES OF APC MATERIALS*, `https://www.americanpiezo.com/apc-materials/physical-piezoelectric-properties.html`, [Online; accessed 05-Nov-2022], March 2020.

[99]E. Mercadelli, A. Sanson, and C. Galassi, *Porous piezoelectric ceramics*. INTECH Open Access Publisher, 2010.

[100]A. R. Studart, U. T. Gonzenbach, E. Tervoort, and L. J. Gauckler, "Processing routes to macroporous ceramics: A review", *Journal of the American Ceramic Society*, vol. 89, no. 6, pp. 1771–1789, 2006.

[101]C. Bowen, A. Perry, A. Lewis, and H. Kara, “Processing and properties of porous piezoelectric materials with high hydrostatic figures of merit”, *Journal of the European Ceramic Society*, vol. 24, no. 2, pp. 541–545, 2004.

[102]H. Kara, R. Ramesh, R. Stevens, and C. R. Bowen, “Porous pzt ceramics for receiving transducers”, *IEEE transactions on ultrasonics, ferroelectrics, and frequency control*, vol. 50, no. 3, pp. 289–296, 2003.